AN EXPERIMENTAL DRIVING MECHANISM FOR
A RIGID OSCILLATING FOIL PROPELLER

ANTONINO M. CALDERON

The author has granted a non-exclusive licence allowing the National Library of Canada to reproduce, loan, distribute or sell copies of this thesis in microform, paper or electronic formats.

The author retains ownership of the copyright in this thesis. Neither the thesis nor substantial extracts from it may be printed or otherwise reproduced without the author's permission.

L'auteur a accordé une licence non exclusive permettant à la Bibliothèque nationale du Canada de reproduire, prêter, distribuer ou vendre des copies de cette thèse sous la forme de microfiche/film, de reproduction sur papier ou sur format électronique.

L'auteur conserve la propriété du droit d'auteur qui protège cette thèse. Ni la thèse ni des extraits substantiels de celle-ci ne doivent être imprimés ou autrement reproduits sans son autorisation.

0-612-62374-2

Canadä

An Experimental Driving Mechanism For

A Rigid Oscillating Foil Propeller

By

©Antonino M. Calderon, BSME, BVocEd.

A thesis submitted to the School of Graduate

Studies in partial fulfillment of the

requirements for the degree of

Master of Engineering

Faculty of Engineering and Applied Science

Memorial University of Newfoundland

January, 2001

St. John's   Newfoundland   Canada

ABSTRACT

This thesis is about an experimental design of a drive mechanism, which was fitted with a rigid, oscillating foil intended to provide propulsive thrust to any 4-6 m boat. The driving device allowed an innovative, tail like fin, to flap vertically up and down with simultaneous change of pitch simulating the characteristic motion of a whale's tail. The work included all the construction of the drive mechanism, the installation of this mechanism to a typical 4.8 m, open, flat bottom boat. Transducer gauges were placed in strategic locations to measure dynamic forces produced by the drive mechanism and moving foil.

This experiment emphasised the practicality and development of a drive mechanism that would accommodate subsequent practical work of other foil propellers of various parameters. It is hoped that more research will follow in the prototype stage to concretely give credence to the practicality of foil propulsion in marine vessels.

THE GREATEST WORK OF ALL

IN MARINE PROPULSION

PSALM 104:24...

....

The Earth is full of thy riches.

So is this great and wide Sea.

Wherein are things creeping innumerable.

Both small and great beasts.

There go the ships;

There is that leviathan, whom thou hast made to play therein.

Acknowledgements

And most of all, I will always remember and truly appreciate the understanding and sacrificing graces of my sons and wife in my absence because of the workload demand.

Contents

List of Figures

List of Tables

List of Graphs

CHAPTER 1

BACKGROUND

1.1   CONCEPTS AND EXPERIMENTS

Man has always been very interested with the concept of motion. Animals of the air, land, and of the sea have much peculiar locomotions inherent to each.

The study deals with the carangiform mode of motion, Lighthill (1969) of a particular group of cetacean mammals, the whales and dolphins. The main interest lies in the ability of these marine dwellers to propel their bodies with great speed over long distances.

Since the study is about a particular mode of motion, it is fitting to see how these mammals and other fishes perform this motion.

Among many living things in the sea and its environment, locomotion has been described as anguilliform and carangiform, Lighthill (1969). The mechanics of anguilliform are undulatory in nature. This paper described the interesting nature of "thrust" from an undulating body such as the typical eel. Lighthill (1970a) explained that this motion could be illustrated in figure 1.1 which shows how this thrust is made available.

1

Undulatory Motion
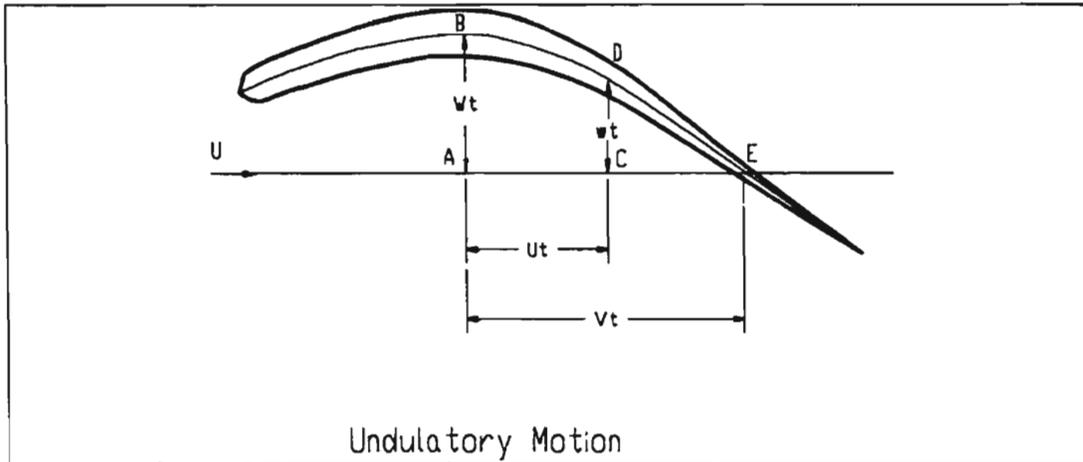
Figure 1. 1 Undulating body

Where U - stream velocity (Thus U is the mean swimming speed relative to the stream)

V - differing speed of undulation going backward

W - lateral velocity relative to animal

w - centre body normal velocity relative to the water

At time interval **t**, Wt takes position AB while the wave moves backwards, Vt, a distance AE. At the same time, the water moves a distance Ut so that relative to the water the centreline moves a distance CD equal to wt. From these positions we have a slope, W/V.

If $K_N w$ is the resisting force per unit length of this normal velocity w and if this is multiplied by the slope W/V, the forward *thrust* is obtained. There is however, a tangential component to the W velocity and this is expressed as W times the slope, which with K_T reduces the forward thrust to a net amount of thrust per unit length, $P = (K_N w - K_T W)(W/V)$. K_N and K_T are resistance coefficients for normal and tangential resistance. Anguilliform propulsion is then the side to side undulations that are propagated

2

backwards as a propulsive wave.

In the carangiform mode. the anterior body stays steady while the posterior part increases in amplitude peaking at the trailing edge as a peculiar undulatory stroke is in progress. Lighthill (1970a) suggests that scombroid fishes and cetacean mammals have adapted the carangiform mode of propulsion. causing their tails converged to a high aspect ratio crescent moon shape through an evolutionary process, where the environment supports the life cycle of the food chain - predators and vice versa.

Now that the tail as the main focus of interest, specifically the one called a lunate tail, that portion of the mammal's after end which is attached horizontally and moves vertically up and down. many researchers have helped to unfold its high efficiency function as a body propulsor.

One study by Hertel (1963). suggests that a fish has three basic strokes: one active, which is a vertical motion with the tail fin; one passive stroke. as in the horizontal sweep using the high lateral surface of the tail; and one natural stroke, which twists the fin about its longitudinal axis for manoeuvre. Although the fish tail is vertical in this study, shifting the axes by 90° would result to similar motion characteristics common to the lunate tail.

Similarly, Lighthill (1970) uses a linearized two dimensional theory of oscillating aerofoil which considers the movements of the lunate tail's vertical motion with pitch angle fluctuating in phase with its heaving velocity. Accordingly, the introduction of $\omega c/U$ (reduced frequency parameter, ω=radians, c=chord of the tail under study, and U=

3

forward speed) and θ=Uα/ωh (feathering parameter, ωh= oscillating amplitude, α=pitch yawing motion) are two relevant variables that demonstrate the propulsive effect of the oscillating tail as these are plotted with variables C_T and η, which, respectively, are the thrust coefficient and efficiency. The significance of this theory indicates that thrust and efficiency are highest when the location of the pitching axis is somewhere between the third and the last quarter chord of the section of the lunate's tail.

Chopra (1974) used a three dimensional analysis which "gives modified values of thrust coefficient and propulsive efficiency for a wide variety of the physical parameters, taking into account the streamwise wake vorticity." This study confirms that a lower aspect ratio of the fin results in a decrease in the thrust coefficient. Following this work, Chopra (1976), considered the fin's large amplitude motion analysis, which demonstrated the increased efficiency due to increased heave and high frequency oscillations. As well, thrust is increased with larger angles of attack so long as the point of separation is not exceeded.

The paper of Chopra and Kambe (1987) considered small amplitude motion of thin plates with general planform similar to the actual lunate tails of fast marine animals. In this study, thrust and propulsive efficiency depended on the following parameters:

(i.) aspect ratio ($span^2$ / planform area)

(ii.) reduced frequency (angular frequency x typical length / forward speed)

(iii.) feathering parameter (the ratio of the tail slope to the slope of the path of the pitching axis)

4

(iv.) position of the pitching axis and

(v.) the curved shapes of the leading and trailing edges.

From their study, it is found that a curved leading edge like the lunate tail's, reduces the portion of thrust related to the leading edge suction and that efficiency is sacrificed when the leading edge sweep back angle exceeds 30°.

Katz and Weihs (1978 and 1979) described their analysis of large aspect ratio airfoils performing large amplitude unsteady motion using the dimensional theory. The result is a comparison of propulsive efficiencies of both a rigid foil and a foil with chordwise flexibility. The latter showed an increase of 20% efficiency when both performed the same motion. Furthermore , it showed that there is an increase of thrust and efficiency when there is large amplitude with increasing frequency and that thrust coefficient is highest when the phase difference between heave and pitch is close to 90°.

Cheng and Murillo (1984) developed an asymptotic theory of a high aspect ratio wing in an incompressible flow. The analysis includes the planar lifting surface, oscillating at a reduced frequency based on the half span, which is of the order of unity at the limit. Application to the lunate tail swimming propulsion model shows physiological and kinematic data consistent with that reported in the literature summarised by Wu and Yates (1978).

The Karpouzian, Spedding, and Cheng (1990) paper is a sequel to the above study and is a performance analysis of lunate tail swimming propulsion. It highlights the role of the proportional feathering parameter,Θ, along with the influence of sweep and the effect

5

of centerline curvature of the oscillating model while holding a certain thrust threshold. One particular point of interest concerns the interchangeable roles of centerline sweep and peduncle(near the major pitch axis) movement at an optimum propulsive efficiency.

Bose and Lien (1989) published their work showing the geometric sizes of the flukes and the flexible feature of the fluke's span and chord dimensions. In their calculations, assuming the foil to be rigid, the hydromechanical efficiency of a whale's fluke is around 87% with the pitch angle at 30° and advance ratio(π x speed of advance / ωh) of 4.5.

Liu (1991) used the QVLM (quasi-vortex lattice method) theory by Lan to predict the thrust coefficients and propulsive efficiencies of three geometric planforms of cetacean's flukes during pitching and heaving motions.

Furthermore, Liu and Bose (1992), using the theory above, predict the propulsive performance of three naturally occurring fin foils. These are the white whale *(Delphinaptera)*, white sided dolphin *(Lagernorhynchus acutus)*, and fin whale *(Balaenoptera physalus)*. Propulsion efficiencies were 90%, 96%, and 96%, ignoring friction and drag, respectively.

These theories uncover the varied functions of a lunate tail's high hydromechanical thrust and efficiency that encourage experimenters to do physical design, modelling, and construction of a foil propulsion simulating the geometry and motion of a fish tail hoping to unravel its practical applications to marine vessels.

6

1.2   Construction for Service/Experimentation:

There were tests and experiments that were conducted several years ago pertaining to the hydrodynamics of a tail fin. Some of them were built for commercial service while others were prototypes made for further experimentation. Three of these will be described in this paper as examples to clearly illustrate how the various works were set up and how their conclusions were drawn concerning thrust generation of the foil.

Cuypers (1984), discusses the merit of monopale propulsion in riverboats. He described the foil propulsion used in a shallow draught riverboat as a non-stationary propeller in comparison with stationary screw propellers. Figure 1.2 is a schematic arrangement of its operation. From this, the single blade moves up and down with simultaneous change of pitch, which simulates one motion of a fish tail. The heave amplitude is determined by the circular drive attachment. Also shown is the non-stationary propeller's K_T - K_{V_a} diagram. K_T is defined as the thrust coefficient equal to

$$T / [\rho_w A P^2]^{1/3}. \tag{1.1}$$

And, K_{V_a} as speed coefficient, expressed as

$$V_a / [P/\rho_w A]^{1/3}. \tag{1.2}$$

Units of each variable are: T, thrust (N), V_a(m/s), P(kW), ρ_w(kg/m^3), and A(m^2). From the diagram, it is suggested that a Voith Schneider propeller has a higher K_T value than the monopale's at high propeller loading. Despite this, the papers suggest that its main advantage is the capability of the monopale to operate in shallow waters.
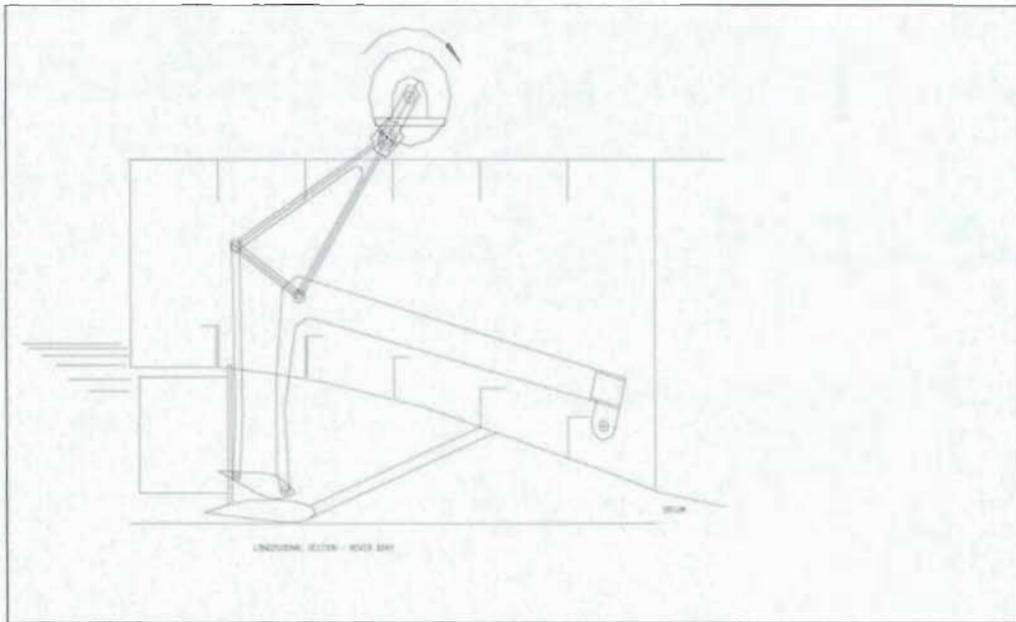
Figure 1. 2 River boat section
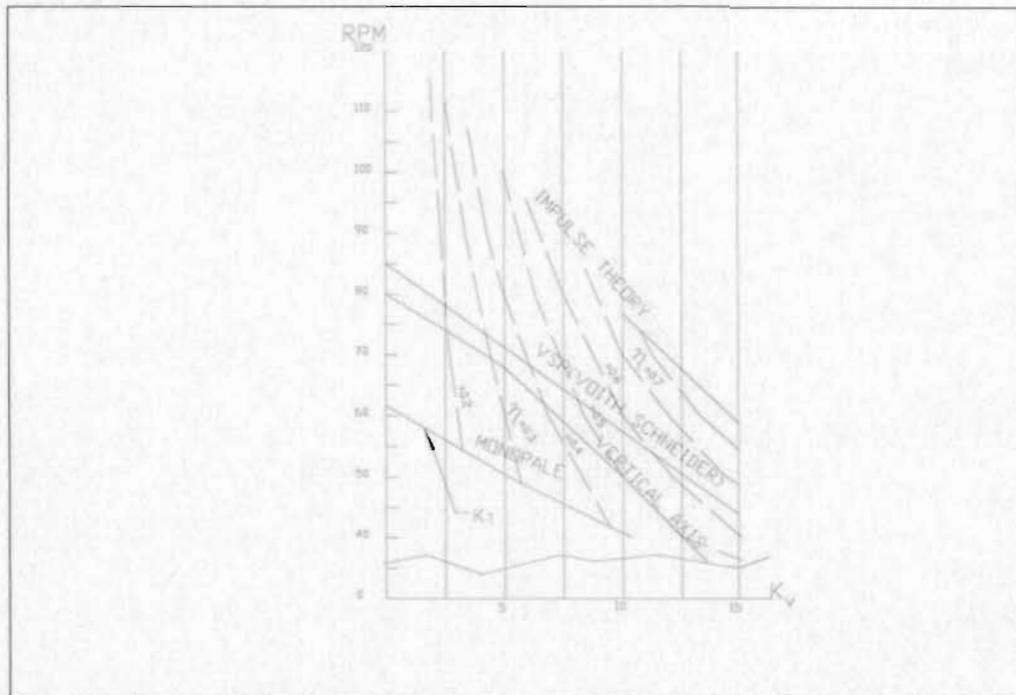
Figure 1.2 a Cuyper's K_T and K_V diagram

Isshiki et al. (1987) states that their experimental single oscillating fin wing as in the figure below proves the measured thrust to be reliable for further prototype testing. Further experiments as conducted by students from Tokyo Institute of Technology and Nihon University led them to outfit a 3m boat with an oscillating fin at its after end. Through this experiment, an encouraging result of 60%-65% efficiencies was measured. Foils of rigid and flexible constructions were used. In the report, the conclusion favours the flexible wing to be a little better in performance than the other.
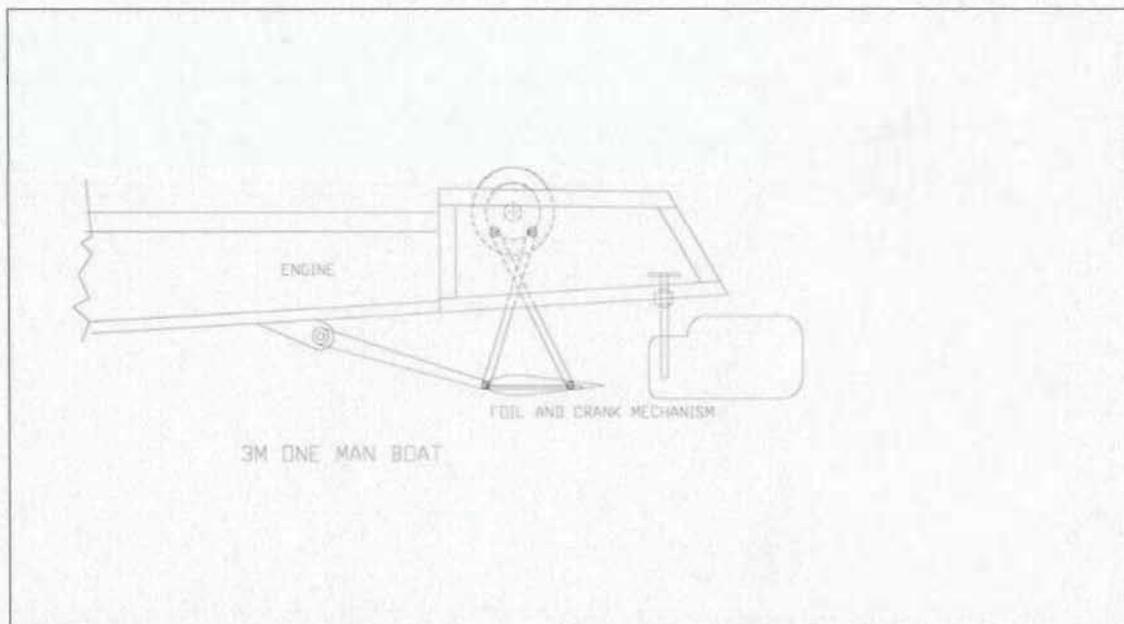
Figure 1. 3 Japanese 3 m experimental boat

Norway's Wave Control Company (1983) tested wave power for ship propulsion. Horizontal hydrofoils mounted below a 7.5m hull reached six knots under wave power. The report also suggested that a powered version could have a 30% saving in fuel when

compared with the common screw propeller.

The design consisted of a horizontal submerged hydrofoil placed just aft of the side of the bow section. A vertical support attached to this section supports the foil, which is restrained by a mechanical force that keeps the foil in a neutral position. Energy is either extracted, when the fixed foil moves vertically due to wave power of the surrounding water, or expended, when thrust is generated due to orientation of angle of attack of foil as it moves vertically up and down. The size of each foil is $0.5m^2$. The foil propulsion arrangement is shown below.
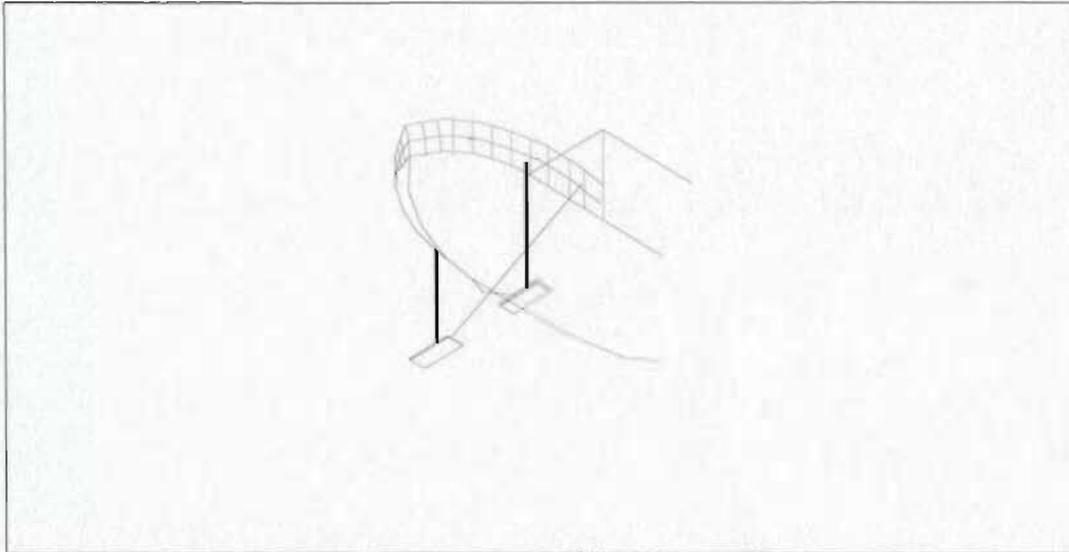
Figure 1. 4 Hydrofoils for wave power

The foregoing studies and experimentation highlighted the parameters that influence the lunate tail's propulsion performance. Again, to name a few, these are feathering parameters, reduced frequency, aspect ratio, sweep back, heave amplitude,

angle of attack, and others. These factors according to the literature survey above would affect the operational performance of a man made fin or foil that would simulate some of the fish tail's character and motion.

CHAPTER 2

DEVELOPING THE PREDICTING EQUATION OF
THE FOIL PROPULSOR

2.1   PARTIAL ANALYSIS

The use of partial analysis (Sharp 1981) is a powerful tool in developing non-dimensional products which give the relationships of the various parameters in describing the physical phenomena that are under study. In order to strengthen this approach, the three factors of geometry, kinematics, and dynamics should combine together in the evaluation of the case under study. Upon their consideration, the technique of dimensional analysis such as Rayleigh, Buckingham, matrix, and even linear proportionality could be used and the result should give some non-dimensional relationships that govern the conditions of the phenomenon under study.

Partial analysis is also an approach to simplification. This claim is verified through the use or consideration of all the important variables and the elimination of redundant ones. Data or record handling becomes manageable since only the variables are considered.

The next benefit of partial analysis is that it provides information prior to experimentation. Identification is made of the most significant non-dimensional relationships. Also, it gives the experimenter latitude to set aside parameters with less significance in the immediate experiment.

The last benefit is attributed to report presentation. Since the terms in the non-

dimensional products are grouped that emphasise the predicted or hypothesised result, the graphical plotting of these non-dimensional relationships is a good way to present the data. Managing and control over of these non-dimensional products allows the experimenter to make decisions in various situations where recording of trends in the early part of the work could predict a certain outcome, which could assist the individual in deciding whether to continue on the present work. Sometimes. this trend dictates adjustments that help the work progress as expected.

2.2 THE PARAMETERS

The following lists each variable and its corresponding description with the applicable dimensional unit. Altogether, they are the parameters considered in describing the morphological aspect of the design under study.

SYMBOLS	DESCRIPTIONS	DIMENSIONAL UNITS
S	Area of foil	L^2
B	Span of foil	L
U_o	Undisturbed velocity	L / T
H	Heave amplitude	L
C	Chord of foil	L
A_1	Sweep back angle	Radian
α	Angular amplitude of pitch	Radian
Ω	Angular frequency	rad / T
Sg	Reduced gravity	L / T^2
G	Gravity	L / T^2
ϕ_{ph}	Phase angle(pitch lead/lag heave)	Radian
D_w	Density of water	M / L^3
D_s	Density of foil	M / L^3
μ	Dynamic viscosity	M / LT
F_t	Thrust	ML / T^2
C_r	Pitching moment point on chord	L
E	Elasticity of foil	M / LT^2
P	Vertical force on heaving motion	ML / T^2
K	Roughness surface	L
δ	Deflection(flexibility of foil)	L

2.3   DIMENSIONAL ANALYSIS

Using the matrix method, the variables are grouped in the following relationship.

$\Theta \{ P, F_t, E, \mu, C_r, \Omega, \alpha, A_l, c, g, sg, S, B, U_o, \phi_{ph}, h, d_w, d_s, \delta, k \} = 0$

	d_w	C	U_o	P	F_t	E	d_s	ϕ_{ph}	A_l	C_r	sg	g
M	1	0	0	1	1	1	1	0	0	0	0	0
L	-3	1	1	1	1	-1	-3	0	0	1	1	1
T	0	0	-1	-2	-2	-2	0	0	0	0	-2	-2

S	B	Ω	α	μ	H	k	δ
0	0	0	0	1	0	0	0
2	1	0	0	-1	1	1	1
0	0	-1	0	-1	0	0	0

Evaluating this matrix, the result is shown in the table below.

d_w	1	0	0	1	1	1	1	0	0	0	0	0
c	0	1	0	2	2	0	0	0	0	1	-1	-1
U_o	0	0	1	2	2	2	0	0	0	0	2	2

0	0	0	0	1	0	0	0
2	1	-1	0	1	1	1	1
0	0	1	0	1	0	0	0

The numbers exhibited in the table are expressed in the resulting non-dimensional products, thus

$$\Theta \{ P / d_w c^2 U_o{}^2, F_t / d_w c^2 U_o{}^2, E / d_w U_o{}^2, d_s / d_w, \phi_{ph}, A_l, C_r / c, sg\,c / U_o{}^2, g\,c / U_o{}^2, S / c^2, B / c, \Omega\,c / U_o, \alpha, \mu / d_w c U_o, h / c, k / c, \delta / c \} = 0 .$$

Rationalising these terms through compounding and combination, the final expression is written as $F_t = d_w c^2 U_o{}^2 \, \Theta \{ P/d_w c^2 U_o{}^2, P/SE, d_s/d_w, C_r/c, sgc/U_o{}^2, gc/U_o{}^2, B^2/S, \Omega^2 c/g, d_w c U_o/\mu, h\Omega/\pi U_o, h\Omega/\alpha U_o, \phi_{ph}, A_l, k/c, \delta/c, B/c \}.$

Looking at the various terms, many familiar non-dimensional products and numbers are present. Specifically, the left-hand term denotes the THRUST, which according to this equation is a function of the following terms inside the parenthesis, which are:

1st term... input force to generate thrust, $P/d_w c^2 U_o{}^2$

2nd term... strain in the foil, P/SE

3rd term... the material composition of the foil, d_s/d_w

4th term... the location of the pitching axis, C_r/c

5th & 6th term... Froude numbers, $sgc/U_o{}^2$, $gc/U_o{}^2$

7th term... aspect ratio of the foil, B^2/S

8th term... oscillating frequency of the foil, $\Omega^2 c/g$

9th term... Reynolds number, $d_w c U_o/\mu$

10th term.. advance ratio of the foil, $h\Omega/\pi U_o$

11th term.. feathering parameter, $h\Omega/\alpha U_o$ and the others define geometric sizes,shapes.

16

and roughness.

Many of these parameters were identified also in the literature surveyed earlier. From the terms identified, one could eliminate for example the Froude numbers, strain on the foil, and deflection on the foil, to simplify the set-up of the experiment. The remaining parameters would correlate experimental data with respect to the Reynolds number, the geometry, the kinematic, and the dynamic parameters. All of these factors suggest that more experimental work and studies are required to fully explore the benefits of fabricated fin foils.

CHAPTER 3

THE FOIL PROPULSION DESIGN AND CONSTRUCTION

3.1 APPLICABILITY

The design and construction of the oscillating foil propulsion system had to meet the following objectives:

- Applicability to boats in the range 4 – 6 m length.

- A practical-drive mechanism that produced the correct motion to create this (Yamaguchi 1992).

- Interchange-ability of foil propulsion planform to test variety of fins including flexible foils.

- Economic construction materials and methods to keep construction cost down.

3.2 PARAMETERS FOR DESIGN AND CONSTRUCTION

Like the lunate tail, the propulsion design must have a motion characteristic similar to that of a whale's flukes. Its geometric form would include parameters such as sweep back angle, aspect ratio, shape, and surface finish. The motion would be sinusoidal with pitch either leading or lagging at a certain angle. Although flexibility is an important factor, a rigid foil was considered to simplify construction. Weight was also important because it influenced the size and strength of the components of the mechanism.

There were many specific parameters to consider as suggested by the various
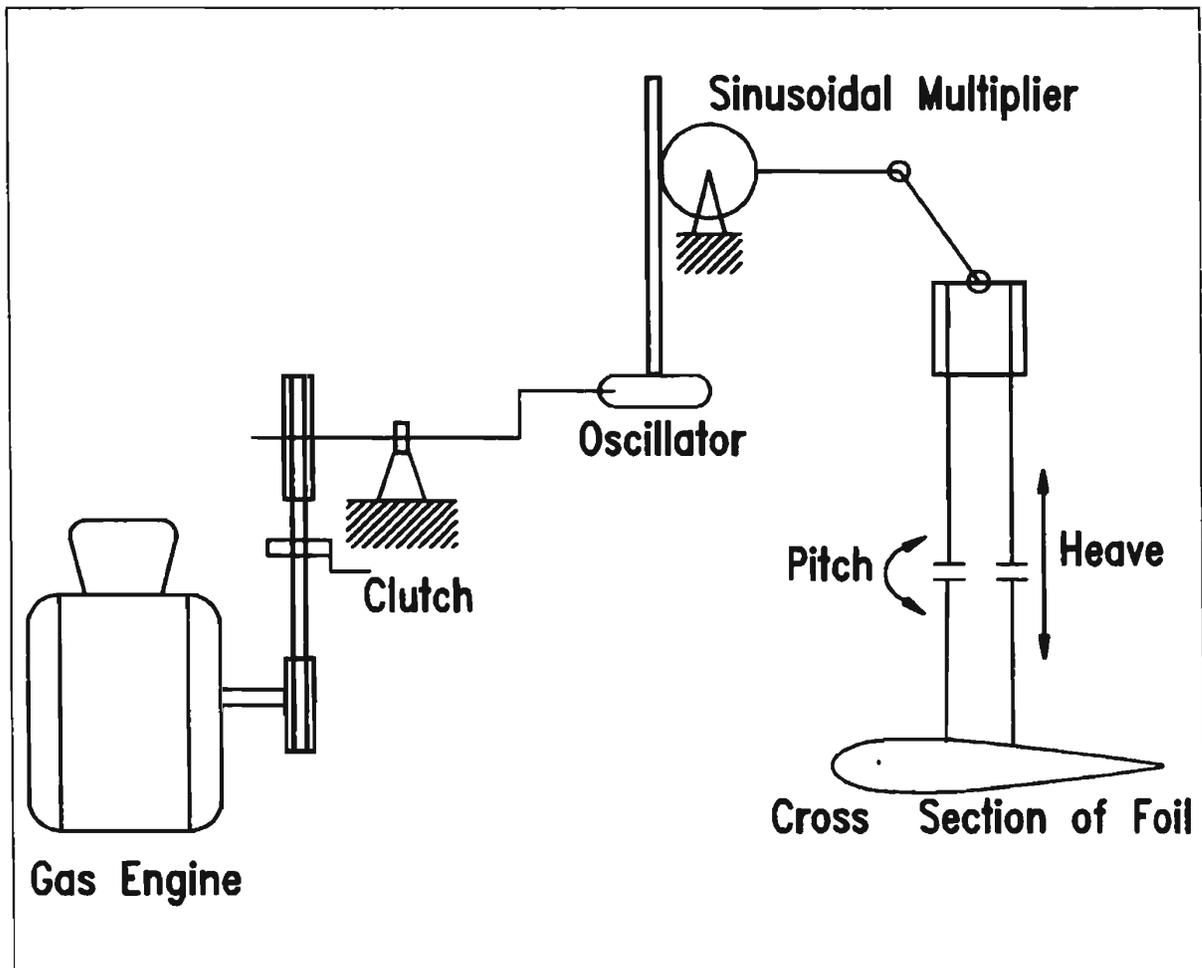
Figure 3. 1   Schematic drawing of the foil propulsion system

reports in the survey and as confirmed by the partial analysis. Unlike the physical factors

mentioned above, there are dynamic variables like frequency, heave amplitude, pitch

setting, advance ratio. feathering parameters, etc. which were identified as the work

progressed. Another matter of interest in the design is the applicable size range of the

boat. The size of the foil was a function of the total resistance of the boat.

The line drawing in fig. 3.1 is the diagrammatic arrangement of the proposed

design of the foil propulsion system. It shows the power plant (a gasoline engine)

connected to gears and pulleys that reduce the speed of the engine to within the required oscillating speed at which the foil would be functional. The foil is considered to be fully submerged. Its motion is vertical and the pitch changes as it moves up and down. The speed of its oscillation depends on the throttle adjustment in the carburetor of the engine. It is imperative that however fast this engine runs, the frequency transmitted to the foil is within its functional range. Also, since the foil is attached to a sliding mechanism, there is the chance of excessive vibration occurring.

3.2.1 THE POWER PLANT

A gasoline engine was the drive mechanism chosen for this propulsion system. It was easily available, economical, and reliable. The problem was sizing the rated capacity required for this particular application.

The conditions to calculate the power requirement of the designed foil and to operate within its designed conditions were as follow:

Aspect Ratio = 6.0   Area of foil, $S = 0.13$ m^2

Amplitude = Heave of foil / 2= 0.530 /2 m   Chord$_{max}$, c = 0.254 m

Chord$_{mean}$ = 0.18 m   Density of salt water, d_w=1026 kg/m^3

Lift force, $L = \frac{1}{2} C_L d_w U^2 S$ Power = Force * Speed /η(Efficiency)

Span (breadth of wing) = 0.81 m

Reynold's number, Re $= d_w c\, U_o/\mu = 1026\,(0.254)\,(1.2)/1.11 \times 10^{-3} = 2.98 \times 10^5$
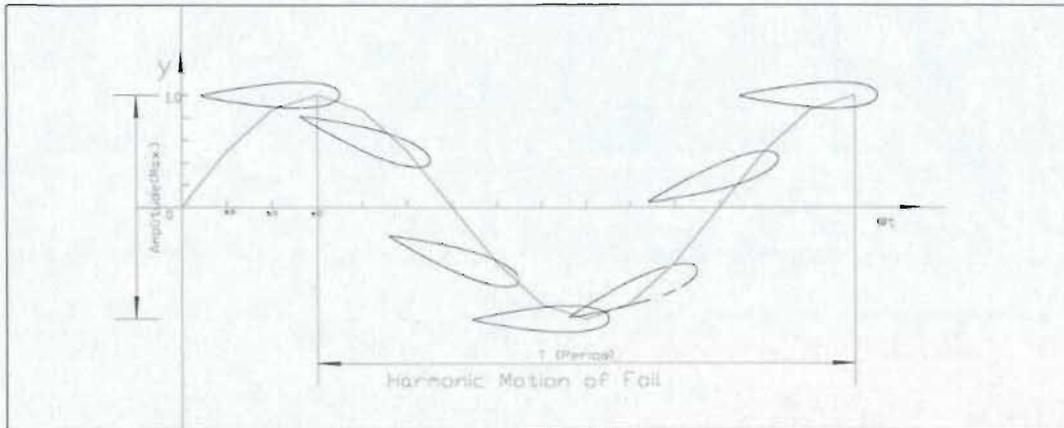
Figure 3. 2 Oscillating motion of foil

The foil motion is considered harmonic and moving transversely as shown. It follows a displacement path, which is

$$y = A \cos(\omega t). \tag{3.1}$$

$$y' = -A \omega \sin(\omega t), \text{ and} \tag{3.2}$$

$$y'' = -A \omega^2 \cos(\omega t). \tag{3.3}$$

The differential results represent the vertical velocity and acceleration respectively of the foil. The angular velocity, ω, of its motion was due to the reduction gearing in the drive oscillator mechanism, which range from 20 to 60 revolution per minute (2.1 to 6.28 rad/s).

21

It was anticipated that fluid, body, and added virtual mass forces were the basis for power calculation of the foil. The first was the lifting body that will provide the thrust component. The second was the body force that comprised the mass of the moving body (foil and slider) and determined as 13.6 kg. The other was the added virtual mass, which pertained to the foil operating in a fluid environment.

Substituting in equations (3.2 and 3.3) the amplitude and the upper ω range, the transverse velocity of the slider and foil was $y' = (-0.53\ /2)$ m (5.23 rad/s) sin(5.23 x $180°/\pi$ * t) = **1.2 m/s**, and the acceleration was calculated as $y'' = (0.53/2)\ (5.23)^2$ cos(300)= **3.13 m/s^2**. These motions were to be considered in the upper range. Calculating the body and added virtual mass forces respectively were

$$F = ma \text{ or } 13.6 \text{ kg } (3.13 \text{ m/s}^2) \text{ equal to } \mathbf{49.3 \text{ N}}. \text{ and} \tag{3.4}$$

$$F_{avm} = \pi c^2 (span)^2 d_w\ /\ 4\ \{(span)^2 + c^2\ \}^{0.5} * (y'') \tag{3.5}$$

or $= 3.14\ (0.18)^2\ (0.81)^2\ (1026)\ /\ 4\ \{(0.81)^2 + 0.18^2\}^{0.5}\} * (3.13) = \mathbf{17.1 \text{ N}}.$

Note the added mass was taken from the mass of a flat plate, which was considered similar to that of the fin, Bose and Lien (1989).

The components of V_R, which are y' or V_f and V_A in figure 3.2a are the basis for calculating the thrust. The value of V_R is assumed to be 1.72 when β is considered to be between 40°-50°.
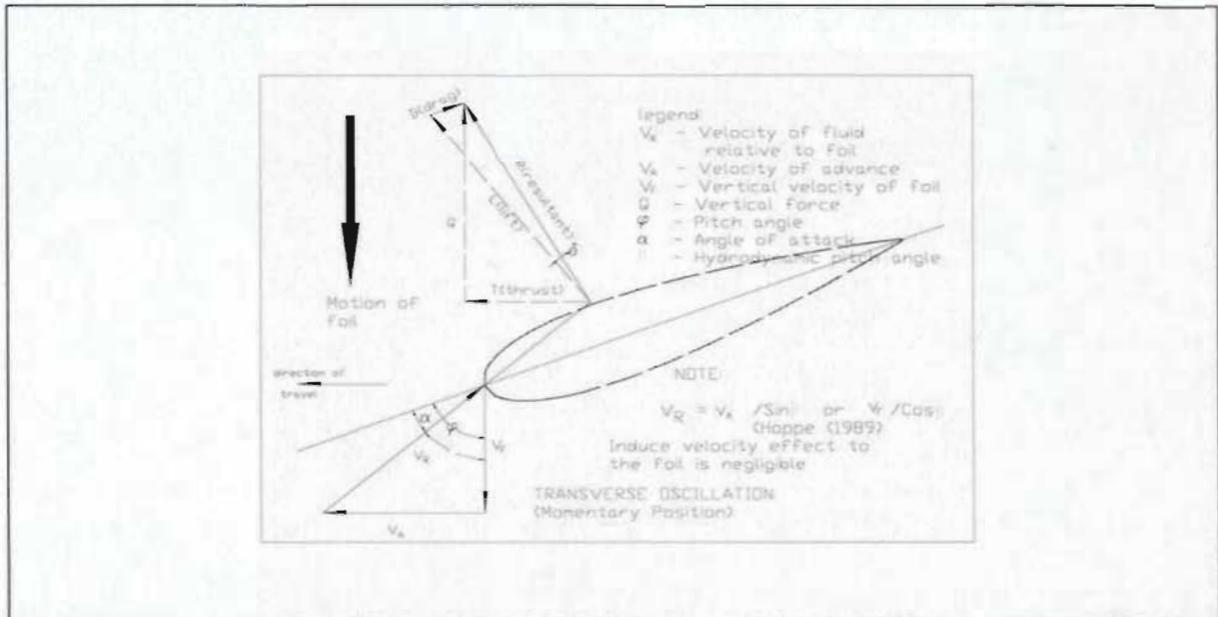
Figure 3.2a   **Momentary motion of foil**

The thrust was taken from Hoppe (1989) indicating thrust was

$$T = L \cos(\beta_I + \delta) / \cos \delta \text{ or } L \cos(\beta + \delta) / \cos \delta, \tag{3.6}$$

where β_I became β since the induced velocity effect was negligible. Vector components are indicated above. From Comstock (1967) the coefficient of lift was, $C_L = 0.0715 \, \alpha$ for small angle of attack up to its stall position. Using 20° for α, it gave 1.43 or from Streeter (1985) fig. 6.17 page 266, it was about 1.6 for 20°. Using the lesser value of 1.43, the lift component, L, in equation (3.6) was (½ $C_L d_w U^2 S$) or substituting the values for $C_L \, d_w S$ and U^2 became V_R^2 according to the diagram above, then {1/2 x 1.43 x 1026 x 1.72^2 x 0.13 } equaled to 282 N. The values for $\cos(\beta + \delta) / \cos \delta$ were in the range of 0.51 to 0.71 for δ to be between 5° and 10° and β to be between 40° and 50°. T was {282 (0.51)} or **144 N**. These forces added to **210.4 N**. Next, the form and induced drag were

23

considered, $D_o= \frac{1}{2} C_D d_w V_R^2 S$ was the profile drag. (3.7)

The value of C_D equaled to $0.74 Re^{-0.2}$ or $0.74(2.98 \times 10^5)^{-0.2} = 0.006$. Then, D_o indicated **2.3 N** (2 sides) and

$$D_i = C_L d_w V_R^2 S / 2 \pi b^2 \text{ was the induced drag,} \quad (3.8)$$

which after substitution, $\{1.43 \times 1026 \times 1.72^2 \times 0.13 / 2 (3.14) 0.81^2\}$ indicated **137 N**. These forces, thrust and resistances, were attributed to the foil. Altogether, these resulted to **349.7 N**, which represent an optimum value in one best position of the foil in one oscillation, at 50 rpm. Since the drive mechanism was designed to run between 20-60 rpm, compare the calculated thrust value of 144 N to the table below. Using Bose and Lien (1989) methods, the table of thrust and power deliveries of the designed fin foil is shown.

Table 3. 1   Thrusts and Powers of the Fin Foil

Thrusts and Powers of the Fin Foil when oscillating at 20 rpm or 2.09 rad/s					
Speed, V (m/s)	0.5	1	1.5	2	2.5
Advance ratio, J	2.8	5.6	8.5	11.3	14.1
Pitch angle (deg.)	50	20	10	5	5
Efficiency	0.84	0.85	0.84	0.8	0.75
Thrust coefficient	0.38	0.25	0.2	0.2	0.1
Thrust (Newton)	6.3	16.7	30.0	53.3	41.68
Power (Watts)	3.8	19.6	53.6	133.4	138.9
Thrusts and Powers of the Fin Foil when oscillating at 30 rpm or 3.14 rad/s					
Advance ratio, J	1.9	3.8	5.7	7.5	9.4
Pitch angle (deg.)	50	40	20	10	10
Efficiency	0.76	0.84	0.85	0.82	0.8

Thrust coefficient	0.26	0.22	0.24	0.27	0.18
Thrust (Newton)	4.3	14.7	36.0	72.0	75.0
Power (Watts)	2.85	17.5	63.6	175.7	234.5

Thrusts and Powers of the Fin Foil when oscillating at 40 rpm or 4.19 rad/s					
Speed, V (m/s)	0.5	1	1.5	2	2.5
Advance ratio, J	1.4	2.8	4.2	5.6	7.1
Pitch angle (deg.)	Off chart	50	30	20	10
Efficiency	Not app.	0.84	0.84	0.85	0.82
Thrust coefficient	Not app.	0.38	0.25	0.24	0.28
Thrust (Newton)	Not app.	25.3	37.5	64.0	116.7
Power (Watts)	Not app.	30.2	67.0	150.6	355.8

Thrusts and Powers of the Fin Foil when oscillating at 50 rpm or 5.23 rad/s					
Speed, V (m/s)	0.5	1	1.5	2	2.5
Advance ratio, J	1.1	2.3	3.4	4.5	5.7
Pitch angle (deg.)	Off chart	50	40	20	10
Efficiency	Not app.	0.83	0.85	0.8	0.78
Thrust coefficient	Not app.	1.4	0.6	0.6	0.48
Thrust (Newton)	Not app.	93.4	90.0	160.0	200.1
Power (Watts)	Not app.	112.5	158.9	400.1	641.3

Thrusts and Powers of the Fin Foil when oscillating at 60 rpm or 6.28 rad/s					
Speed, V (m/s)	0.5	1	1.5	2	2.5
Advance ratio, J	1.0	1.9	2.8	3.8	4.7
Pitch angle (deg.)	Off chart	50	40	30	20
Efficiency	Not app.	0.76	0.84	0.84	0.82
Thrust coefficient	Not app.	1.6	0.7	0.55	0.4
Thrust (Newton)	Not app.	106.7	105.0	146.7	166.7
Power (Watts)	Not app.	140.4	187.6	349.3	508.3

The construction of the table was based on figure 6, page 195 of the Bose and Lien (1989) paper. The important factor used was the advanced ratio, $J=\pi V/\omega h$, where V is the velocity of advance (m/s), ω is the oscillating frequency (rad/s), and h is the heave amplitude (m). For each given oscillation, in the range of the design drive mechanism, and if V is assumed, J is calculated at the designed heave amplitude, h= 0.53/2 or 0.265 m.. Then, J was referred to figure 6 (a), which relates J (abscissa) and η (Efficiency, ordinate) corresponding to closed curves of pitch amplitude 50,40,30,20,10,5, and 1.25

25

degrees. The matched efficiency and pitch amplitude readings for each J are referred to figure 6 (b). A thrust coefficient reading is matched and this led to a corresponding thrust calculation from $T = \frac{1}{2} C_t d_w S V^2$. This procedure was repeated for each oscillation and given speed.

The table data at 50 rpm with the thrusts 90 N and 160 N were closely comparable to the earlier calculated thrust of 144 N using the Hoppe (1989) method. This point showed that the foil at higher oscillation would generate higher thrust. As well, the drag resistance of this particular design at this frequency was high too. The table demonstrated the varying thrusts in the range covered by the design.

Continuing on to predict the power requirement, the hull resistance of the boat can not be found using the conventional Froude's resistance formula, $R_f = f S V^n$ or others similar to it. In this work, a smaller boat with corresponding similarities and weight was towed to get R_f, which resulted in 976 N at 2 m/s.

Adding the earlier calculated 348.7 N, attributed to the foil's thrust and resistances, to the hull's 976 N resistance, resulted to 1325.7 N. An assumption was made that the foil operating at 50 rpm nearly approaches the 2 m/s velocity, which the resistance of the hull was taken. Then at this speed, F x V = 1325.7 x 2 = 2651.4 Watts. Assuming efficiency at 80%, the power needed was approximately 3314.25 Watts or 4.4 horsepower. Calculating the power requirement another way, the following description is made.

The hull resistance of the boat was the major component in matching the foil's

power requirement. For a flat bottom boat with parameters described in section 3.3.2, page 48, was comparable to the flat bottom utility boat in the range of 12-15 ft, which was recommended by the editors of the "Time Life Books" (1975) to take up a 5-15 bhp power outboard engine and this conformed to the industry standard. The length-width factor charts of both the American Boat and Yacht Council Safety Standard (1974) and the Boat Data Book (1978) published in England verified this estimated power requirement for small craft as shown in the charts of graph 3.1. Estimating the power requirement was to multiply the length of the boat and its transom width. The Americans used the English foot measure while the British used the SI unit in meter. The resulting product was represented in the horizontal scale of the left chart as 15.75 ft x 4.03 ft = 63.5 or 4.8 m x 1.23 m = 5.9 of the right chart and their corresponding brake horsepower was read from the vertical scale. Both indicated a little over 10 bhp for a flat bottom boat.

From the foregoing exercise, it was determined that a safe horsepower rating between 5 to 15 bhp of any engine was acceptable. The search for a gasoline engine in this power range was not difficult because there are many household and recreational appliances around that use similar engine to what was needed. The engine drive used in this project was a 12 rated horsepower, which was taken from a snow mobile vehicle. With this engine, the horsepower rating used in this project could easily absorb the calculated foil forces demonstrated above.

Graph 3. 1 Chart for estimating power requirement

3.2.2 CROSS SECTION OF NACA FOIL VS WHITE WHALE'S FIN

Comparing the NACA 0019 foil with the offsets of a white whale's profile Bose et al. (1990), the profile or cross section outline is shown below. Other offsets were considered like that of the NACA 0010 and NACA 0006 foils, both of which were used by Isshiki et al (1987) on his foil propelled craft. The contour of the NACA 0019 foil is a close likeness to that of the white whale fin. It was decided that this would be the adapted form for the prototype construction. An additional advantage in choosing this foil was the large leading edge of the form. It was expected that this would improve the performance of the oscillating foil by minimising leading edge separation and maximising the potential leading edge suction.

Sizing was next done to determine the final geometric shape of the actual foil for fabrication.
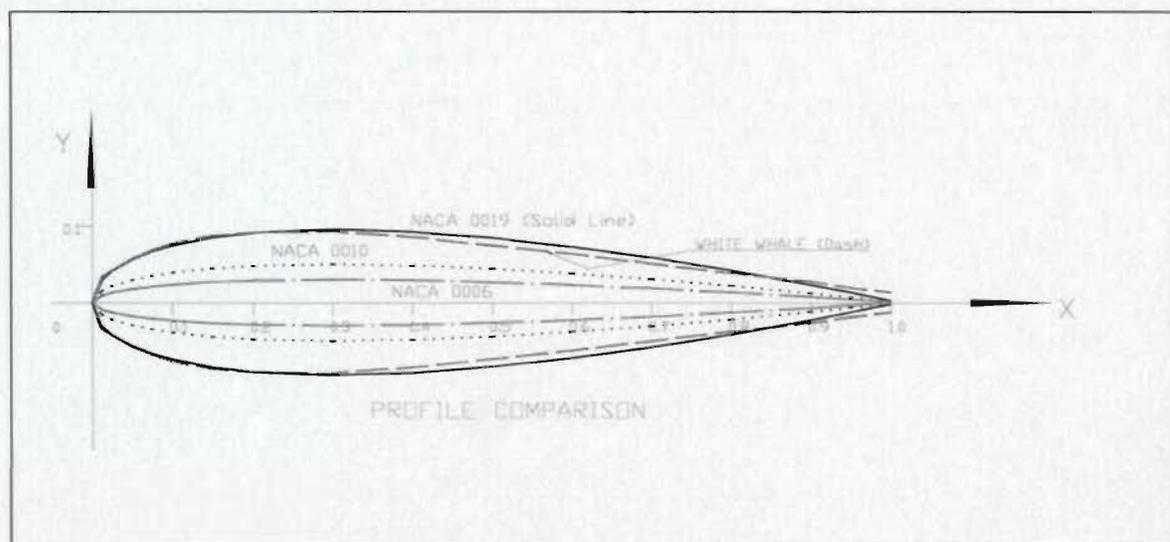
Figure 3. 3   Different profiles for consideration

3.2.3 THE FOIL PROPULSOR

On the 3m prototype boat built by the Tokyo Institute of Technology and Nihon University, the span of the foils experimented on were nearly as wide as the beam of the boat. Cuyper's (1984) riverboat or reduced draft vessels, used in the inland waters of Africa, had a similar width of foil or monopale. Yamaguchi (1992), suggested a width of 0.9 times the breadth of the vessel is a good guideline.

Since the intention of the foil design was to apply to a vessel of any 4-6m in length, the beam of this type of vessel was taken into consideration. It was thought that the width of the foil should be less than the size of their transom's width. The geometric sizes are as follows:

Span: Wing tip to wing tip: 0.81m

Chord (max): 0.254 m   Chord (min.): 0.63 m

Sweep back: 30°   Profile: NACA 0019

Aspect Ratio: 6.0   Area: 0.13 m^2

The sweep back angle and aspect ratio sizes are based on the fin whale's tail characteristics, Bose et al. (1990). The configured foil is shown below in figure 3.4.

The aluminum metal shown at the center in the figure was the foil support. It was a 50mm by 8mm Aluminum bar, which was carefully bent at the middle with little heat to avoid cracking. The end was then inserted with a small piece and welded in place. The dimension was sized to accommodate the foil and the front tip was rounded to avoid undue drag and to avoid flow disturbances around the leading edge shoulder of the foil.

GEOMETRY OF FOIL
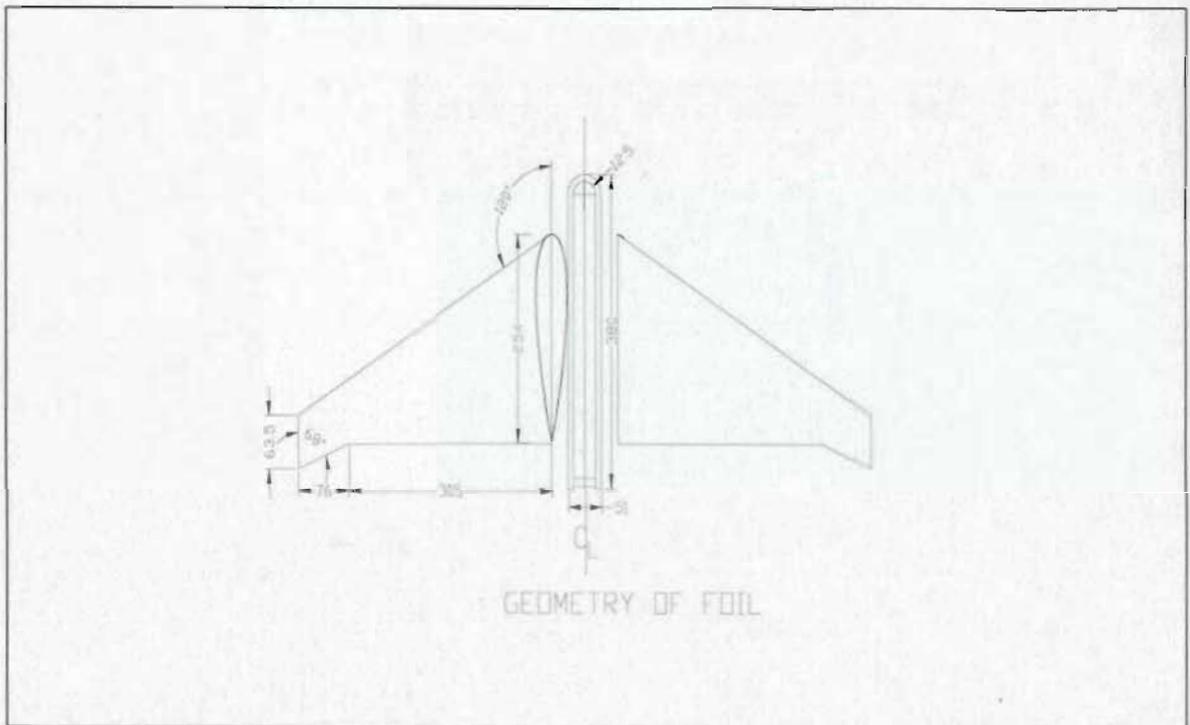
Figure 3. 4   Shape and size of foil

3.2.4 CONSTRUCTION OF THE FIN

The structure should be rigid enough yet not heavy so one person could easily handle it during construction, assembly, and testing. Also, low mass means low inertia which is a consideration for an oscillating body. The metals of choice were aluminum and light gauge steel. Thin aluminum flat bars easily warp and required a jig for manufacture. So it was decided to use gauge number #12 steel strips. Joining required the use of TIG (Tungsten Inert Gas) welding to avoid too much distortion. The foil shape of each station was made of steel and held in position by stringers. The skeletal form shown below was the pattern used for fabrication.
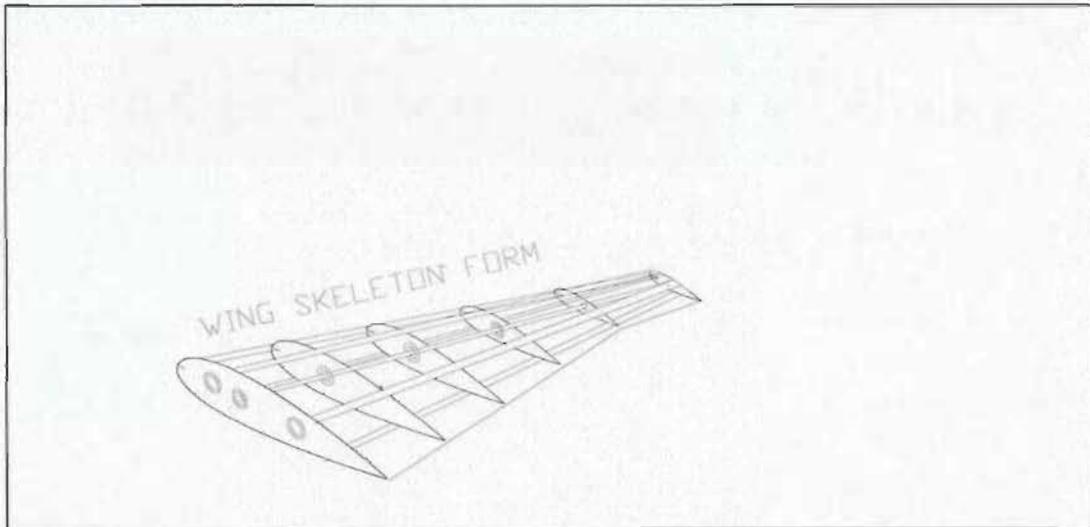
Figure 3. 5 Fin skeletal form

With the skeletal form ready, the spaces inside were stuffed with polyethylene foam, and then shaved to follow the contour of the surface. Automotive metal filler was applied on the exposed surface and immediately scraped to form the rough contour

required. Concave template profiles were applied at required specific stations to guide the sanding process. The form was dried for at least twenty-four hours to let the applied materials set. Sanding was again done to prepare for the fibreglass resin application. Fibreglass cloth was immediately pressed to the surface and scraped to let go any visible bubbles. Again, it was dried. Touched up areas were smoothed out and paint was applied. The wing foil was set aside for installation.

3.2.5   THE OSCILLATING RIG

The sliding mechanism and the attached foil comprised the propulsion sub-assembly. There were two designs. One was an electro-mechanical assembly and the other was an all-mechanical components assembly.

The first design was a complicated set-up. It was thought that the motion characteristics that this machine would exhibit parallel those of the lunate tail. As the foil moved upward, a pitch actuator adjusted the value of the pitch to its maximum as it reached the mid-point of its vertical travel. After it had passed this point, the pitch value was gradually decreased in such a way that it went from maximum to zero as it reached the maximum displacement.

During the downward movement, the pitch actuator repeated the same operation until it reached the starting position. The cycle was repeated and oscillation was varied depending on the speed setting of the engine.

The oscillating rig assembly was constructed according to the installation

33

assembly of figure 3.6. The components of the pitch mechanism were the connector pitch link bar of the foil, which was hinged at the other end to the sliding pad pitch actuator. This part had a horizontal hole where a pin was slid in to raise it up or down. In turn, its motion came from the sprocket wheel actuator that rotated on a linear chain track as the slider rig moved up or down. Limit switches were located so as to activate the DC motor, which rotated one revolution, for each stroke. When this happened, the pitch adjustment reversed in operation and the vertical motion was opposite from the first occurrence.
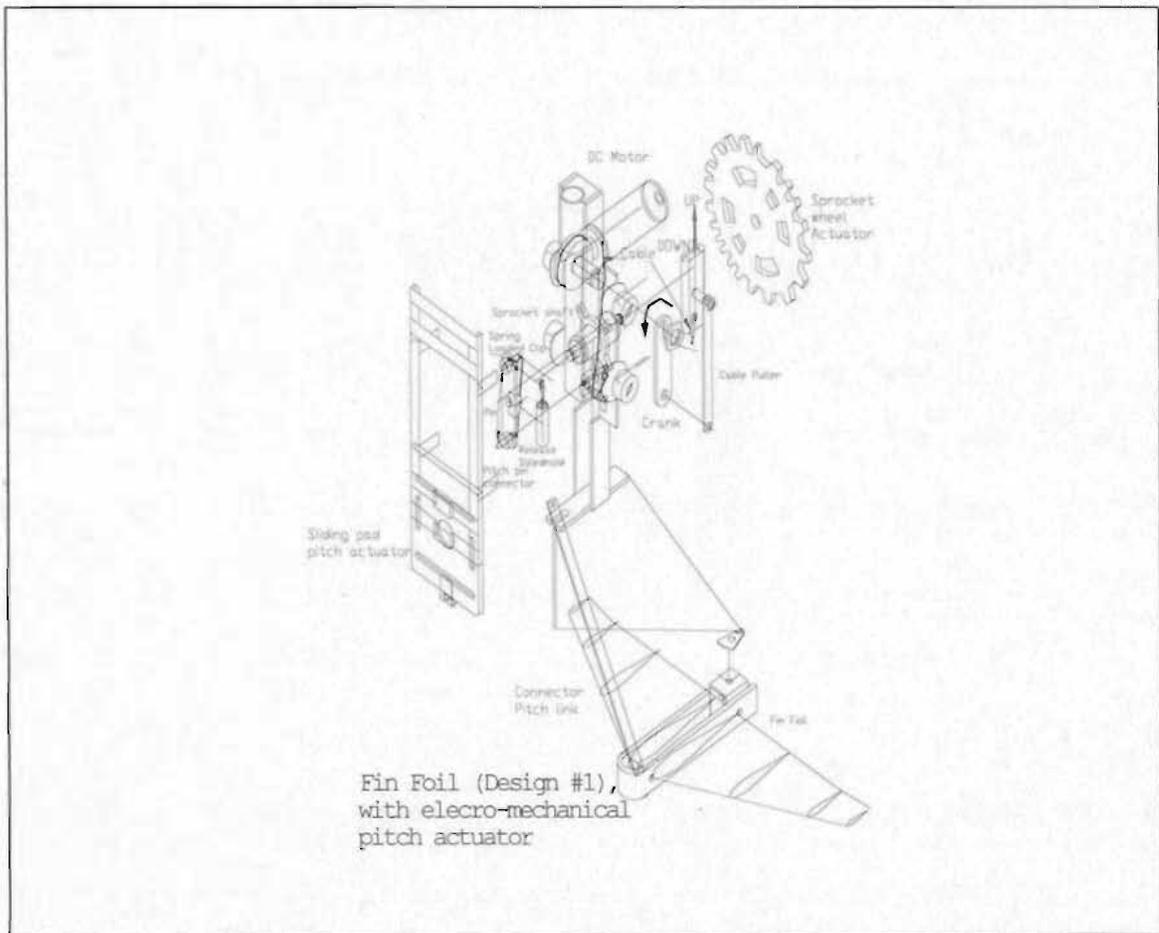
Figure 3. 6 Installation assembly of foil design #1 and slider sub-assembly

The rig assembly oscillated up and down guided by two vertical channels fixed at the transom frame. The oscillation was critical because the masses that were heaving up and down were not well distributed. What would be the operating frequency? From Cuyper's (1984) monopale's range of rpm (i.e. 62 rpm) and the Japanese 3m experimental boat, Isshiki et al. (1987), the foil's frequency ranged from 8 Hz and below. Actually, getting down to this range of oscillation frequency required gear or pulley reductions. Practically, with many small engines the starting idle speed range from 1800 to 2000 rpm. From our workshop experience, it was difficult to get to this range without incurring expensive reduction gears. Our first trial set up was shown below.
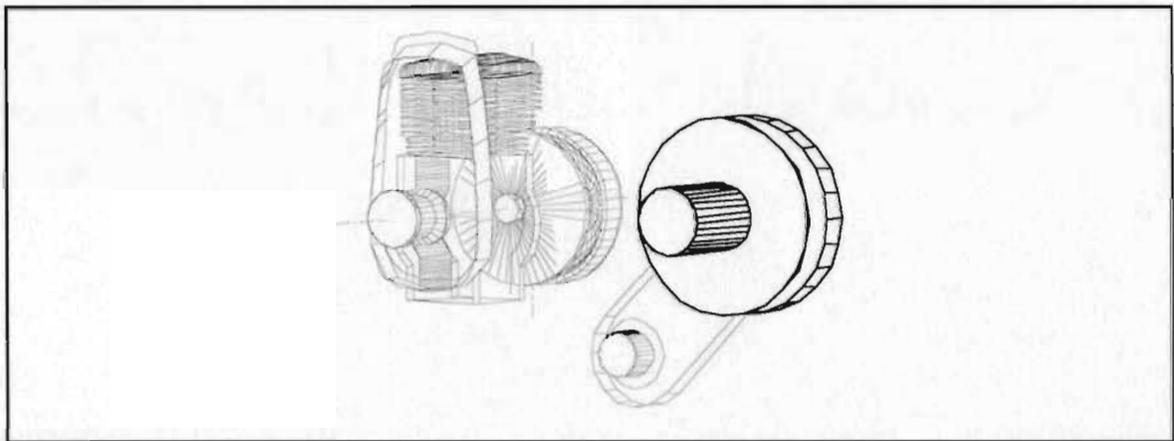
Figure 3. 7   Pulley arrangement drawing

The engine ran at 1800 idle rpm on a 38mm diameter shaft and this was transmitted to a 254mm pulley via a cogged V-belt. With the pulley shaft turning at 270 rpm and the 25 teeth sprocket gear at its opposite end, a chain transmitted this speed to a 10 teeth sprocket gear reducing the output rpm to 108. Knowing this, a reduction gear with a 0.25 ratio was required. A standard reduction gear was used. However, this still

gave 27 rpm at idle. Adjusting the engine output pulley to 32mm diameter shaft finally allowed an acceptable idle frequency of 0.4 Hz (22 rpm).

Maintaining a minimum amount of weight for the sliding assembly required an all aluminum structure. The reason was that this metal was less heavy than steel because its density was only 2.9 kg/cm^3 as compared to steel's 7.8 kg/cm^3. The joining process used was GMAW (Gas metal arc welding) as opposed to SMAW (Shielded metal arc welding) for steel. The sliding sub-assembly, the wing foil, the supporting vertical channels, and the seat for this channel sub-assembly comprised the modular, compact design of these sub-assemblies. Fitting them together took longer because clearances between parts had to be adjusted just right and its compact feature maintained. The following picture shows fin foil design #1 built inside the three sub-assemblies during the fit –up.
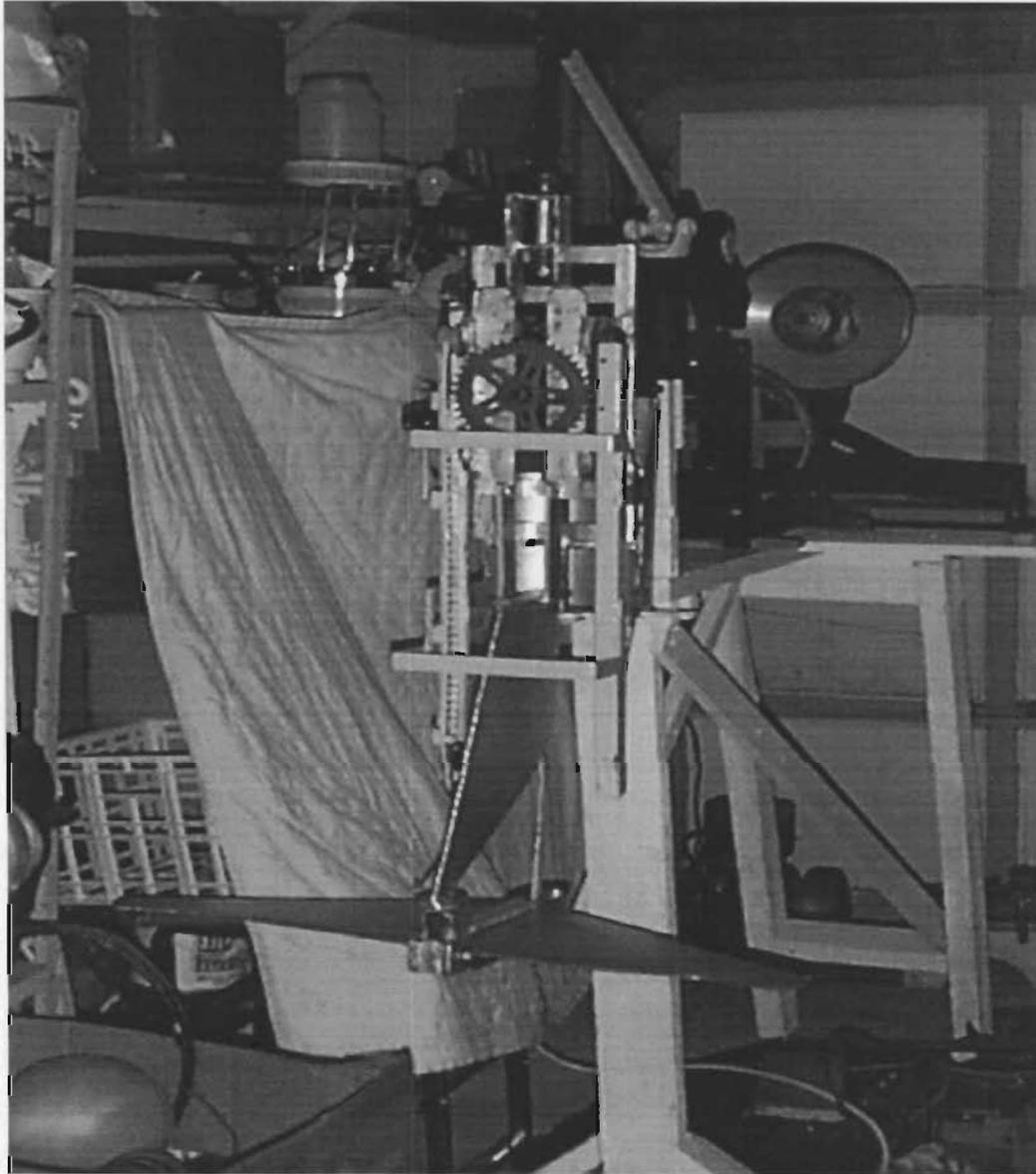
Figure 3. 8   Fitting installation of design foil #1 with respect to other assemblies

3.2.6 THE SINUSOIDAL MULTIPLIER (Lever arm)

The lever principle is used here. The lever is made of steel and sized to provide rigidity and strength. Figure 3.9 shows the basis for its construction.

A cross-formed ½"steel shaft with two steel ball bearings mounted on one shaft provided the lever steady support. This shaft was the pivot axis of the lever arm. The cross shaft was welded to the base of the lever for rigidity and strength. The long arm in the direction away from the boat will move to an arc, which gives the maximum heave of the foil. This arc could be adjusted by either moving the pivot forward or backward. However, this solution is not practical since the pivot body is clamped to the base of the seat. Another approach was to make several holes forward, which will provide some minor height adjustments. The pictorial drawing in figure 3.9 depicts its construction.

The opposite end was the shorter arm and was connected to the oscillator mechanism that provided a permanent height displacement. This height depended on the diameter of the rotating wheel of the oscillator mechanism. A connecting rod was pinned to the hinged part of the oscillator while the other end was connected to the shorter arm of the lever. An extra 16 pounds of padding was welded at the shorter end. This extra weight counter balanced the weight of the sliding mechanism and the foil so it provided a smoother start up because of the near balance of the oscillating masses. (See Appendix E, page 119, for beam size and material used.)

38
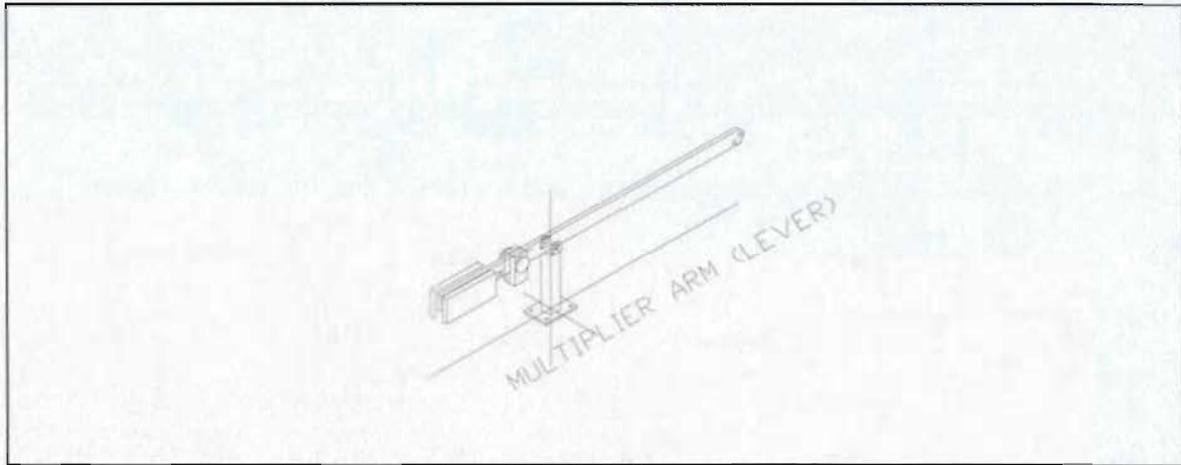
Figure 3. 9 Lever arm, heave multiplier

3.2.7 THE OSCILLATOR

The assembly comprised of a rotating wheel of a fixed diameter. Near the periphery of the rim was connected a small shaft closely coupled to a slider pad. This pad moved along a circular motion but translates this motion up and down as the pad slides in a channel that encloses it. In turn, the channel has vertical guides so its movement follows the up and down stroke. It was this output motion that supplied the sinusoidal motion of the foil assembly through the lever arm. Mid-point of this channel, a hinge- bracket was welded to provide the pivot point for the connecting rod that was attached to the shorter end of the lever arm. The hinge-bracket was visible on top of the slider pad as shown in the reducer-oscillator sub-assembly drawing in figure 3.10. (See Appendix E, page 121, for coupling and key sizes.)
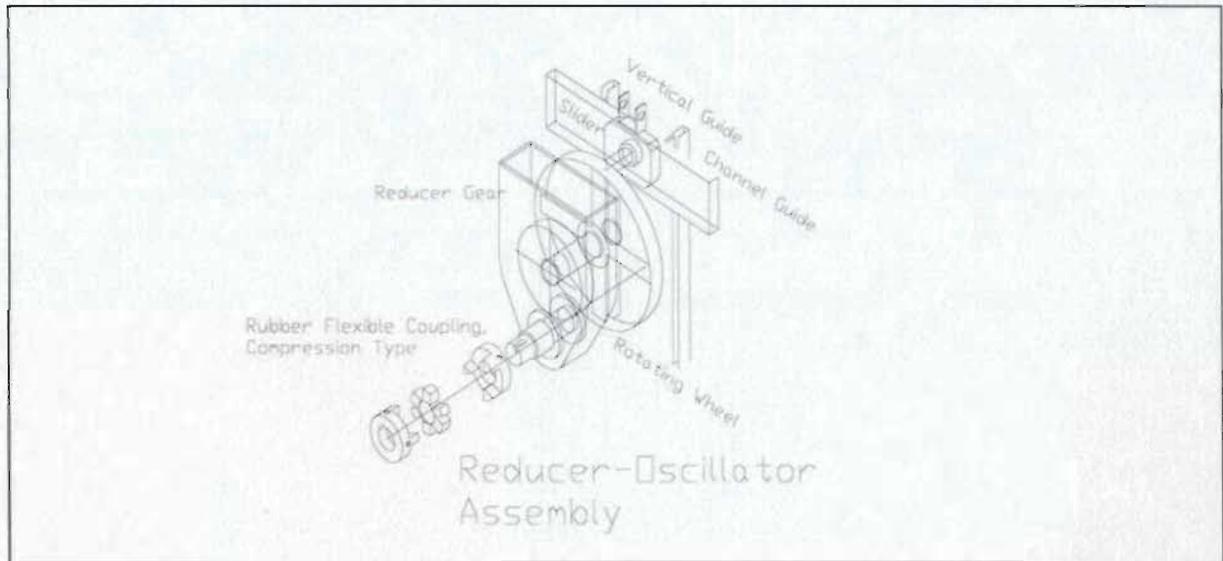
Figure 3. 10   Installation assembly of coupling, reducer gear, and oscillator mechanism

3.2.8   THE POWER TAKE-OFF

As seen from figure 3.11, the engine and its sheave and gear parts comprised the power take off sub-assembly with its short shaft protruding. This and the reducer-oscillator shaft were mated via a rubber flexible, steel coupling. This was used because it allowed angular and linear misalignments of the shafts for assembly. The clearances were checked to manufacturer specifications. The assemblies were then constructed together with their respective mounting seats and supports adjusted accordingly. The power take-off sub-assembly and the gear reducer-oscillator sub-assembly were installed in close quarters as shown in figure 3.12. (See Appendix E, page 121, for power- take off shaft size and material).

40
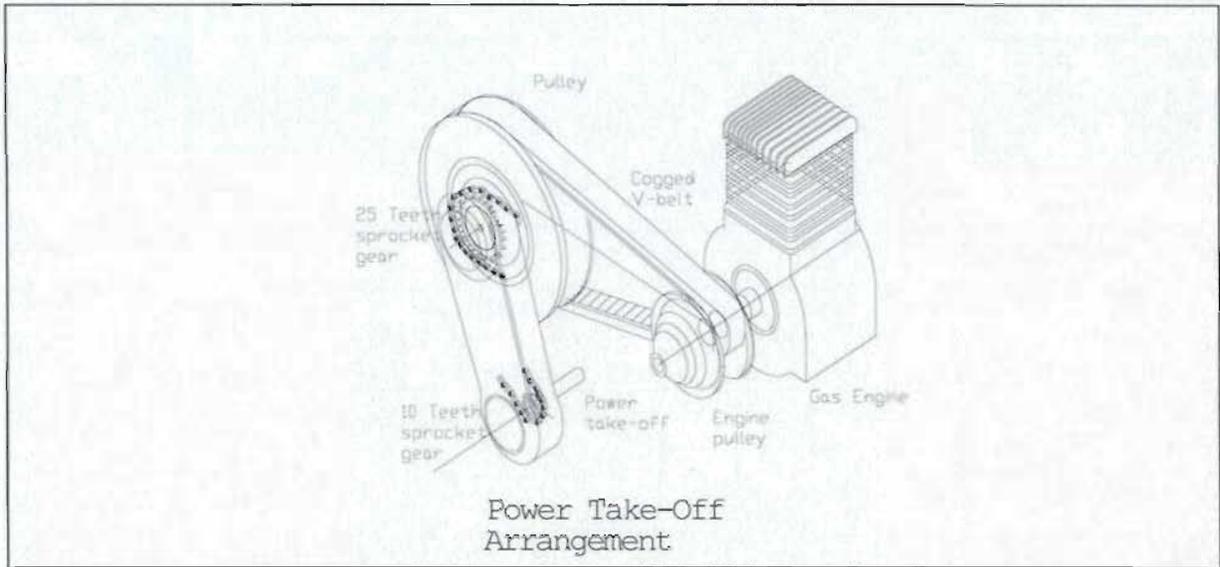
Figure 3. 11   Installation assembly for pulley and sprocket gears
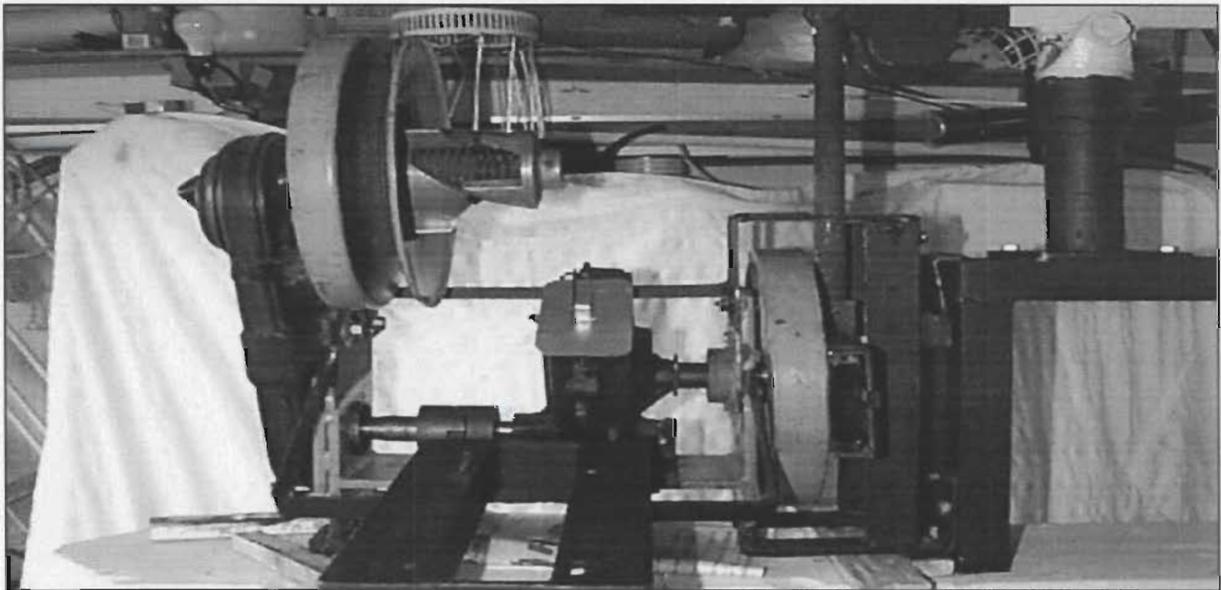
Figure 3. 12   Actual assembly for reducer-oscillator gear and mounting brackets and seat

41

3.3   THE INSTALLATION AND ASSEMBLY (DRY RUN)

The other components such as the seat for the lever arm, the suspended seat

support for the slider sub-assembly channels, and the slider sub-assembly guide were

constructed to support the moving assemblies mentioned earlier. Included in the

construction were the connecting rods, pins, and spring dampers. They are shown in the

figure 3.13 to describe their relationship with the other assemblies. (Bigger drawings are

attached in the appendix)
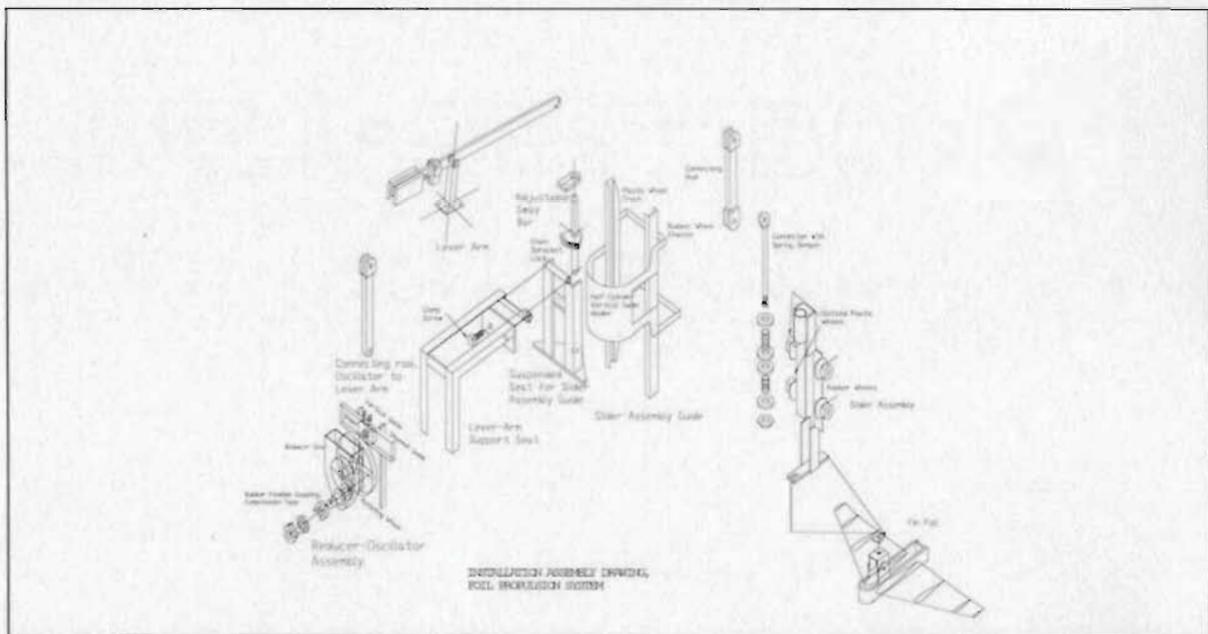
**Figure 3. 13   Installation assembly for the various sub-assemblies of the propulsion
system**

A jig platform was built in an enclosed garage to test the sub-assemblies of the

mechanism. This elevated structure took up the various components and placed these in

their respective places. Without the engine, the whole assembly was checked for motion displacements and the integrity of the functional components. A template was made for the seating arrangement after a satisfactory assembly was carried out.
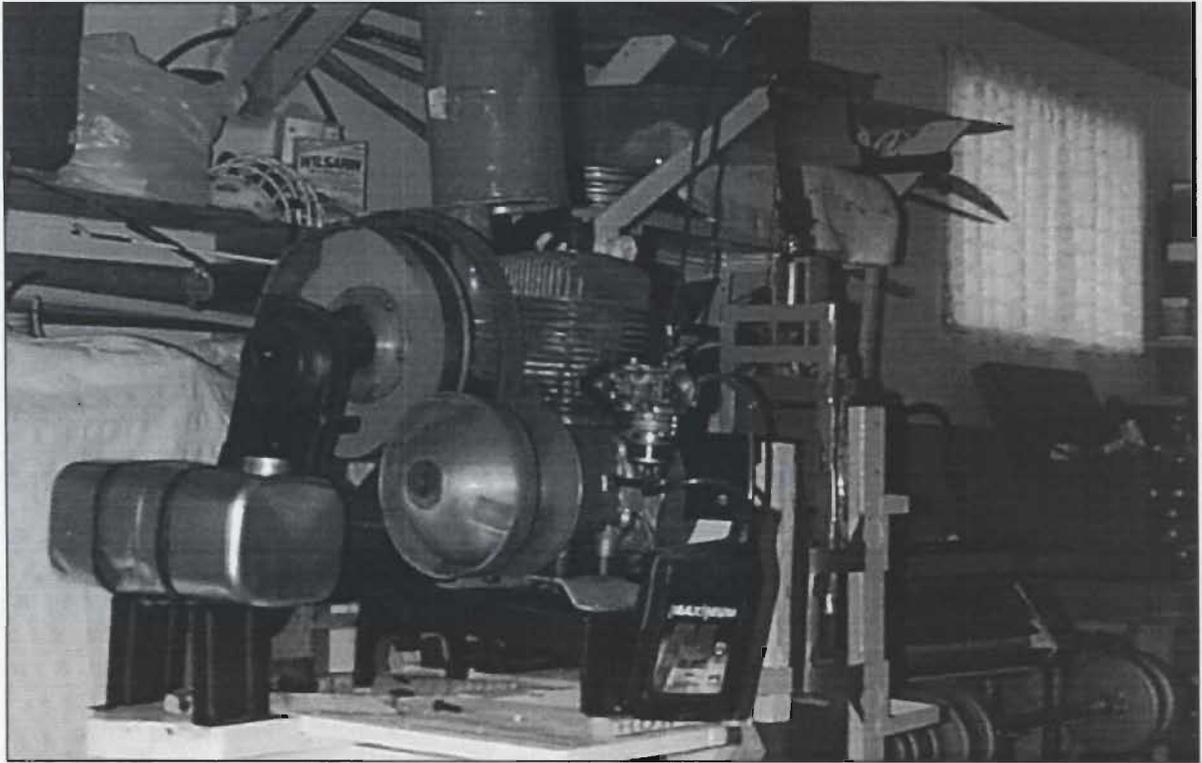
Figure 3. 14   Fitting -up of the various assemblies in their respective places

As could be seen from figure 3.14 and 3.15, maintaining a close assembly was necessary to simulate the small space where its actual installation took place. The boat's interior was then reinforced to take up the mounting beds to insure a good set-up. While in the garage, different assemblies were fitted together. These fittings were made to work according to the motion applied. Some of these pictures are shown in the following figures.
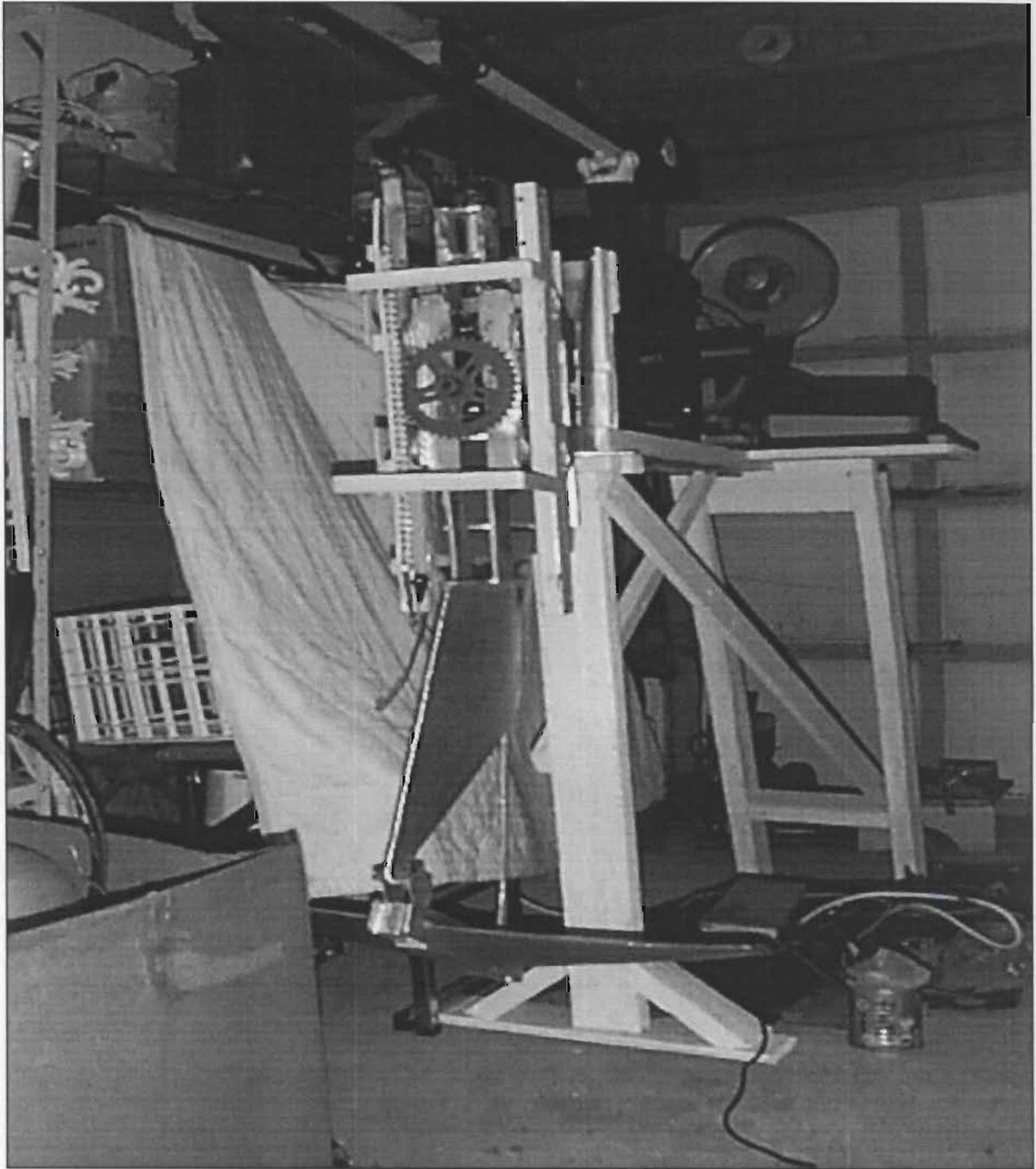
Figure 3. 15   Design foil #1 during fit-up

In this assembly, the foil design #1 mechanism was fitted together with the slider

and guide sub-assemblies connected to the lever arm's eyebolt.
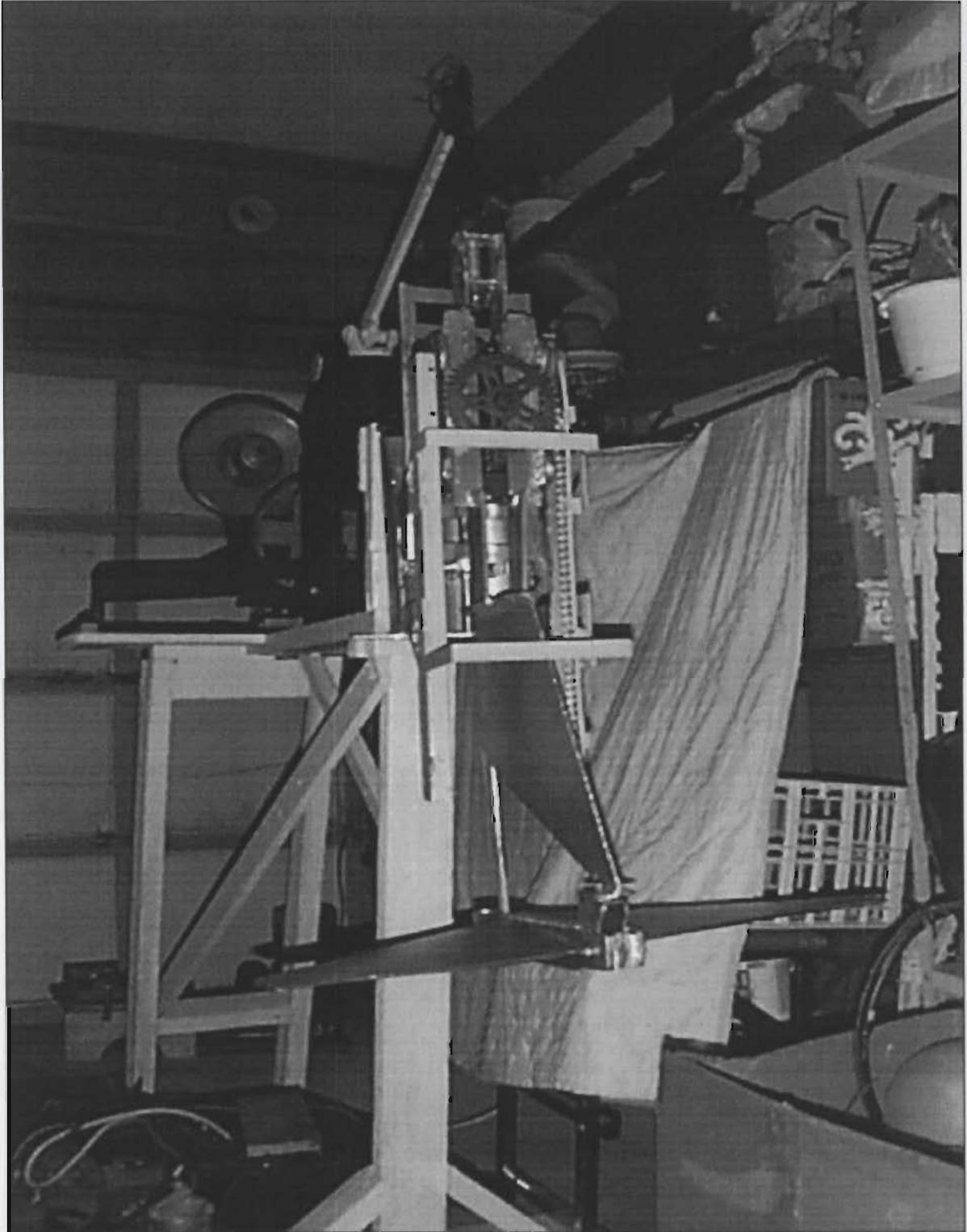
Figure 3. 16   Another scene while design foil #1 was fitted -up in place
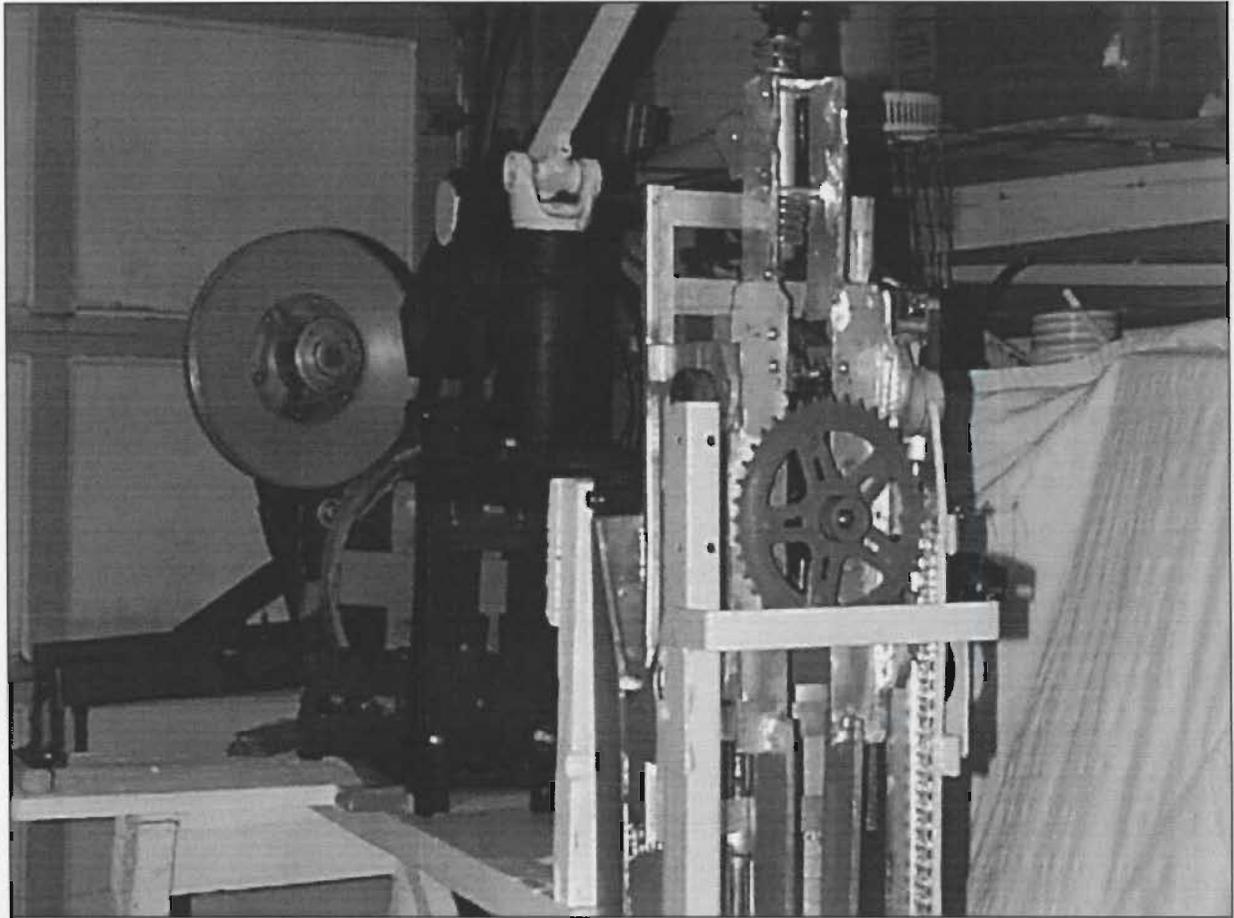
Figure 3. 17   A close up view of the various assemblies in place

In this view, the sprocket gear was engaged with the linear chain track to control the pitch adjustment. The rollers on top the tracks are shown enclosed at the left and slotted at the right. The design prevents sway of the slider sub-assembly because of the clearance between the roller and its track enclosure when moving up and down.

3.3.1 THE LOAD CELL

The linkage between the oscillator assembly and the lever arm multiplier was identified as the component that took up two strain gauges. These strain gauges were located near the end of the bolthole connected to the shorter end of the lever arm. These gauges would measure the input force generated by the oscillator assembly. Accordingly, these gauges were attached to the smallest cross section of the connecting rod. A spreadsheet was made to ascertain that the gauges would be able to measure the forces that are loaded in this linkage. Only tensile and compressive forces would be registered since the oscillation was up and down motion. The linkage (connecting rod) was drawn showing the strain gauge rosettes attached.
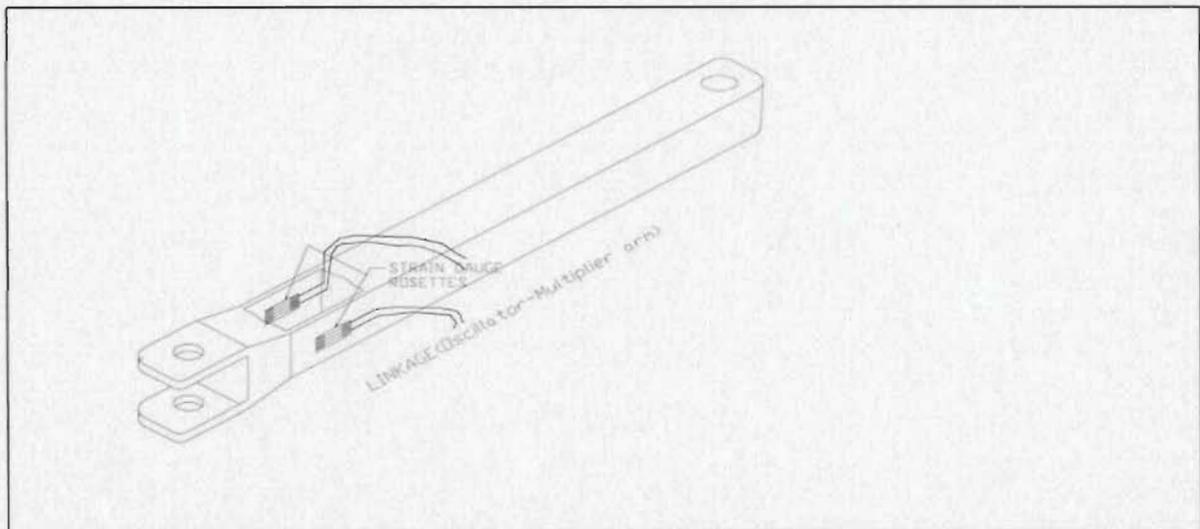
Figure 3. 18   Strain gauges shown attached to the connecting rod

The other transducer set-up was positioned at the lower frame of the transom. The arrangement consisted of two-cantilever beams with the gauges mounted at the fixed end.

47

These were positioned under the suspended seat of the slider guide assembly. Since this assembly was lightly leaning outward by a few degrees, there was no load or force affecting the load cell when the foil was not running. These load-cells measured the thrust force when the foil was operating.

These gauges operated below waterline and were water proofed by rubber and plastic wrappings. Since these were fully submerged, temperature changes had to be taken into consideration. The water temperature and the load cells must be the same before any reading had to take place. Its location was approximated as shown in the drawing below.
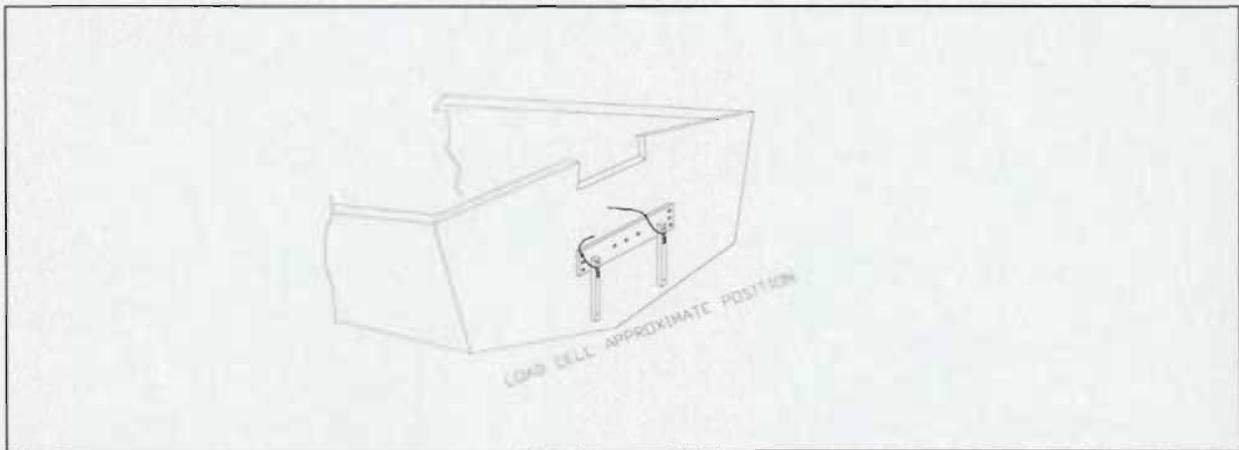
Figure 3. 19   Approximate location of thrust cell

3.3.2   OPEN BOAT

This was an economical, dinghy like, flat bottom boat of a design similar to the Newfoundland dory. The length from stem to its transom measured 4.8 m (15ft-9in).

48

Empty, it weighed about 400lb (182 kg). Maximum breadth was 1.52 m and the upper

transom beam was 1.23 m while the bottom part was 0.95 m. Draught when empty was

approximately 150 mm (level or trim). The flat bottom area was approximately 3.62 m².

3.3.3   DATA ACQUISITION SYSTEM SCHEMATIC
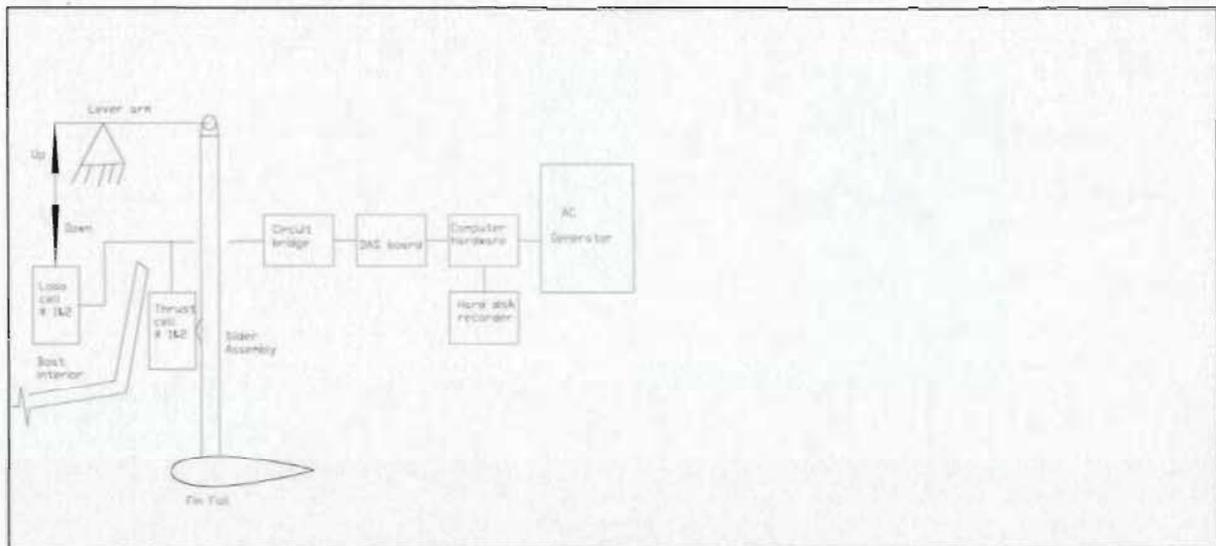
Figure 3. 20 Instrumentation schematic

Altogether, there were eight electrical leads; two from each strain gauge and these

wires were connected to each bridge circuit shown in figure 3.20 a. Each circuit had three

resistors connected to one channel of the bridge circuit box. In turn MUN Materials and

Applied Science Laboratory connected this box to an internal Data Acquisition Board

(DAS) of the PC computer package that was loaned. This equipment would only be

installed during the testing period.
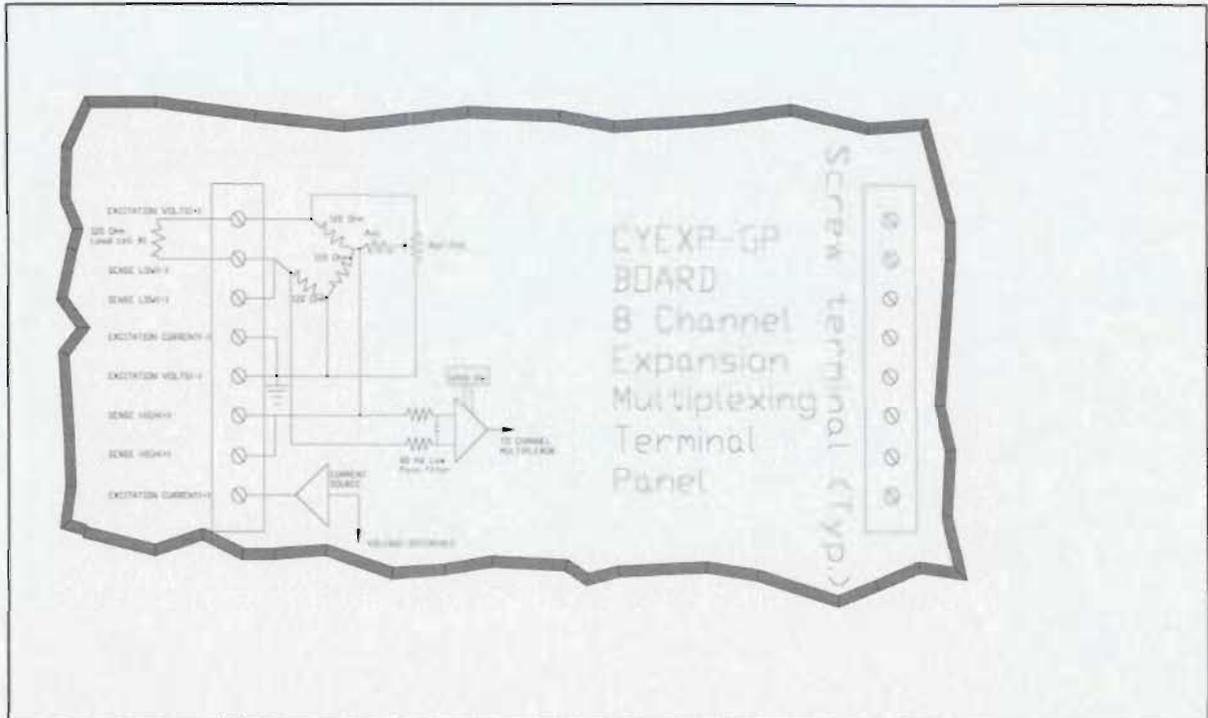
Figure 3.20 a   Load and thrust cells partial schematic

3.3.4   ON BOARD INSTALLATION

After the mounting bed was installed in the boat, the assemblies followed. The first assembly that was installed was the lever arm support seat. Its clamping end was fastened to the middle of the transom frame and its leg rested on the mounting bed. Next were the reducer-oscillator assembly and the power take-off assembly, which were pre-assembled to their supporting seat and brackets. These were bolted to the legs of the lever arm support seat and the mounting bed. Wooden chocks were installed to get them properly levelled. The lever arm was next seated and centred. This too was bolted down firmly to its seat. Figure 3.21 shows a close up view of the supporting brackets of the power take-off, reducer, and oscillator sub-assemblies.
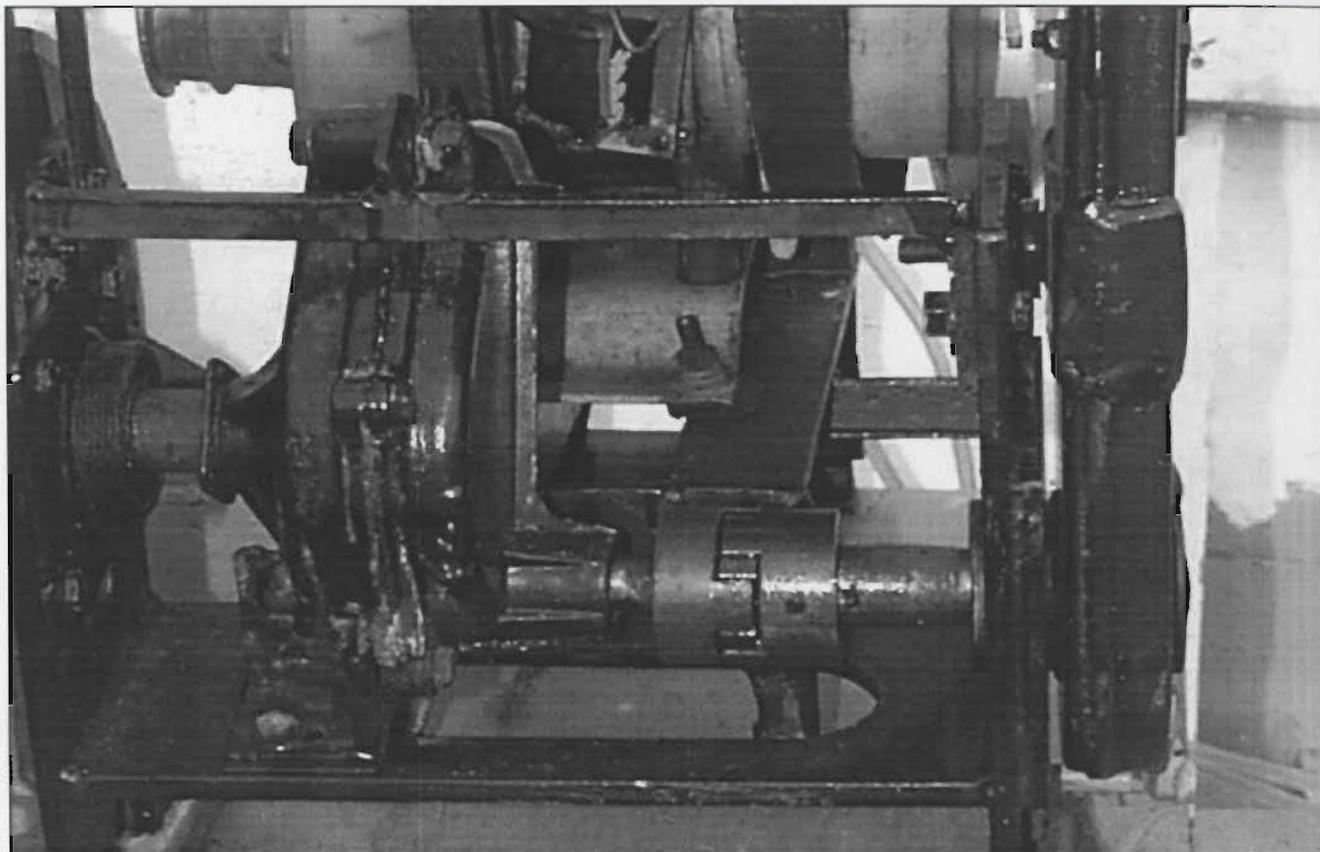
Figure 3. 21   Actual installation of the power take-off gears, reducer-oscillator assemblies

The power take-off and reducer-oscillator sub-assemblies were installed in place. It did not take much space as these assemblies were put together compactly. Holding down bolts were placed at both ends of the assembly seat, which were padded by wooden chocks for levelling.
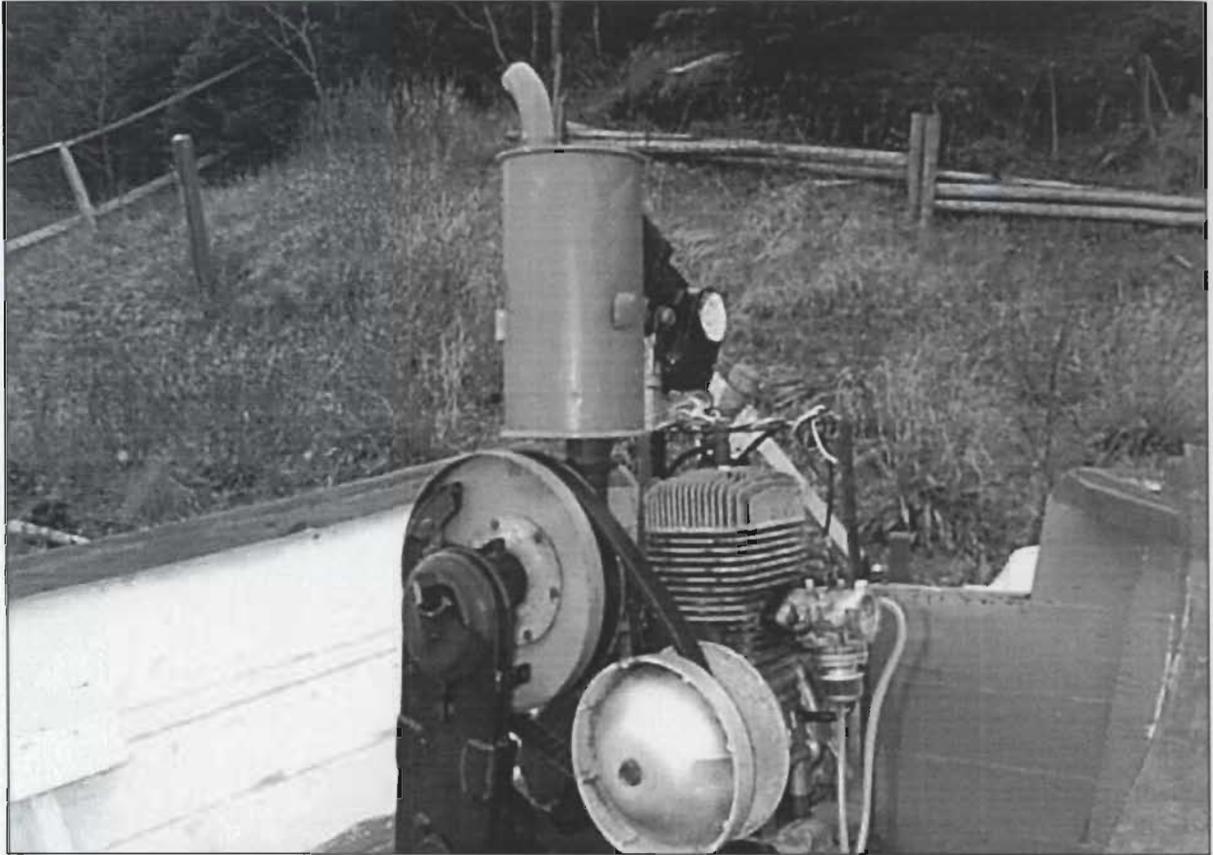
Figure 3. 22 Drive assembly in place with fitted muffler

As the drive mechanism was installed, the exhaust muffler was connected and adjusted to clear all moving parts. As well, the electrical leads from the gas engines were secured to a mounted steel frame together with the throttle lever. Fuel lines were clamped secured and out of the harm's way.

The next figure, shows the installed pre-assembled group of the suspended seat, slider guide and slider sub-assemblies. The fit-up was made for positioning and location of the thrust load cells determined to evaluate the inter-action of parts between each other.
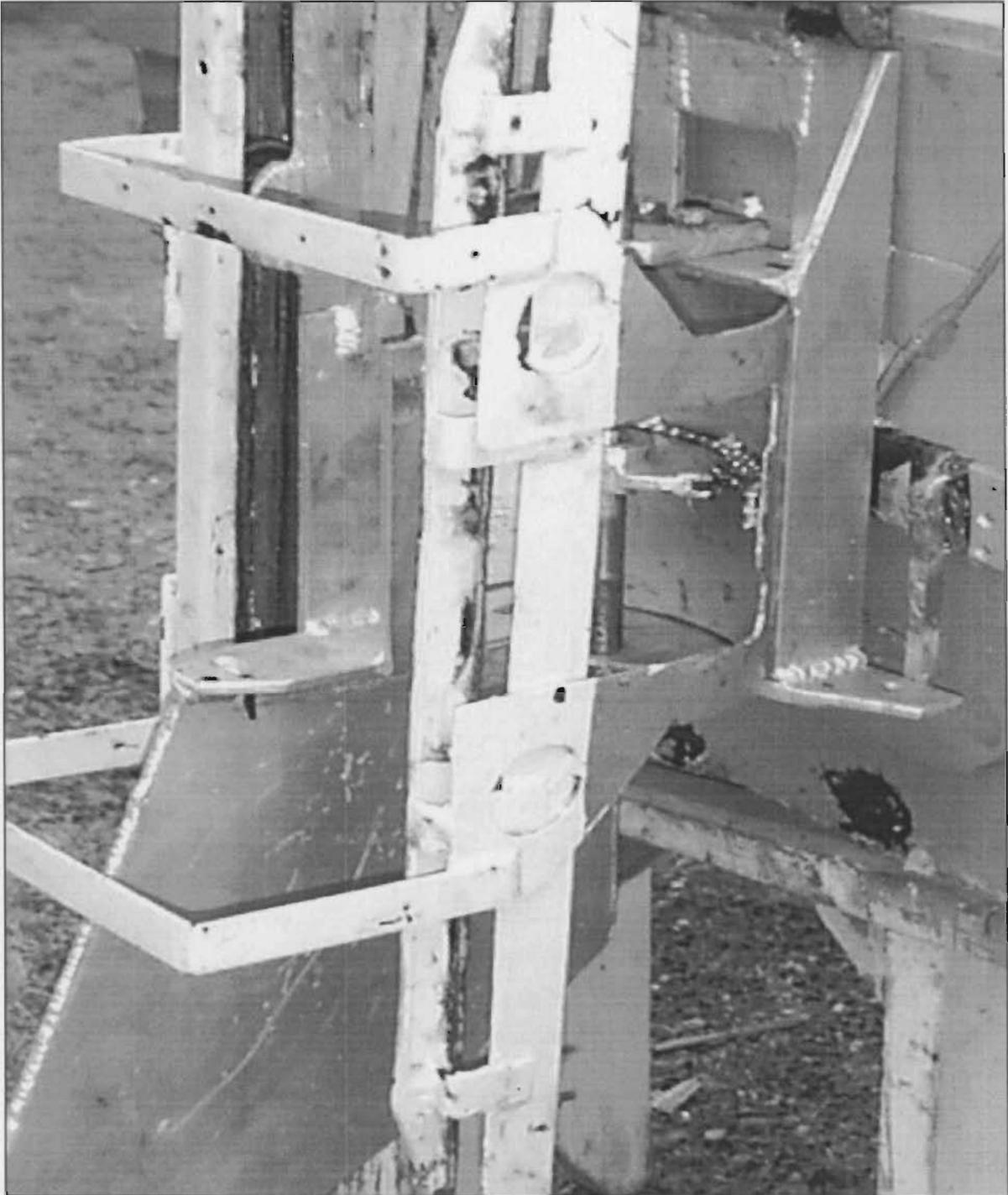
Figure 3. 23   **Slider assembly with rudder like enclosure for the linkage rod**

pitch-actuator

Figure 3. 24   Lever arm fully extended and connected to the eyebolt of the slider assembly

The lever arm was connected to the slider's eyebolt. Maximum heave of the slider was reached as the guide roller reached its maximum run.
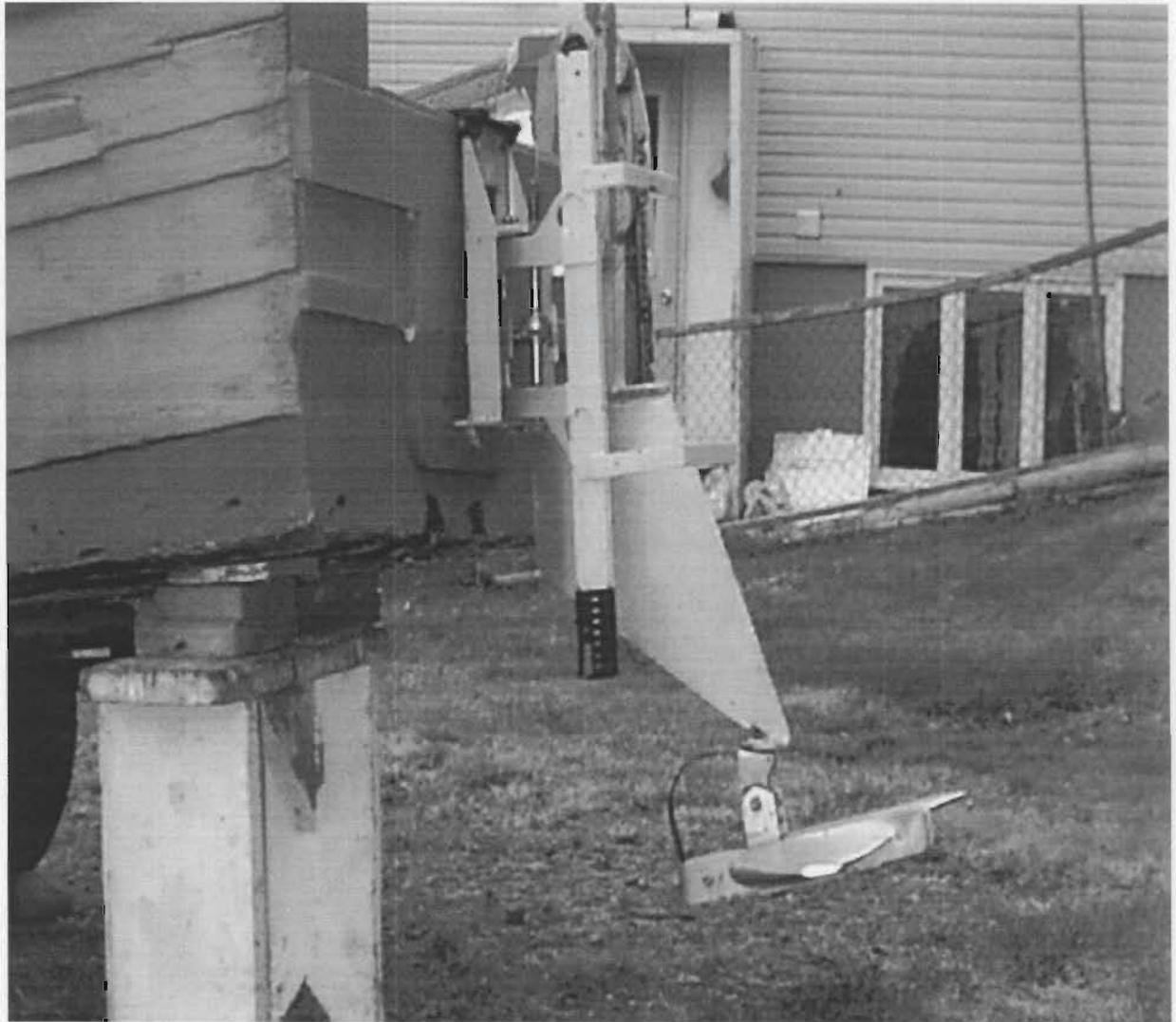
Figure 3. 25   The position of the fin foil at maximum heave
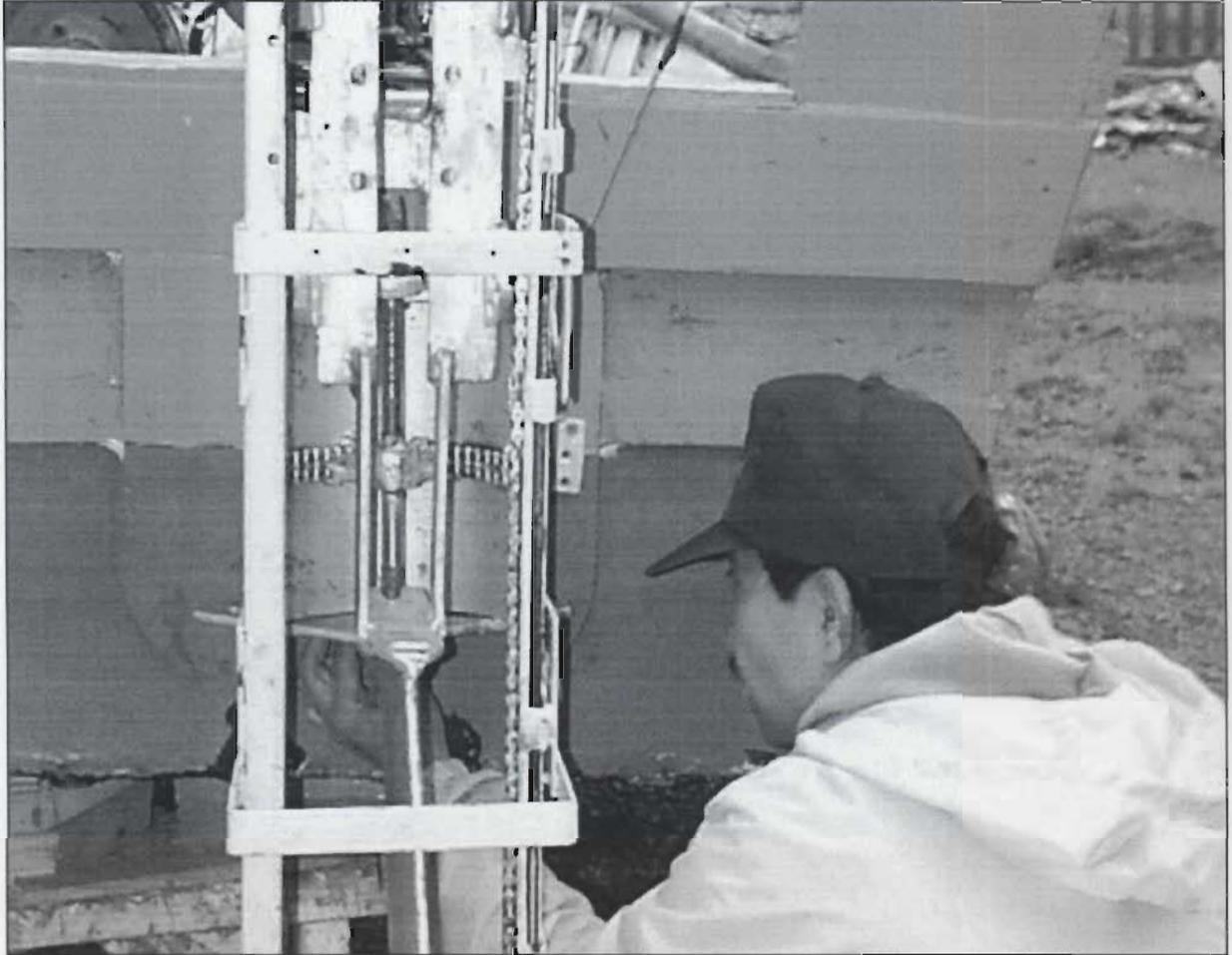
Figure 3. 26   Inspecting the internal part of the slider guide assembly

CHAPTER 4

THE EXPERIMENT

4.1 PREPARATION FOR TESTING

The dry run adjustments and installation of all components on board are depicted in the pictures shown earlier. At this point, the data acquisition system was not yet installed. The DAS system was borrowed for a short time period from the Materials and Applied Science Laboratory at MUN. This comprised a monitor, CPU package, bridge and rectifier box, and small peripherals required for its operation. The Notebook Pro software is an enhanced software package for data acquisition, process control, monitoring, and many more features. Its DAS multifunction, high-speed A/D (analogue/digital) I/O expansion board was internally slotted to the common PC using its DMA (direct multi access) capability for data and signal analysis. This board was connected directly to the bridge circuit box via cable and terminal interface. One disadvantage however, was the need for an AC power source, which necessitated the inclusion of a generator.
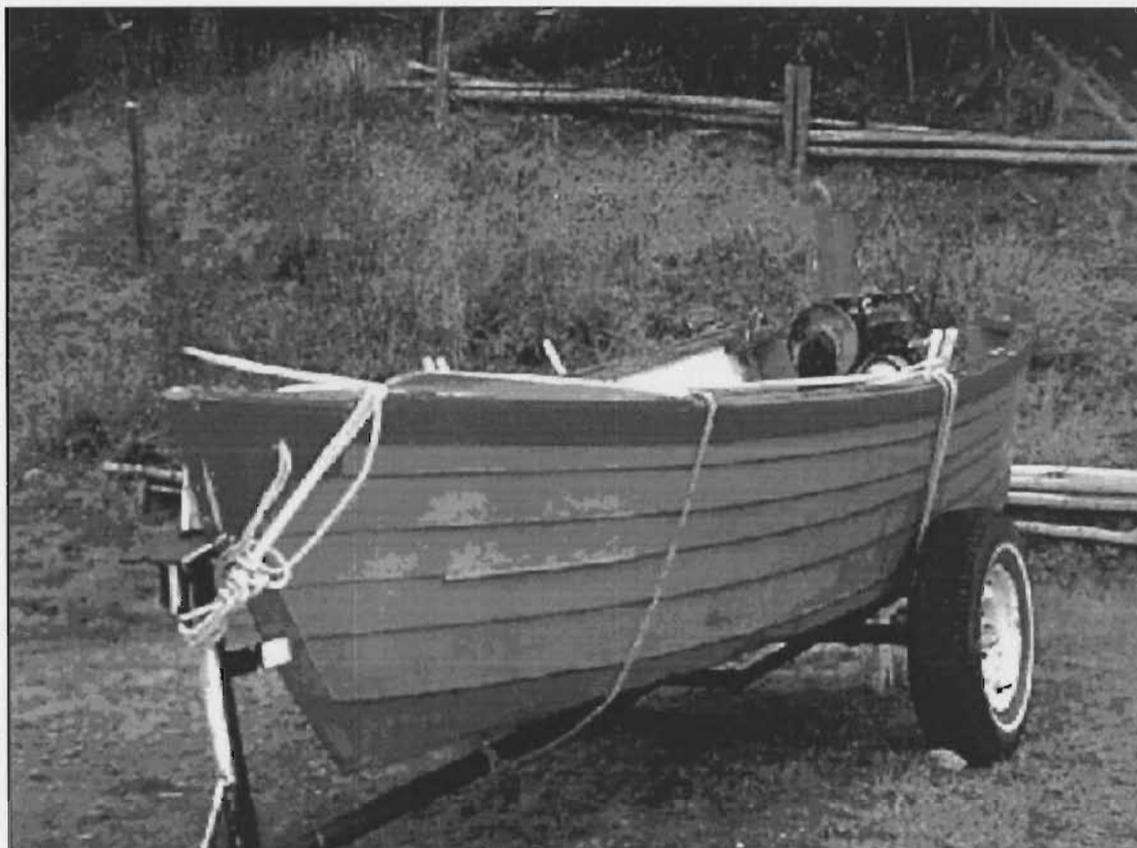
Figure 4. 1   Preparing the launch

On the early morning of August 5, 1999, at a sandbar located in Creston North of Marystown, this boat was launched, moored and was prepared for its first sea trial. The water depth near the sandbar was shallow. However, it gets deeper farther away from the shoreline.

4.2 MAIN OBJECTIVE OF THE EXPERIMENT

This was a two-purpose experiment. The first was to determine whether **foil design #1** would be viable during this time of the experiment. As mentioned earlier, this was an electro-mechanical pitch controlled device and its pitching axis pivots at its trailing edge. Figure 3.6 depicts the version of the design. Since most of the construction works were geared in completing this design, hopes were high during the launch.

The other was to firmly test **design foil #2** that was a simpler version of design #1. This version was the back-up plan in case the first one did not operate as per expectation. The picture in figure 4.2 below shows the fitted version of design #2
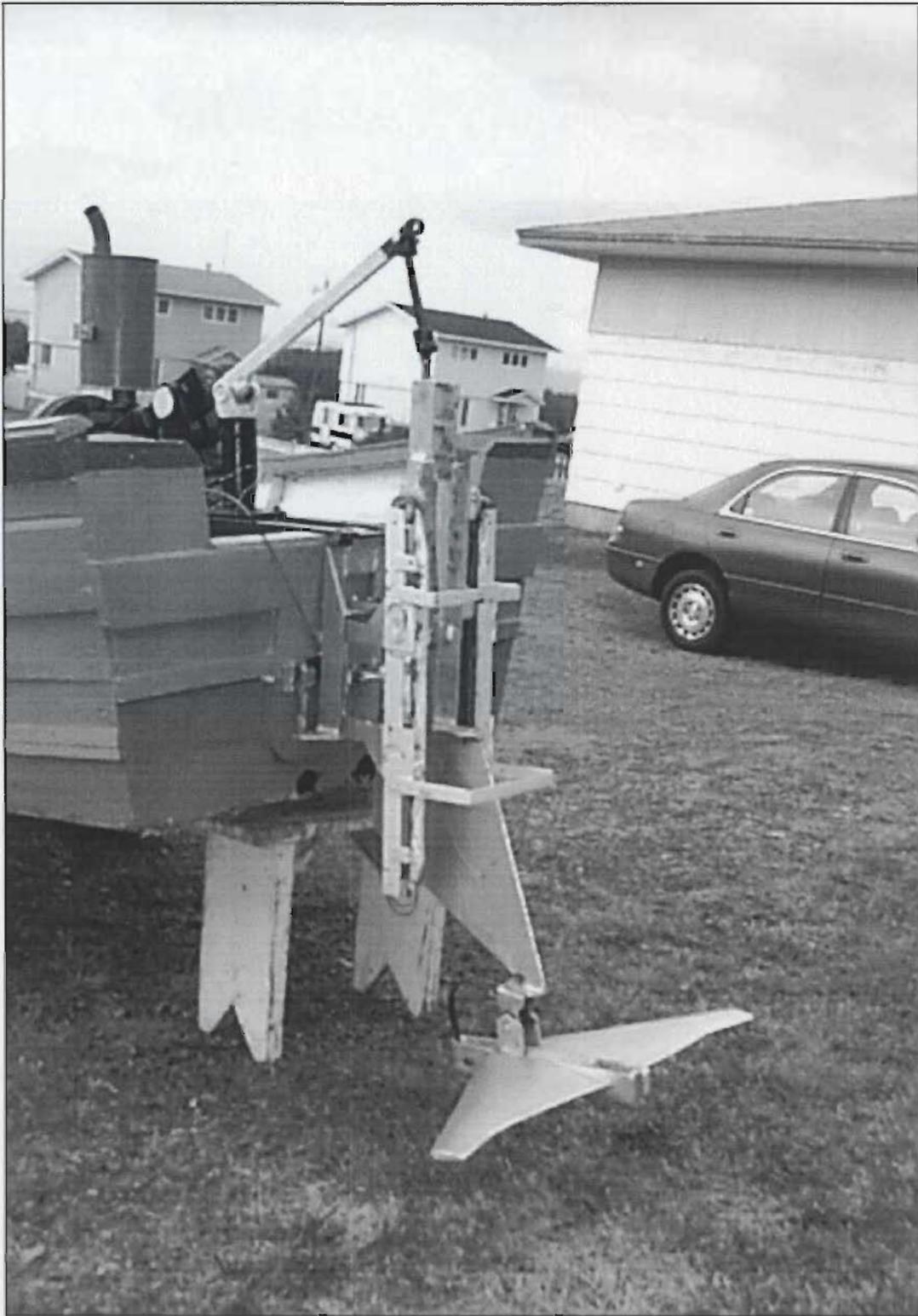
Figure 4. 2 Design foil #2 in pre-test position

To compare both designs, the schematic was drawn to see the difference when both foils are moving upward.
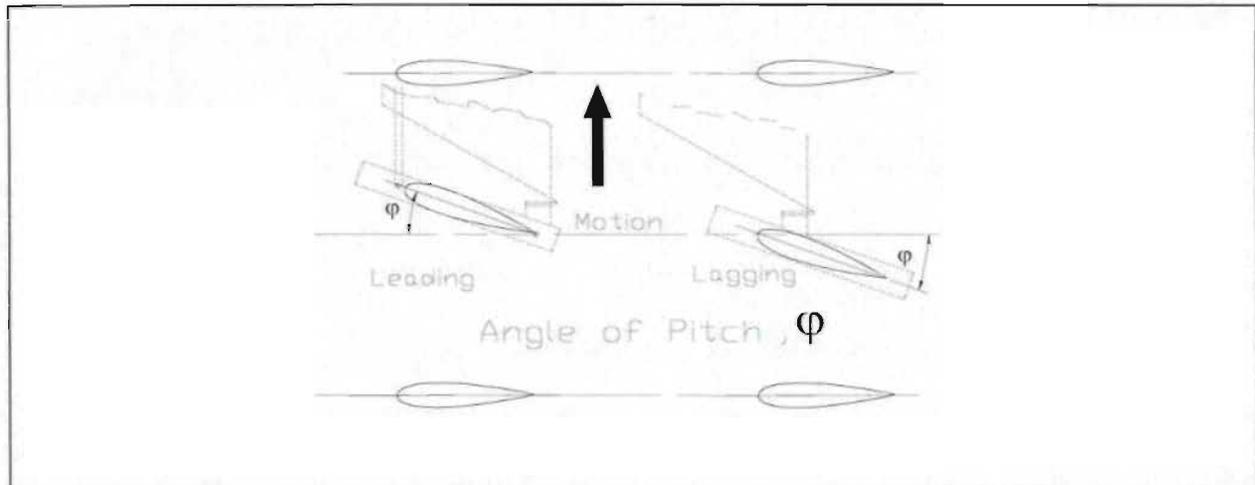
Figure 4. 3   Schematic representation of heave motion of the two foils

The first design was an electro-mechanical contraption at the left. It was quite complicated because it needed a timing mechanism. This mechanism controlled the movement of the linkage rod in front of the leading edge. It was completed first and it worked during the dry run. However, it made the sliding mechanism heavier due to the various mechanical and electrical parts that moved along the sliding assembly. During the initial test, the oscillating frequency of 0.4 Hz seemed fast and the sliding pad pitch actuator guide had a welding joint defect and its clearance with the slider assembly guide widened and the whole slider assembly seized. The engine was immediately stopped. The data acquisition system made some readings but not enough time was recorded. As a result of this test, observation showed the rig demonstrated a desirable characteristic motion. With some modifications and careful assembly this design could operate

61

functionally.

The other was purely a mechanical design as shown in figure 4.2. A torsion spring was installed in the hinge connector between the foil and the holder of the slider mechanism. The foil changed its pitch due to the moment forces acting on it when moving vertically. The angle of pitch opening was limited with a built in stopper.

4.3   THE 1st SEA TRIAL

As indicated earlier, the preliminary sea trial took place on the early morning of August 5, 1999. The preparation took place on the sand bar and the tide was favourable that morning. A snap shot of our preparation shows the extent of our work before the sea trial.

Figure 4. 4   A scene early in the morning prior to testing

Figure 4. 5   Preparing the boat for first day of testing

A close up view of the laden boat revealed the extent of work required before testing. The next two pictures showed the cluttered gears and safety devices on board the boat prior to setting out to the testing area.

Figure 4. 6   A mechanic on standby prior to testing

Figure 4. 7   The prepared boat ready to go out to the testing area

At the site, at a depth measured by the full length of our paddle, we installed the slider assembly with the foil design # 1 attached. The AC generator was started first so the DAS was up and running. Then, the drive engine was started. The foil moved up and down for about a few seconds but there was a malfunction in the mechanism and tests had to be aborted for the day.
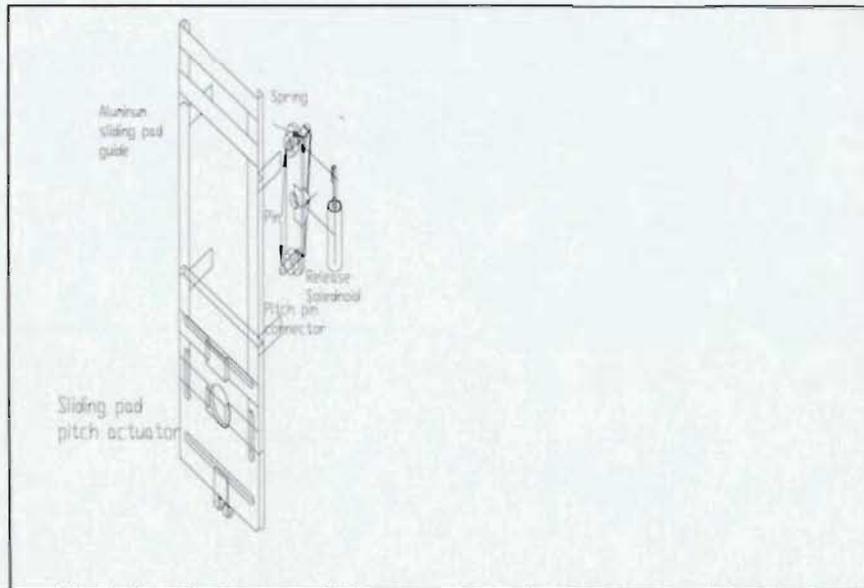
Figure 4. 8   The bracket for the Aluminum slider pad guide broke during the first test

When two of the horizontal brackets of the aluminum slider pad guide broke, its

clearance from the stationary slider assembly guide decreased, damaging other parts.

After evaluating what happened, all of the slider electro mechanical parts were taken off.

With minor modification, design version #2 is shown in figure 4.9.
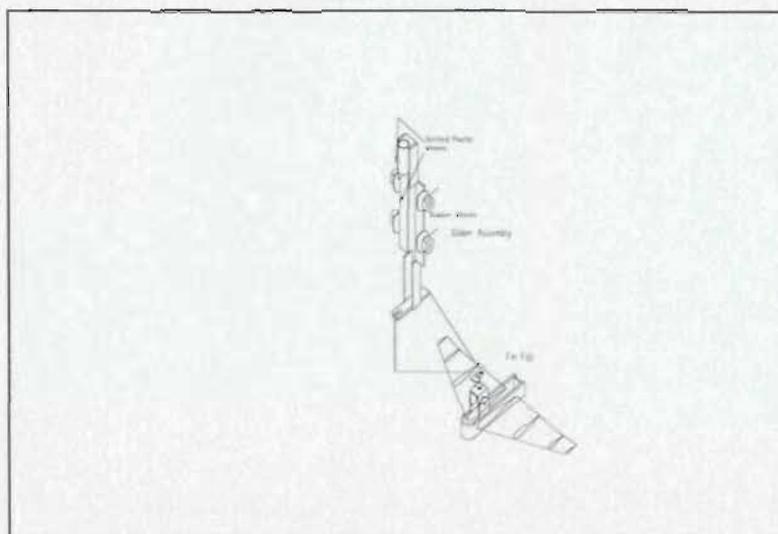
Figure 4. 9   Schematic drawing of design foil #2

4.4   THE 2nd SEA TRIAL

Tests were re-started again on the morning of August 10, 1999. This time, our slider assembly and foil design #2 were all inspected closely. The torsion spring was installed at about a third of the maximum root chord from the leading edge shoulder and at a height of 70 mm from the surface of the highest surface of the foil. The angle of pitch opening, φ, was set at about 30°. The setting refers to the symbol as used in figure 4.3.

A limited success was experienced that morning. The DAS equipment functioned well and recorded about a minute of the foil in operation. The test was halted, however, when the roller of the slider sub-assembly overshot the guide track and the rubber roller got caught at the corner end of its track. This happened a few times which indicated that some adjustments were required.

Figure 4. 10   Preparing the boat for another test

Figure 4. 11   Positioning the thrust cell in place
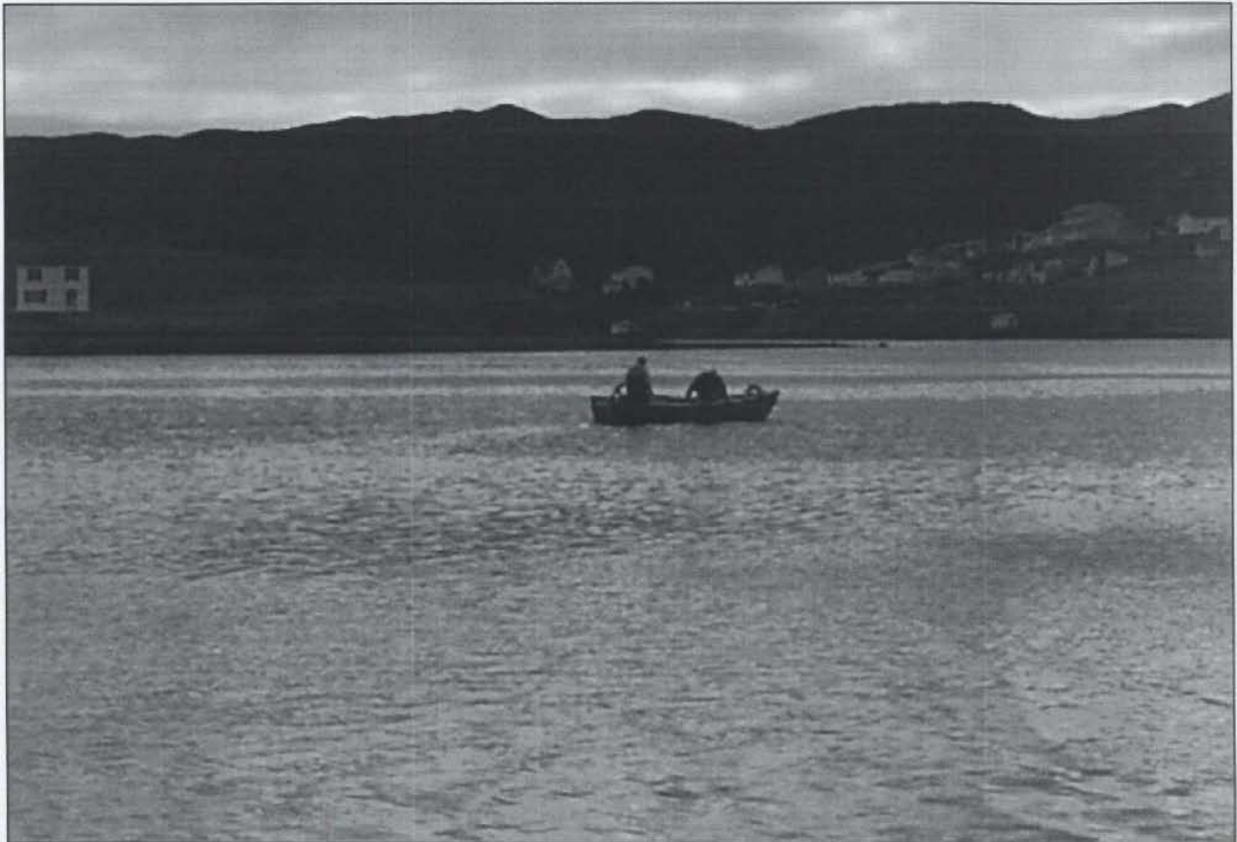
Figure 4. 12   Installing the slider and foil mechanism at the proper water depth

After making repairs, the test continued on the morning of August 14,1999. The test area is shown in figure 4.12 where the slider and the foil assembly module were installed and the test begun. This test was a success because the recorder captured about five minutes out of approximately forty minutes of operation. The speed was approximately over half a meter per second by observation. A measured run trial was not carried out.

Before noon approached, mists and showers of rain did occur. Our DAS equipment, although fully covered by plastic wrappings, went awry during the last stage

Figure 4. 13   View inside the boat
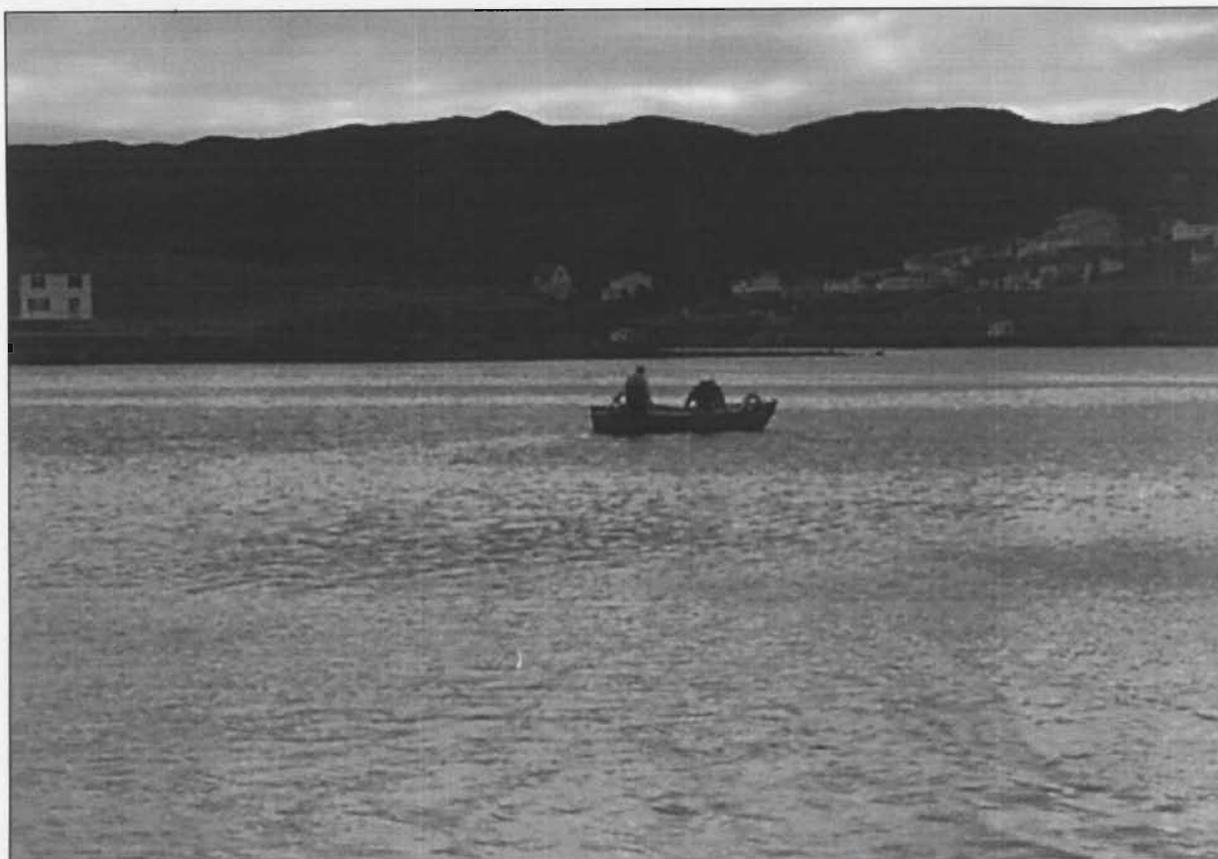
Figure 4. 14   Foil almost lost to shallow point of testing ground

4.6   THE SPEED RUN

The engine was already running and so was the DAS equipment too as the boat ran parallel with the imaginary line between the pole and the buoys. Recordings were made as the boat passed these markings. There were about five runs altogether but only two good recordings were achieved. The reason was the difficulty to run parallel to our markings. During one of these runs, the boat approached near the shoreline where the water depth was shallower. A sudden turn around was made to avoid any disaster.

Figure 4. 15   Buoy still visible as the boat passes marking

The buoy marking was still visible at the right side while the boat was steered back for another run. It ran along side this marking and a recording made as it reached the other end. The foil was working well and had recordings of increased oscillations. At some point, the DAS seemed to be showing some abnormal screen movement. The foreground image on the screen seemed fluid like and not steady so it was decided to head back to shore. Afterwards, a slight mist and shower came in.

Figure 4. 15   Buoy still visible as the boat passes marking

The buoy marking was still visible at the right side while the boat was steered back for another run. It ran along side this marking and a recording made as it reached the other end. The foil was working well and had recordings of increased oscillations. At some point, the DAS seemed to be showing some abnormal screen movement. The foreground image on the screen seemed fluid like and not steady so it was decided to head back to shore. Afterwards, a slight mist and shower came in.

CHAPTER 5

RESULTS AND COMMENTARIES

There were two sets of tests. The first one was a test to try the viability of the first design. It proved that an electro-mechanical controlled pitch mechanism was unwieldy due to the increased mass of the slider mechanism and the cumbersome switches and linkages required of the timing mechanism. However, the foil worked momentarily which indicated that a re-thinking of the design and care in fabrication could be beneficial in the next round of testing.

Subsequent testing was done using design #2 described earlier. The table below shows the results of the tests made on August 10 and 14, 1999.

Pitch Angle	Oscillation Range	Record Time	Distance Covered
30°	20-30 rpm	55 seconds	not taken
30°	20-30 rpm	320 seconds	50 m in 90 sec.

The test came to a halt when the computer stopped working.

Resumption of the tests took place on October 20 and 21, 1999 as soon as the computer became available. Continuing with the sea trials the following data were taken:

Pitch Angle	Oscillation Range	Record Time	Distance Covered
20°	25-35 rpm	100 seconds	50 m in 72 s
20°	25-45 rpm	190 seconds	100 m in 122 s

At this time, the weather and the water were near zero degree temperature. As well the computer was acting strangely so testing had to be stopped.

5.1 COMMENTARY

The graphical records are shown to support the testing that was carried out.

The first one is a record of the input force versus thrust force calibrated in pounds. Load cells number 1 and 2 were positioned to measure the input force taken from the reducer-oscillator sub-assembly of the driving mechanism, while thrust cells 1 and 2 were positioned beneath the suspended seat supporting the slider channel sub-assembly. When the foil was operated, the slider sub-assembly pressed the thrust cells imparting a thrust force for recording.

At the testing ground, the DAS was started and recording immediately followed. The data recording frequency was set at 10 Hz. The mechanical oscillation was fairly smooth i.e. in the 20-30 rpm range and recording started. The early part of the recording showed the signals spiking upwards in the graph of thrust. This indicated an increase in the amount of strain. The reason was that the roller was getting caught at the corner end of the guide track. This momentarily pressed the rig slider sub-assembly to the thrust cells, which in turn relayed the signal to the DAS. Afterwards, the rubber of the roller re-oriented in position and the testing continued while the signals resumed its normal recording. These signals were indications that the driving mechanism and foil design #2 propeller were recording the forces being generated. The test concentrated on the operational aspects of the propulsion system such that measurement for the speed run was not carried out. To avoid any more incident concerning the roller, the test was halted for adjustment.

76
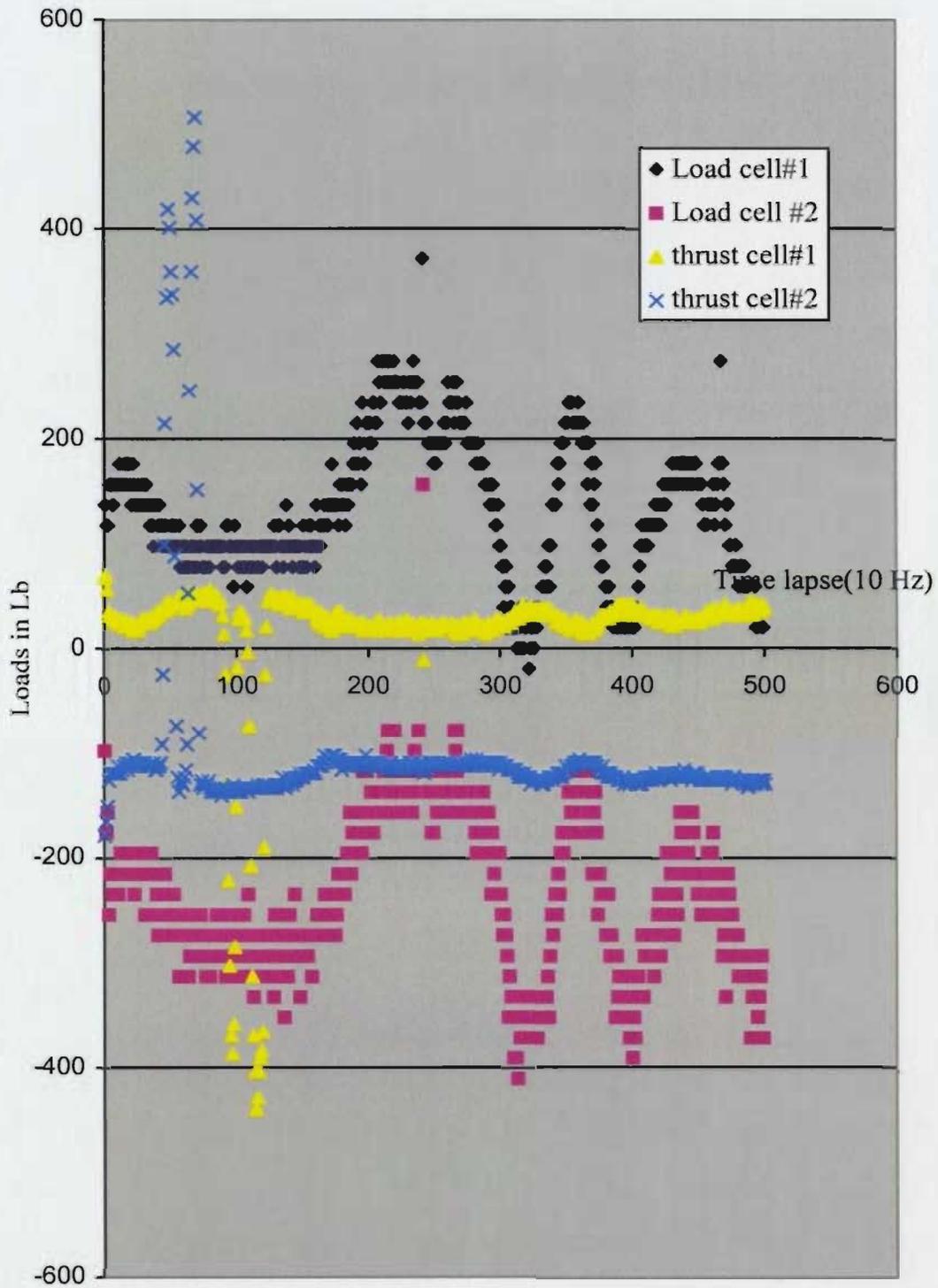
Graph 5.1 Record of test no.1
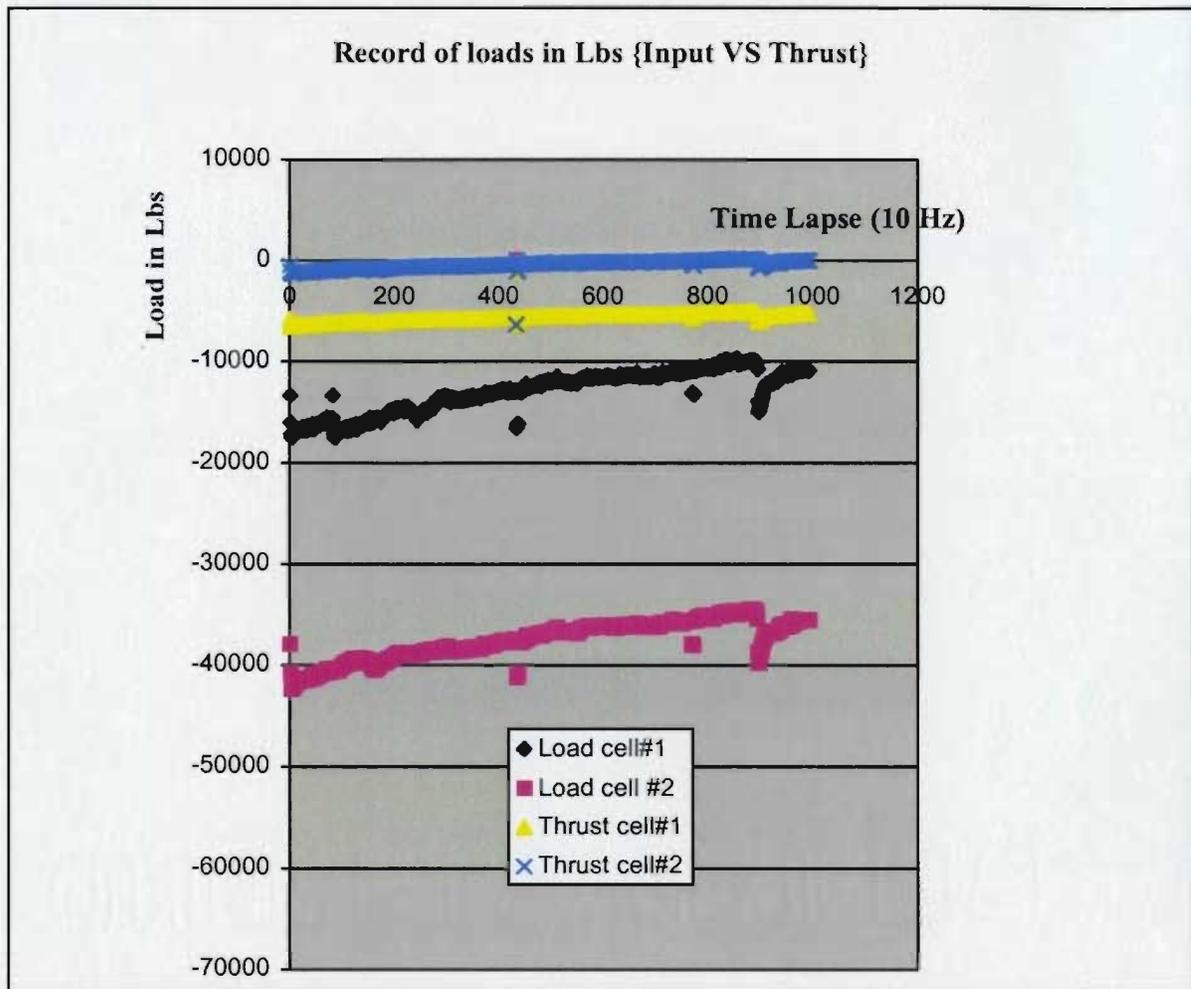
Graph 5.2 Record of test no.2

The second run was longer. The input load cell was behaving properly but the thrust cells seemed sluggish. Though we managed to get some distance and time-lapse recording, it was clear that either our calibration got out of control or zeroes drifted or the computer was starting to malfunction. Shown on graphs 5.2 and 5.3 are recordings with their calibration gone awry as indicated by the high scale of the data numbers. The DAS equipment was returned to MUN for repair and it was found out that the hard disk of the computer had to be replaced. Since students also used this equipment, testing was deferred until it became available again during the fall mid-term.

78

Graph 5.3 Continuation of record no.2

Continuation, Part 2 - Record of Loads in lb {Input VS Thrust}

Time lapse (10Hz)

Loads in lb

- ◆ Input load cell#1
- ■ Input Load cell#2
- ▲ Thrust cell#1
- ✕ Thrust cell#2
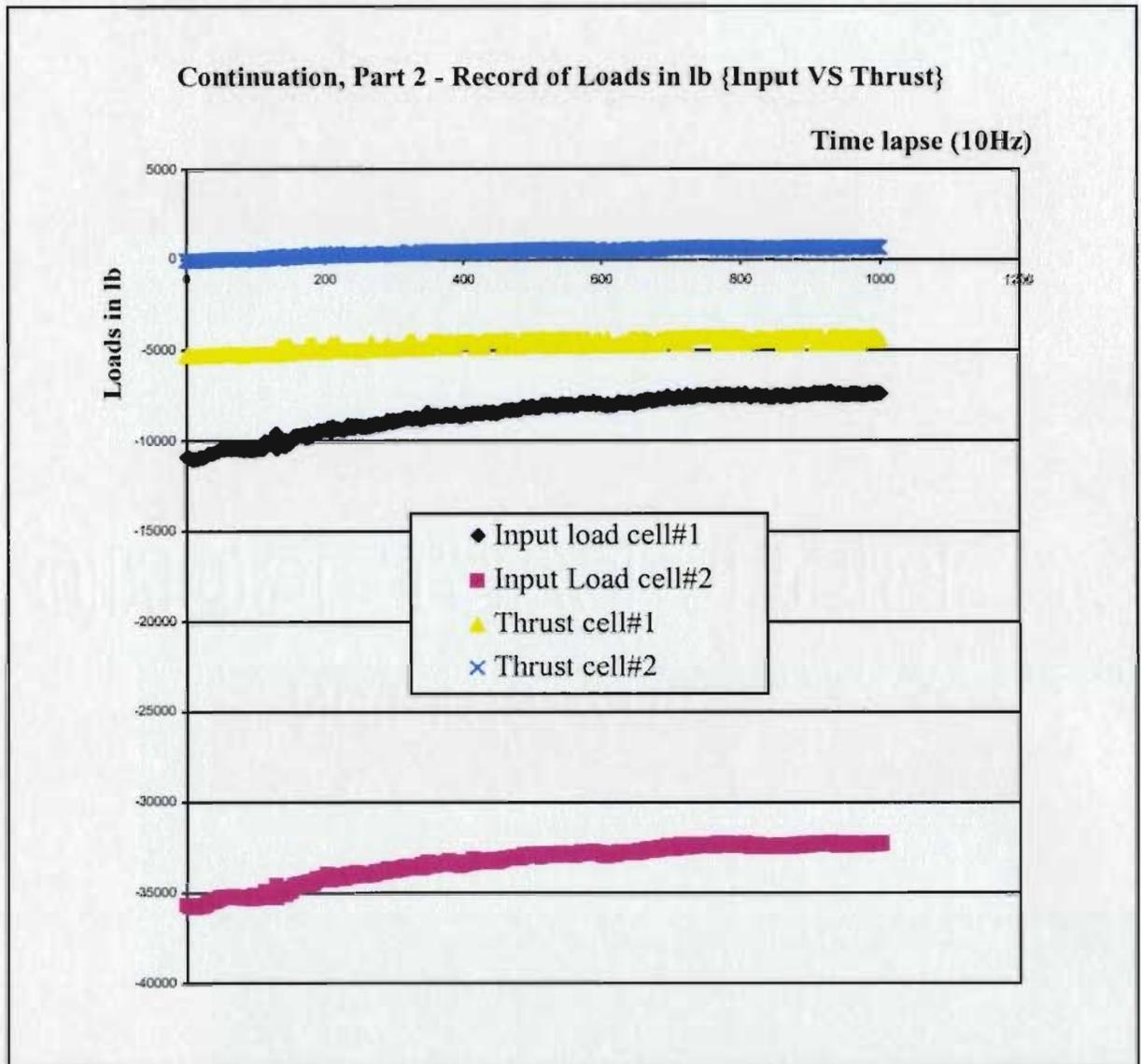
Graph no.5.4 was a recording using units in micro-strain and the signal acquisition rate set to 2 Hz. The instrument recorded the output of the load cells as shown, which indicated a problem with the data despite the satisfactory operation of the foil.

Record of Loads in micro strain{Thrust/Input}
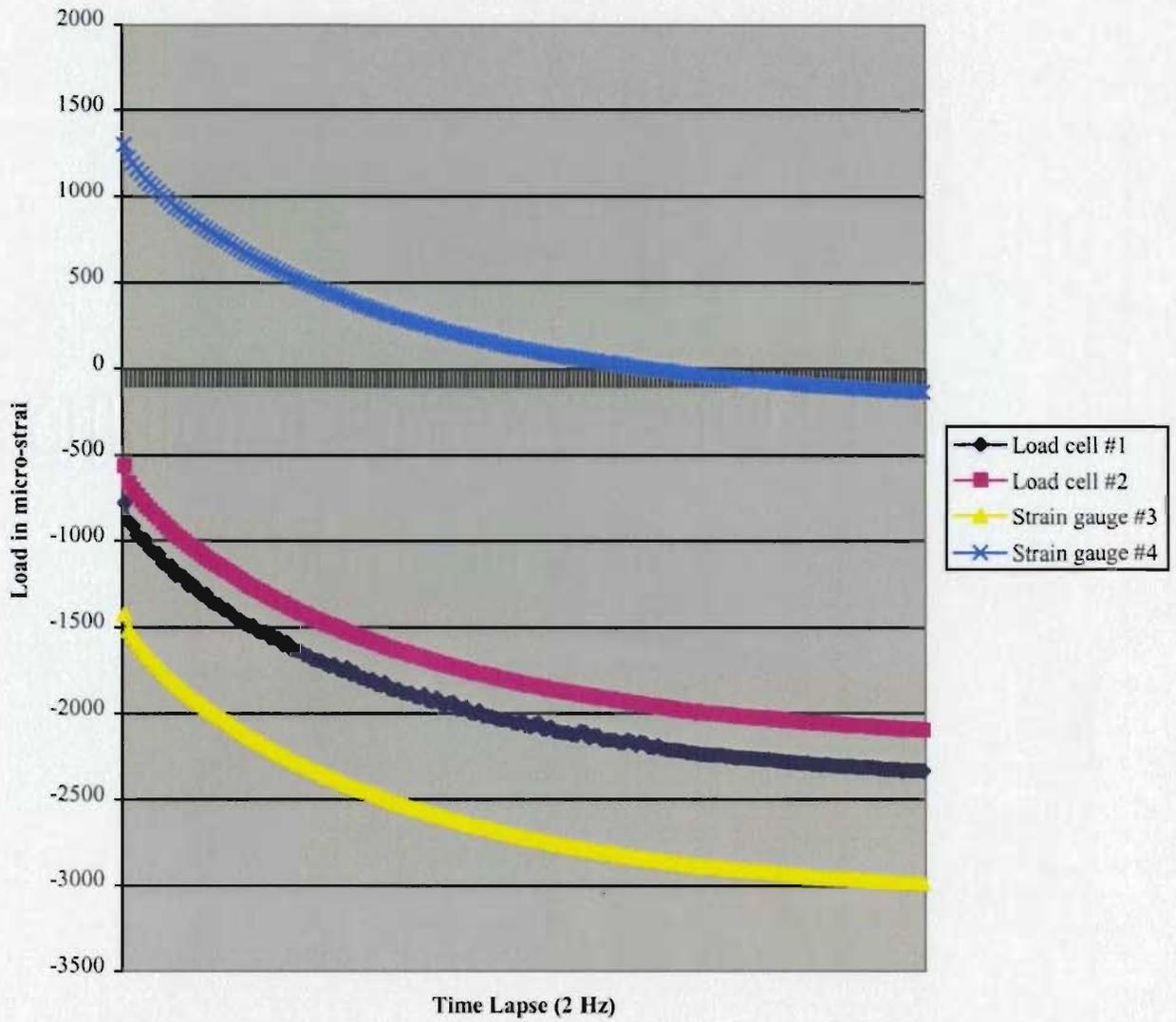
Graph 5.4 Record of test no. 3

The last reading (Graph 5.5) was a record that indicated all cells functioning. In

the upper range of oscillation, the fluctuating reading was very visible.

Graph 5.5 Record of test no.4

Record of Loads in micro-strain{Thrust/Input}
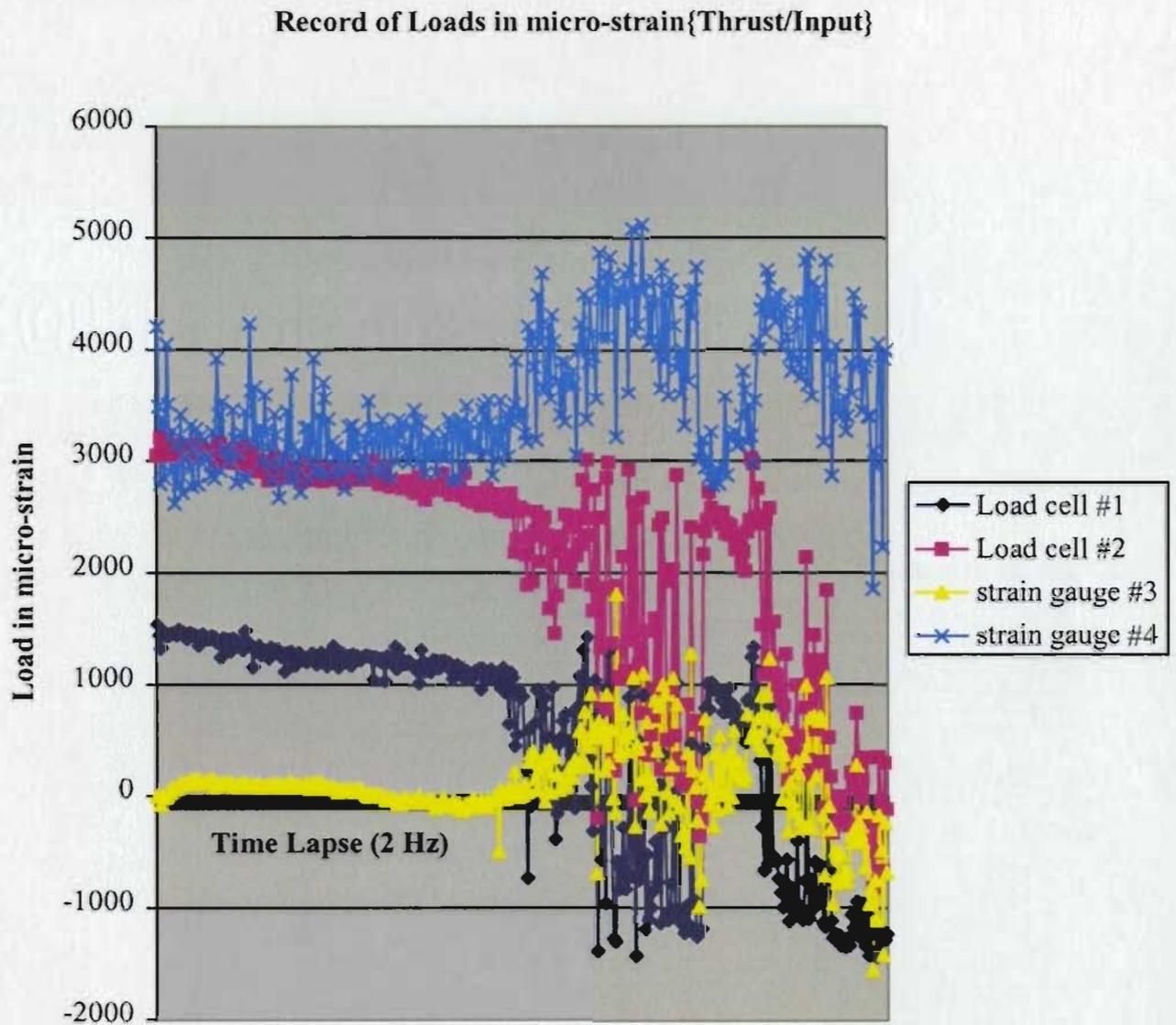
5.2   ANNOTATED DATA

From the foregoing graphical records, it is very difficult to see what the recorded data means as indicated by graphs 5.1 to 5.5. In order to show some significant trend that concerns the performance of the foil from these data, some analysis is required.

Some significant features of these graphs will be discussed to demonstrate the approach taken in interpreting the data gathered by the DAS. These are the frequency signal, curve formation of the graphs, and the scale used.

Data points for graphs 5.1 to 5.3 were recorded at a 10 Hz. frequency, which indicated that there were 10 data points every second during the time the DAS was in operation while graphs 5.4 and 5.5 recorded 2 data points every second since the frequency used was 2 Hz. In the first recording the data points were closely lumped together, which indicated smooth load variation (e.g. fig.5.1) while a later record showed spiked top and bottom forms (fig. 5.5). These formations were indicative that the first test was at low frequency while the last was at a much greater engine speed.

From the description of the two expected graph record formations, graph 5.1 and the latter part recording of graph 5.5 matched this expected curve configuration. The others, graph 5.2 to 5.4 were not used for further analysis because a fault was suspected in the equipment during these runs.

There was difficulty in comparing the two different curves to see an indication of foil performances. Before the annotation exercise was carried out, the raw data points starting 1 to 84 of graph 5.1 were considered. These specifically referred to the record of

load and thrust cells no. 1. Although these data represent a fraction of the whole record, the trend could be established as similar for the rest. Data points between 85 to 120 of the thrust cells were considered an aberration and excluded because, as mentioned earlier, of an interference at the end of the roller tracks during this recording.

Referring to graph 5.5, data points 228 to 275 of load cell no. 2 and thrust cell no.2 were chosen for analysis because of the clarity of the curves in their spiked form. The other cells in this range showed similar curves, which would indicate a similar trend, to cell 2. Thus, further analysis is not required.

Another feature differentiating the first test recordings from the second was the scale used. Resistance reading in lb. (pound) was used in the first and the second used micro-strain ($\mu\varepsilon$). The latter scale was converted to the former to have uniformity in the use of force measurements. The following graphs will indicate the corrected unit of lbs for a clearer comparison.

To illustrate these features in a graphical form would give an indicative trend of how the foil performed during the test runs. Raw data points and the annotated exercise carried out were shown in Appendix F, pages 124 to 132 for reference.

Comparison of Load and Thrust Cells' Record in Lbs
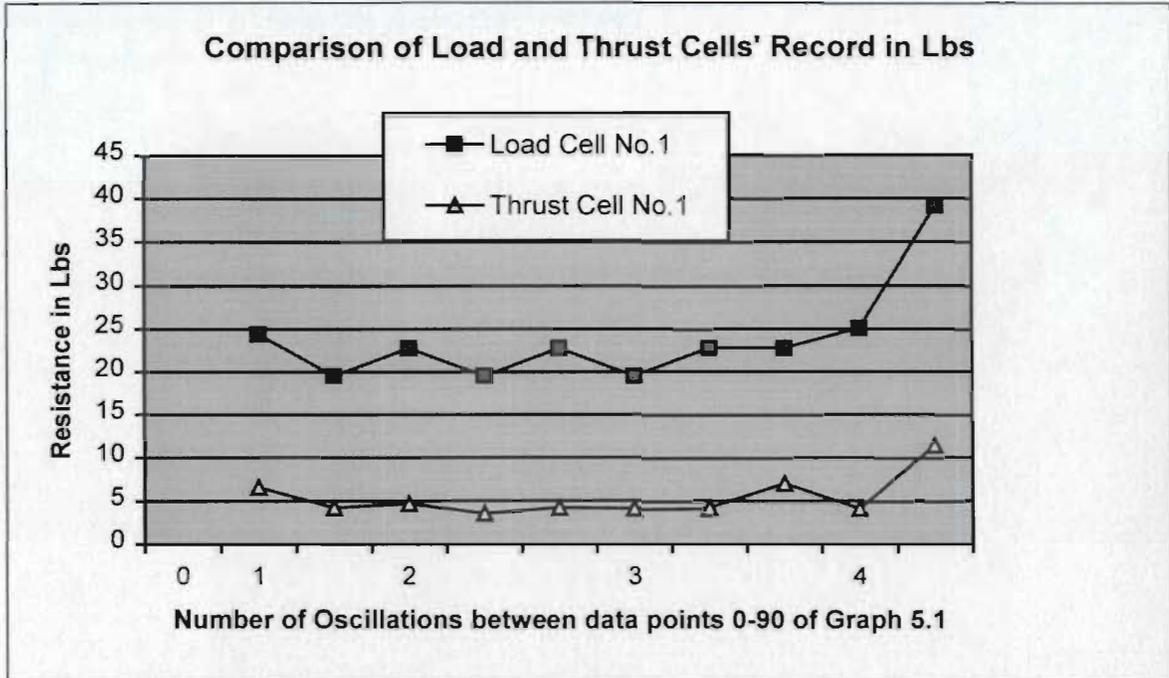
Graph 5.6   Converted graph for load and thrust cells no.1

Graph 5.6 above is the converted representation of load and thrust cells no.1

Record from a portion of graph 5.1. The graph shows three data points for each

oscillation, which was approximated to average 25 rev. per min of the oscillating foil.

From this graph, the average thrust of the foil was about 5 lb. at its 30°- pitch setting and

taking all the points, the thrust versus the load, an approximated average efficiency of

22.7% results. This efficiency compared the running average of all the points, i.e. thrust

divided by load times 100%. Referring back to graph 5.1, it was shown that the level of

thrust did change slightly when there was an increase of oscillation.

The second set of tests, with foil adjusted to a 20° pitch setting and oscillating at

an average of 35 rev. per min., is indicated by graph 5.7 below.

84

Comparison of Load and Thrust Cells' Record in Lbs

Legend: Load Cell No.2, Thrust Cell No.2

Y-axis: Resistance in Lbs (0 to 70)

X-axis: Number of Oscillation between data points 228-275 of Graph 5.5
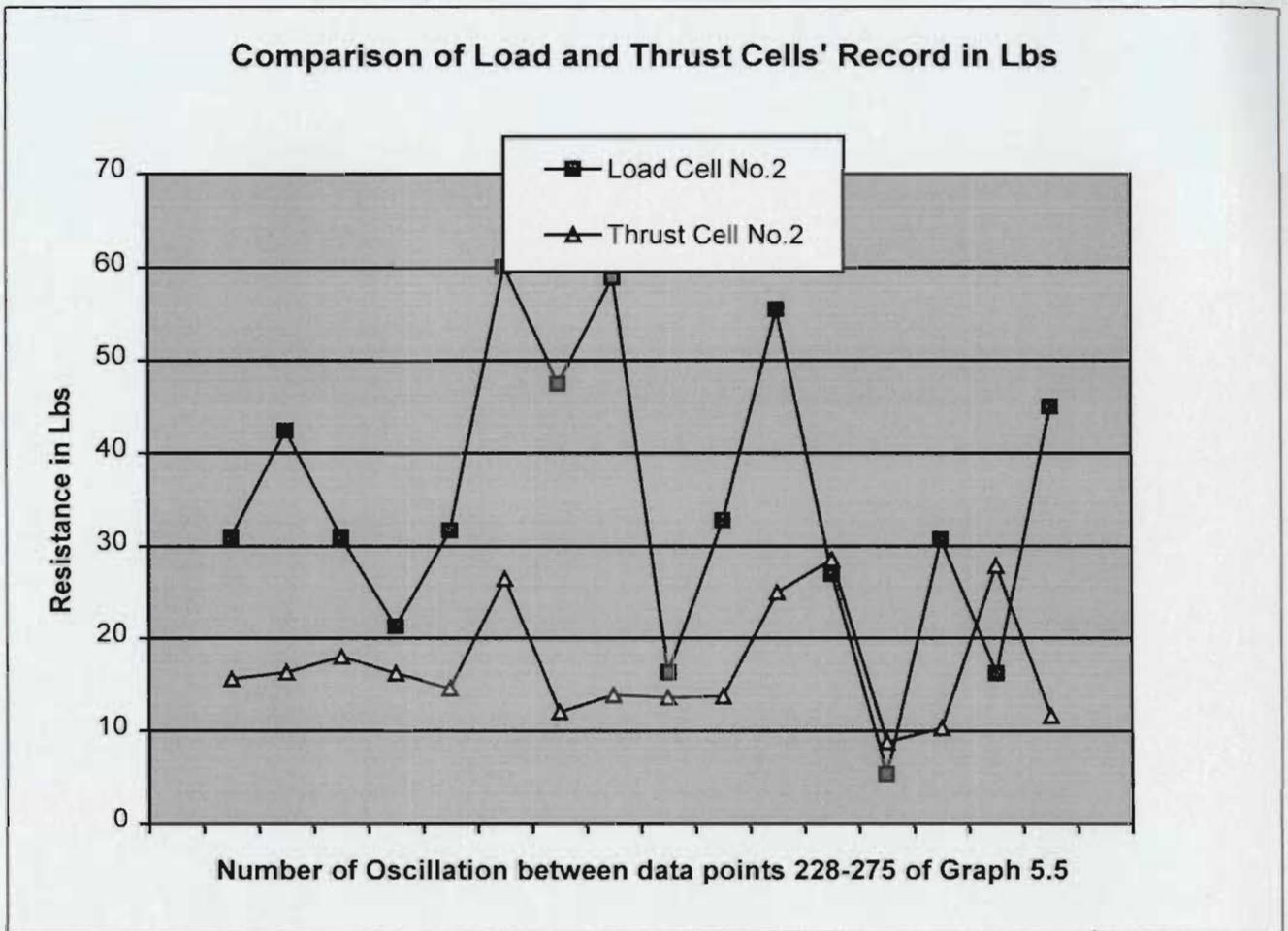
Graph 5.7   Converted graph for load and thrust cells no.2

The original data points were already clustered between 3 to 4 points for each oscillation, not all data points are plotted in graph 5.7. This approach was taken to show more oscillations in the graph.

From this latter graph, the average thrust of the foil was a bit below 20 lb. and repeating the same process as was done for the former graph, the approximate efficiency was estimated to be 48 %. There were increases in both thrust and efficiency of foil when

operated at the setting mentioned. As well, an increase in oscillation contributes to higher thrust as the advance ratio ($h\Omega/\pi U_0$), feathering parameter ($h\Omega/\alpha\ U_0$), and oscillating frequency ($\Omega^2\ c/g$) were affected.

The performance of the foil from the analyzed data was encouraging. It showed promise of improving performance at an optimum pitch setting, still to be determined, and at higher oscillation speed, which the drive mechanism could operate safely. It is, however, not conclusive because the data obtained were not extensive enough.

Appendix F shows the data analysis carried out in this exercise.

CHAPTER 6

CONCLUSIONS

This work concentrated on one specific design of a foil propulsion system applicable to a marine type vehicle. It was based on the work done by various theoreticians and experimenters who have contributed to this field. Along with the great amount of information available, the report also used the partial analysis method in order to assimilate the various parameters that affect the dynamic and physical conditions of the design.

The design and construction of the various assemblies such as the power take-off, the reducer-oscillator assembly, the lever arm multiplier, and the slider assembly guide, which was corrected in the latter part of the tests, performed well according to their functions. These assemblies were connected to the slider mechanism, which supported and provided the up and down motion of foil design #2. In this operation, load cells situated according to their designated positions measured input and thrust forces.

Foil design #1 was built ahead of the foil tested above. It had similar features to the system that was tested. However, the construction of its electro-mechanical pitch mechanism broke down due to a defective component. The experimenter believed that it could be re-worked and re-tested in the future.

87

Connecting
Rod

Connector with
Spring Damper

Adjustable
Sway
Bar

Lever Arm

Plastic Wheel
Track

Rubber Wheel
Channel

Chain
Sprocket
Lock

DC Motor

UP

Sprocket
wheel
Actuator

Cable DOWN

Clamp
Screw

Half Cylinder
Vertical Guide
Holder

Sprocket shaft

Spring
Loaded Clip

Cable Puller

Connecting rod,
Oscillator to
Lever Arm

Suspended
Seat for Slider
Assembly Guide

Aluminum
sliding pad
guide

Crank

Vertical Guide

Slider #1 Channel Guide

Lever-Arm
Support Seat

Slider Assembly Guide

Reducer Gear

Rotaike
Solenoid
Pitch pin
Connector

Pin

Rubber Flexible Coupling,
Compression Type

Rotating Wheel

Sliding pad
pitch actuator

Reducer-Oscillator
Assembly

Connector
Pitch link

Fin Foil

Fin Foil (Design #1),
with elecro-mechanical
pitch actuator

| DRAWING NO. 002 | TITLE: INSTALLATION ASSEMBLY DRAWING FOR FOIL DESIGN #1 PROPULSION SYSTEM | DESIGNED & DRAWN BY: T. CALDERON |

line co-ordinate.

Example. In *Human Powered Racing Hydrofoil* design and built by D.J.Owers.BOC(1984), the hydrofoil profile followed the NACA 4412 offsets. Referring to the section drawing above, the first digit of this foil indicates the maximum camber, $100\ (y_A/c)$. The second digit is the abscissa, $10(X_A/c)$. The last two gives the relative thickness, $100\ (t/c)$. Thus, the NACA 4412 wing section has 4 per cent camber at 0.4 of the chord from the leading edge and is 12 per cent thick (t is $0.12c$).

The NACA four digit series with the first two digit having two zeroes like NACA 0006 and NACA 0010 signify that there is no camber and the profile is symmetrical.

In October of 1958, NACA became the National Aeronautics and Space Administration (NASA) with extended mandate in space exploration.

107

6.1 ENCOURAGING TREND

The analyzed data of section 5.2 showed the performance of a foil improving from a pitch setting of 30° operating at an averaged of 25 rpm oscillation to an adjusted pitch of 20° and running at an averaged of 35 rpm oscillation. The trend indicated much improvement in thrust when the frequency of oscillation increased significantly. The thrust recorded was not solely due to the motion of the oscillating foil but also due to the flow field of the current where the foil was tested. As the boat bobs up and down due to current and waves, these motions aid in increasing the thrust of the foil.

Comparing the average thrust of about 20 lb. from graph 5.7 to the predicted or theoretical thrust of 32.4 lb. (144 N) at a speed of about 1.3 m/s in section 3.2.1, which was calculated solely on the motion of the foil operating in still water, is encouraging evidence that this type of propulsion could be viable. Better performance would have been achieved if the foil was bigger. Glancing at the equation of the induced drag, $D_i = C_L d_w V_R^2 S / 2 \pi b^2$, the span of the foil has to be increased to decrease this resistance. Doing so would lead to a re-design of the fin foil with careful attention to the change of area and aspect ratio.

Since the outcome of the experiment had thrust numbers getting close to the predicted required thrust, is an encouraging sign that further practical testing could one-day achieve the required parameters of a practical foil propeller.

90

OFFSET COMPARISON(NACA # VS White Whale's)
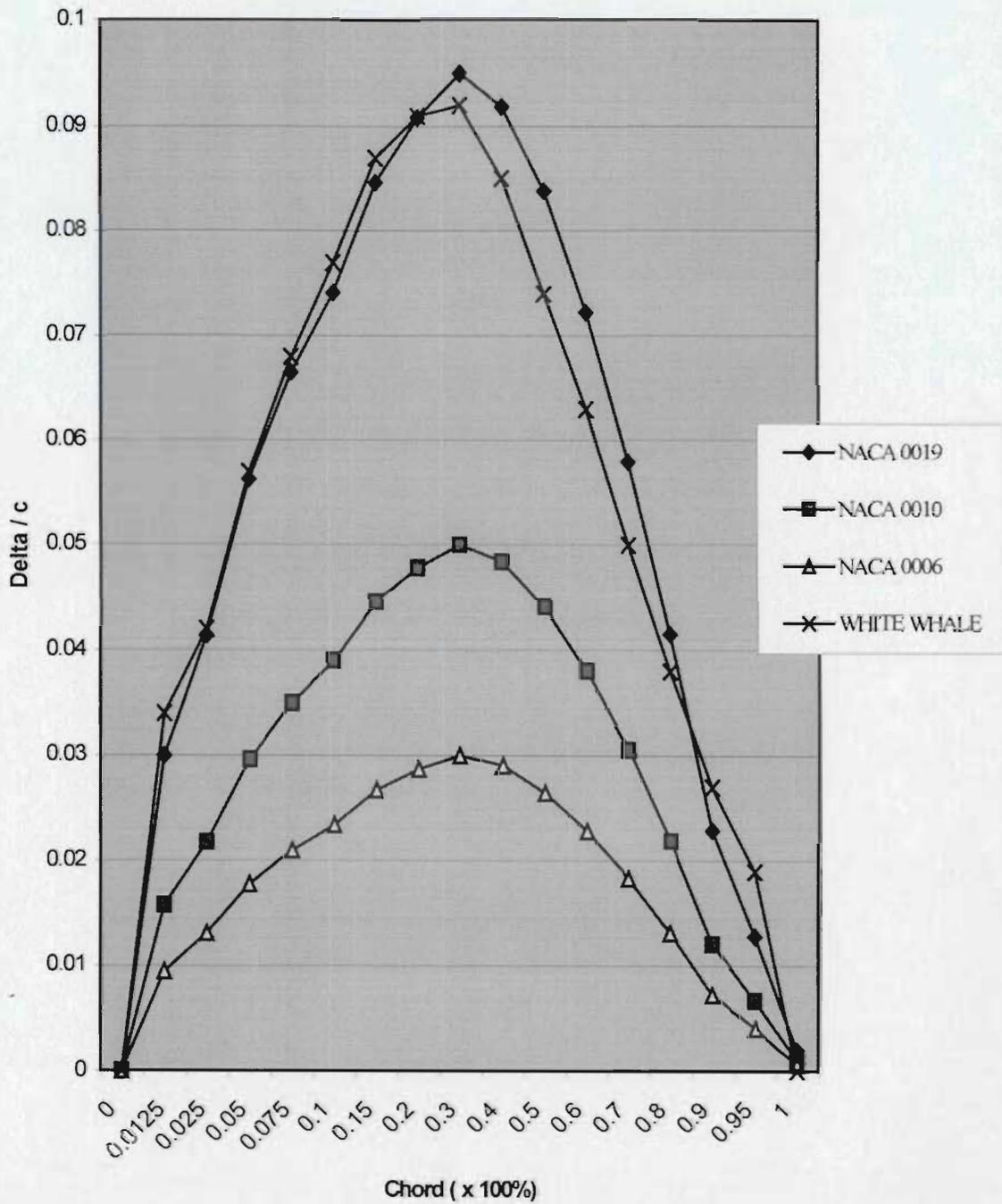
the construction phase. Another factor that influenced this decision was the health issue, which needed attention. This made it difficult to consult as often as preferred with the project supervisor.

In the end, the project was completed, and hopefully, contributes some value to the body of work on fin foil applications in marine propulsion.

REFERENCES

Avallone, E.A. and Baumeister III, T. (1996)." Marks' Standard Handbook for
Mechanical Engineers," McGraw Hill, New York, 10th Ed.

Bhattacharya,R. (1979). "Dynamics of Marine Vehicles," John Wiley and Sons, Inc.,
USA

Baxter, B. (1970). "Naval Architecture," University Press Publishing , London

Bose, N. and Lien, J. (1989). "Propulsion of a Fin Whale is Fast Swimmer." Proc. R.
Soc. London. B237

Bose, N. and Lien, J. (1990). "Energy Absorption from Ocean Waves: A Free Ride for
cetaceans," Proc. R. Soc. London. B240

Bose, N. and Lien, J. (1990). "Measurements of the Bodies and Flukes of Several
Cetacean Species: Designs for Fast and Slow Swimming," Proc. R. Soc. London.
B242

Chopra, M.G. (1974). "Hydromechanics of Lunate-Tail Swimming Propulsion. Part 1." J.
Fluid Mech.,. Vol. 64, Part 2

Chopra, M.G. and Kambe, T.K. (1977)."Hydromechanics of Lunate-Tail Swimming
Propulsion. Part 2," J. Fluid Mech., Vol. 79, Part1

Comstock, T.P., (1967). "Principles of Naval Architecture," SNAME, New York, U.S.A.

Cuypers, E. (1984). "Propulsion of Reduced Draft Vessels," SNAME, New York, U.S.A.

Hertel, H. (1963). "Bio-technique of Oscillating Propulsion Systems and their integration
into the Body," University of Berlin, Germany

Record of loads in Lbs {Input VS Thrust}
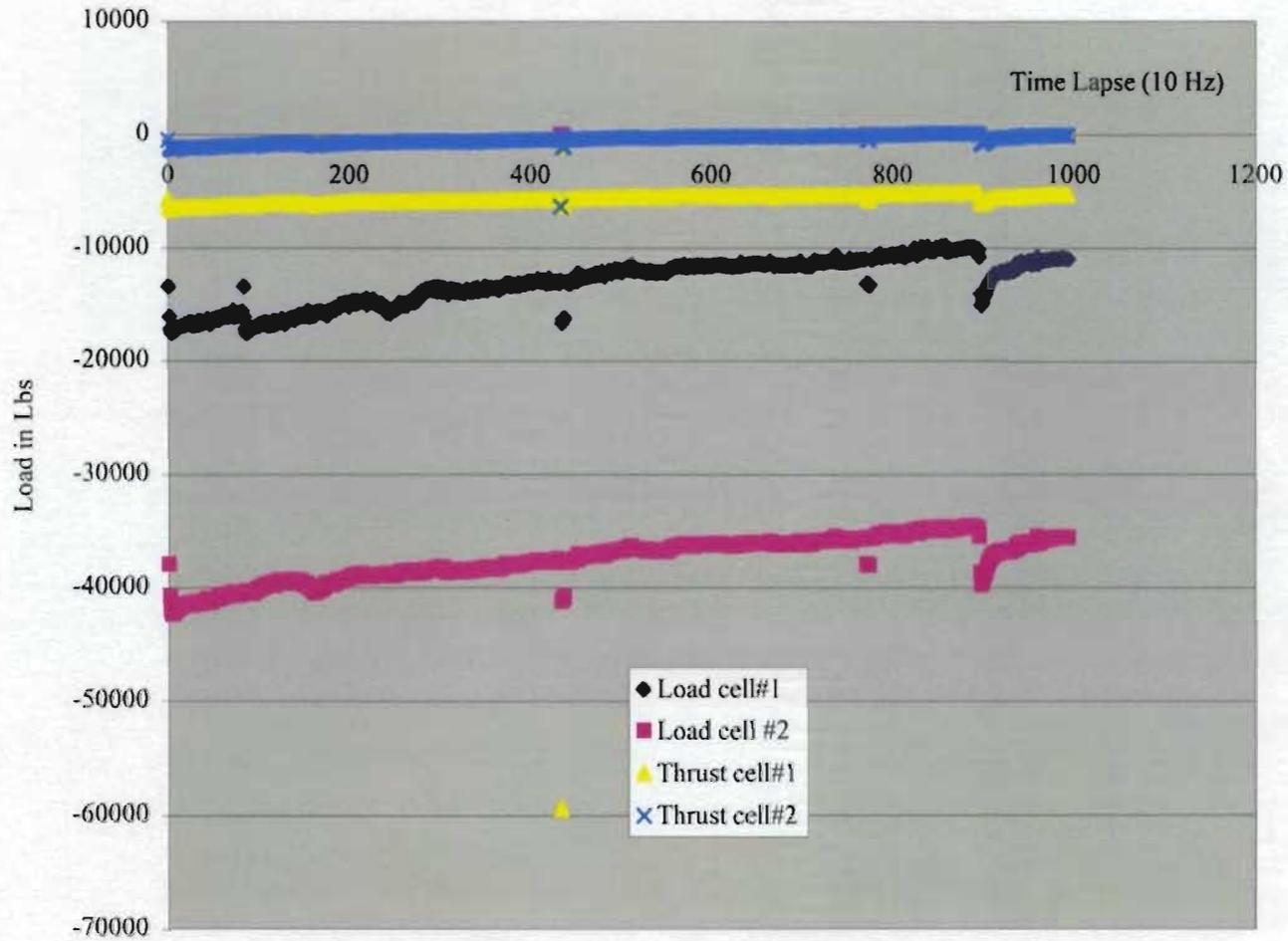
Von Mises, R.(1959). "Theory of Flight." Dover Publications Inc., New York, USA

Wu, T.Y. (1971a). "Hydromechanics of Swimming Propulsion. Part 1. Swimming

Flexible Plate Variable Forward Speed in Inviscid Fluid," J. of Mech., Vol. 46

Yamaguchi, H.(1992). "Hydrodynamic Design of an Oscillating Foil Propulsion," LM-

1992-19, Institute of Marine Dynamics, National Research Council, Canada

Appendix A

Installation drawings for the Foil Propulsion System

Connecting Rod

Adjustable Sway Bar

Plastic Wheel Track

Rubber Wheel Channel

Connector with Spring Damper

Lever Arm

Chain Sprocket Lock

Half Cylinder Vertical Guide Holder

Slotted Plastic Wheels

Connecting rod, Oscillator to Lever Arm

Clamp Screw

Suspended Seat for Slider Assembly Guide

Slider Assembly Guide

Rubber Wheels

Slider Assembly

Vertical Guide

Channel Guide

Reducer Gear

Lever-Arm Support Seat

Rubber Flexible Coupling, Compression Type

Rotating Wheel

Reducer-Oscillator Assembly

Fin Foil, Design #2

DRAWING NO. 001

TITLE: INSTALLATION ASSEMBLY DRAWING, FOIL PROPULSION SYSTEM

DESIGNED & DRAWN BY: T. CALDERON

Record of Loads in micro-strain{Thrust/Input}

Load in micro-strain

Time Lapse (2 Hz)

Legend:
- Load cell #1
- Load cell #2
- strain gauge #3
- strain gauge #4

DC Motor

UP

Sprocket
wheel
Actuator

Cable DOWN

Sprocket shaft

Spring
Loaded Clip

Aluminum
sliding pad
guide

Cable Puller

Pin

Crank

Release
Solenoid

Pitch pin
Connector

Sliding pad
pitch actuator

Connector
Pitch link

Fin Foil

Fin Foil (Design #1),
with elecro-mechanical
pitch actuator
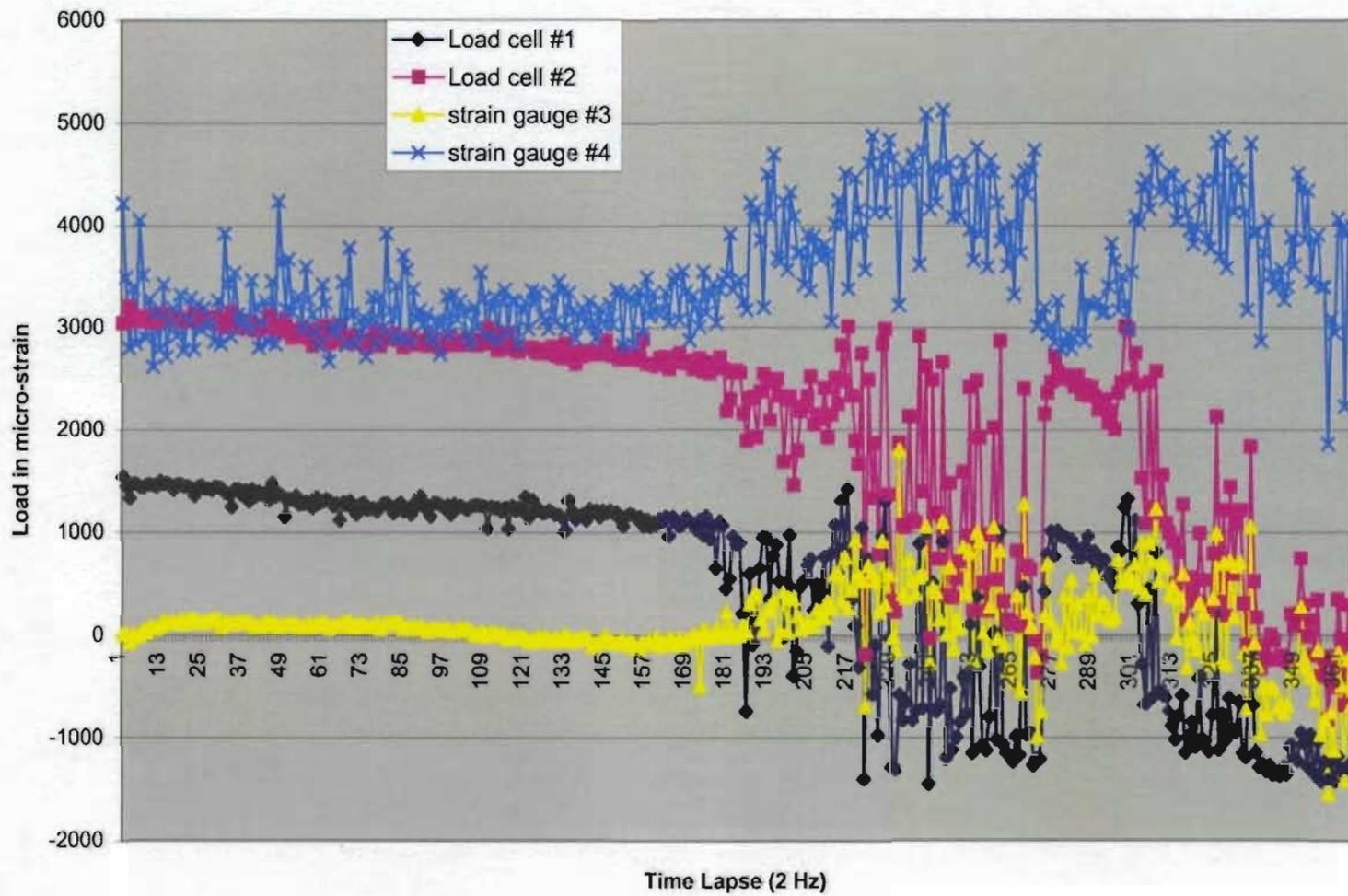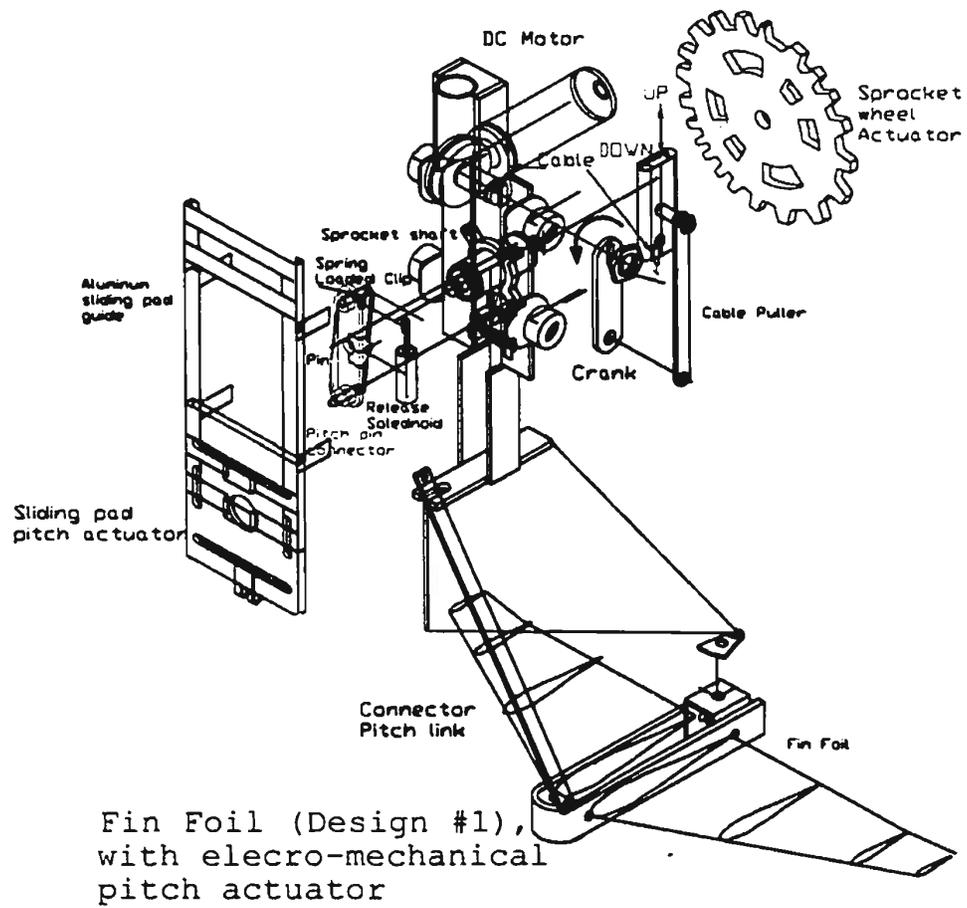
| DRAWING NO. 003 | TITLE: | INSTALLATION ASSEMBLY FOR FOIL DESIGN NO.1 | DESIGNED & DRAWN BY: T.CALDERON |

Record in Lbs {Input VS Thrust}

Pulley

Cogged
V-belt

25 Teeth
sprocket
gear

Gas Engine

10 Teeth
sprocket
gear

Power
take-off

Engine
pulley
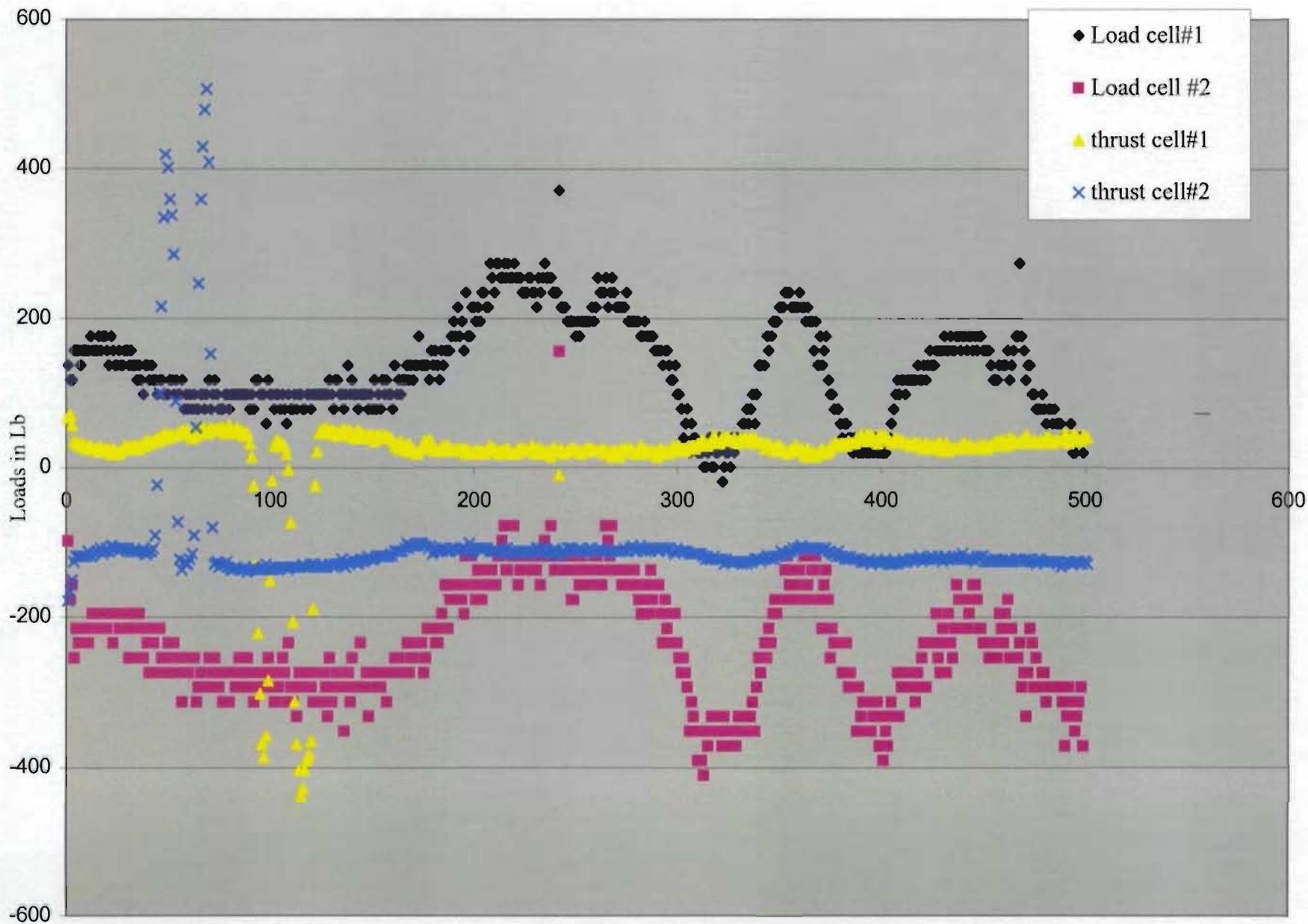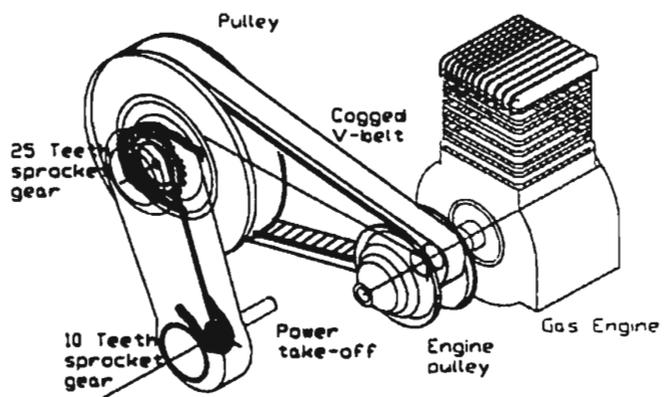
Power Take-Off
Arrangement

DRAWING NO. 005	TITLE: INSTALLATION ASSEMBLY FOR POWER TAKE-OFF	DESIGNED & DRAWN BY: T.CALDERON

Vertical Guide

Slider

Channel Guide

Reducer Gear

Rubber Flexible Coupling,
Compression Type

Rotating Wheel
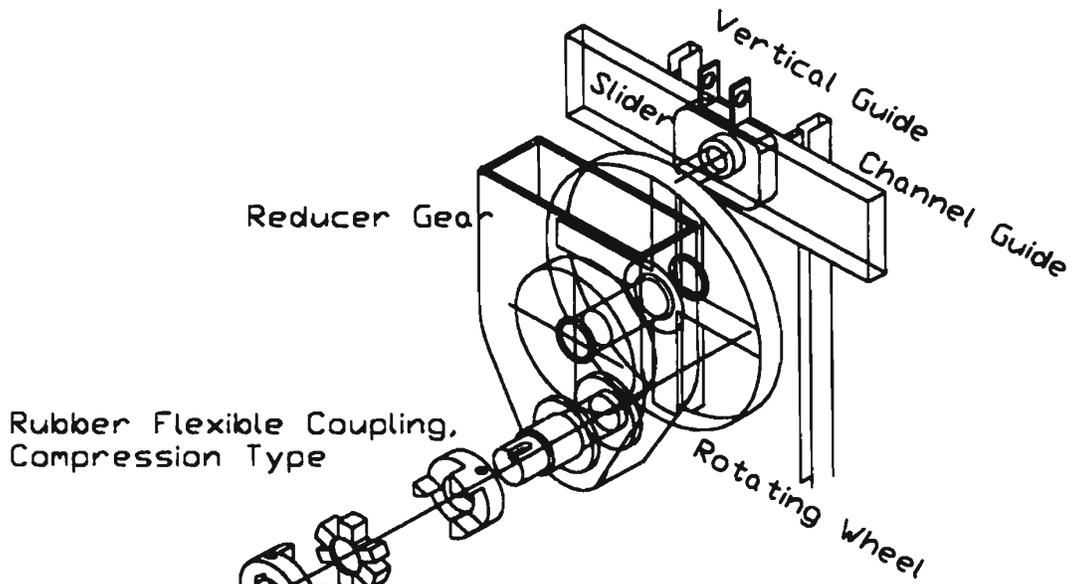
Reducer-Oscillator Assembly

DRAWING NO. 006

TITLE: INSTALLATION ASSEMBLY
FOR REDUCER-OSCILLATOR
GEARS

DESIGNED &
DRAWN BY: T.CALDERON

Adjustable
Sway
Bar

Plastic Wheel
Track

Rubber Wheel
Channel

Chain
Sprocket
Lock

Half Cylinder
Vertical Guide
Holder

Suspended
Seat for Slider
Assembly Guide
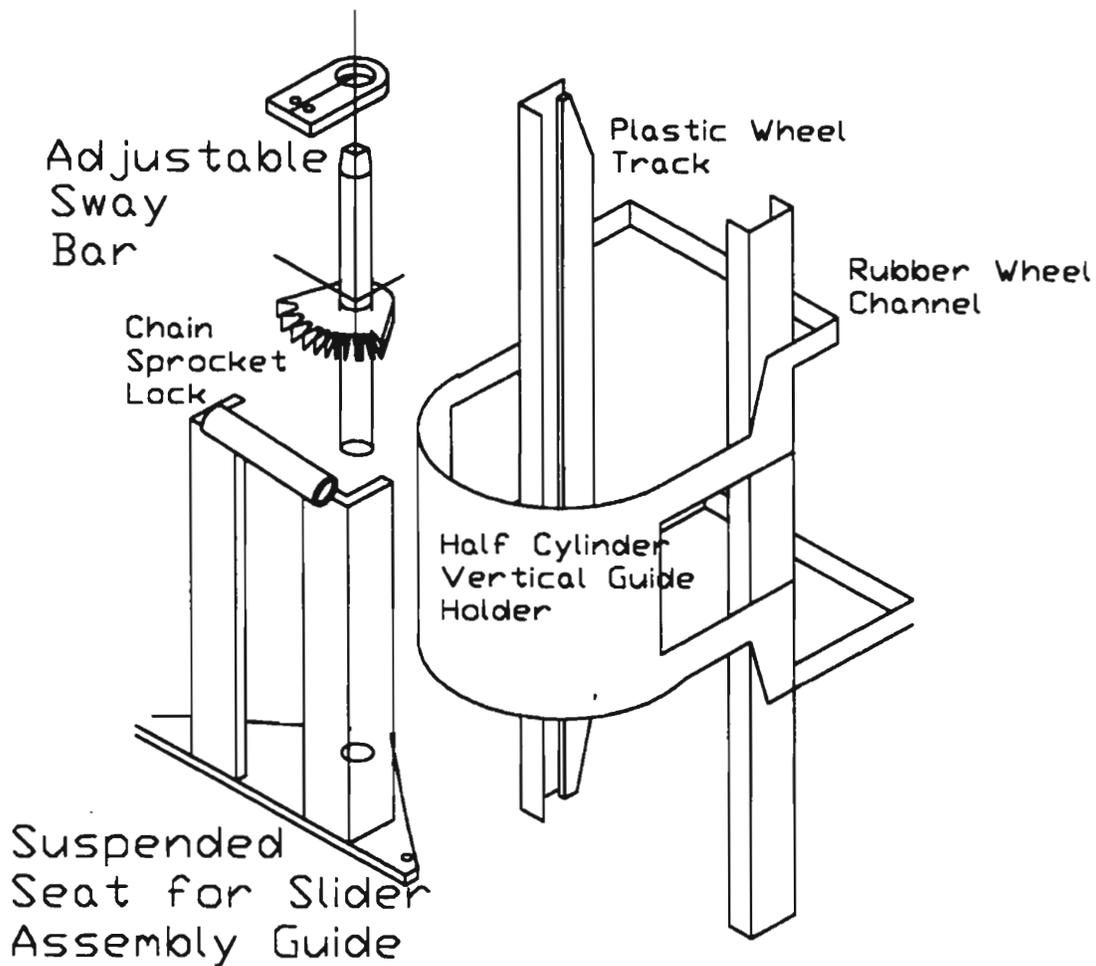
Slider Assembly Guide

| DRAWING NO. 007 | TITLE: INSTALLATION DRAWING FOR SLIDER ASSEMBLY GUIDE AND SUSPENDED SEAT | DESIGNED & DRAWN BY: T.CALDERON |
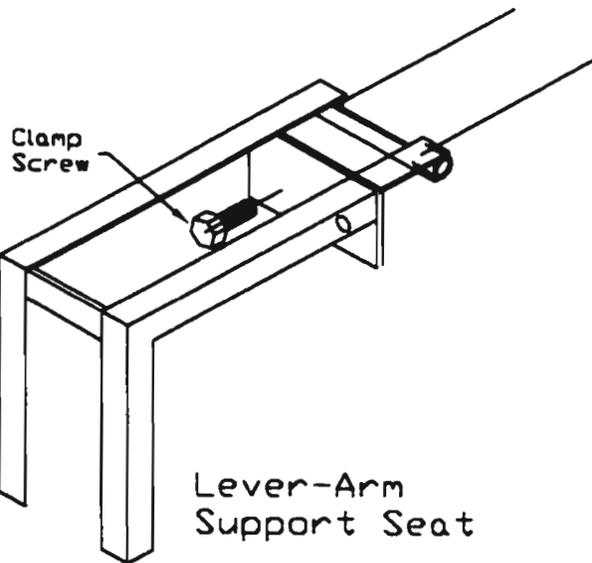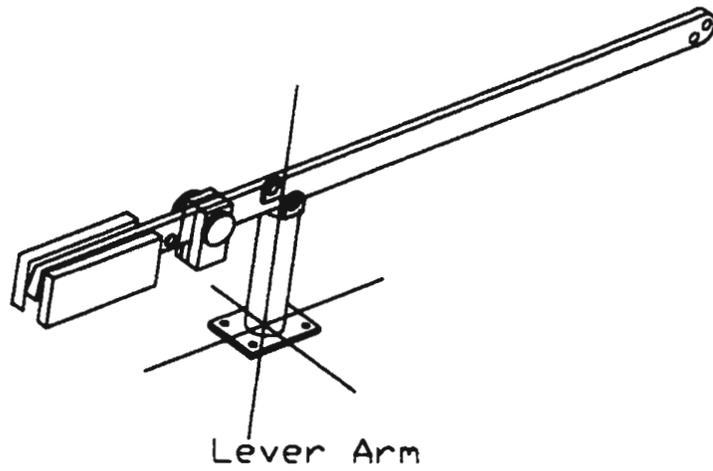
Lever Arm

Clamp
Screw

Lever-Arm
Support Seat

Appendix B

Brief Discussion on Wing Profiles

WING PROFILE DEVELOPMENT

It all started with Otto Lilienthal, universally recognized as the first flying human. He was the first to realise the importance of carefully shaped wing sections. His experiments in wing development in the years 1871 to 1890 led him to adapt **camber**, a curved contour, forming appropriate thickness distribution on the section of the wing as compared with a flat plate. The brothers Wilbur and Orville Wright tested their own profile section designs in 1903. From these works, followed renowned aviation pioneers and scientists like Farman, Antoinette, and Joukowski who were contributors in the first phase of wing development. The next stage were profiles of rounded forms like the Gottingen 360, Mises(1915), and the successful American Profile of 1922(Clark Y). The latter one came about from the laboratory research of the National Advisory Committee for Aeronautics (NACA) which was founded in 1915 to advance US interest in aviation. In 1933, the NACA Tech. Report #460 publication showed the normal symmetrical profile equation,

$$\delta = \pm \{1.4845 \, (x/c)^{1/2} - 0.6300 \, x/c - 1.7580(x/c)^2 + 1.4215 \, (x/c)^2$$

$$- \quad 0.5075(x/c)^4 \}$$

The NACA <u>four and five digit series</u> are the best known wing profiles for study. Basically, the first two digits determine the form of the mean camber line and the last two digits indicate the relative thickness of the profile, *i.e.*, the thickness t expressed in per cent of the chord length c. Specific rules apply to the trace of the mean camber lines which are defined by two parabolic arcs tangent at the position of the maximum camber

line co-ordinate.

Example. In *Human Powered Racing Hydrofoil* design and built by D.J.Owers,BOC(1984), the hydrofoil profile followed the NACA 4412 offsets. Referring to the section drawing above, the first digit of this foil indicates the maximum camber, $100 \ (y_A/c)$. The second digit is the abscissa, $10(X_A/c)$. The last two gives the relative thickness, $100 \ (t/c)$. Thus, the NACA 4412 wing section has 4 per cent camber at 0.4 of the chord from the leading edge and is 12 per cent thick (t is $0.12c$).

The NACA four digit series with the first two digit having two zeroes like NACA 0006 and NACA 0010 signify that there is no camber and the profile is symmetrical.

In October of 1958, NACA became the National Aeronautics and Space Administration (NASA) with extended mandate in space exploration.

107

Appendix C

NACA COMPARISON OFFSETS

OFFSET CALCULATIONS FOR:							
	a. NACA 0019:			b. NACA 0010:			
t=0.19c	*x/c*	*d/t*	*d/c*	*t=0.10c*	*x/c*	*d/t*	*d/c*
0.19	0	0	0	0.1	0	0	0
0.19	0.0125	0.157825	0.029986	0.1	0.0125	0.157825	0.015782
0.19	0.025	0.217893	0.041399	0.1	0.025	0.217893	0.021789
0.19	0.05	0.296223	0.056282	0.1	0.05	0.296223	0.029622
0.19	0.075	0.349991	0.066498	0.1	0.075	0.349991	0.034999
0.19	0.1	0.390230	0.074143	0.1	0.1	0.390230	0.039023
0.19	0.15	0.445430	0.084631	0.1	0.15	0.445430	0.044543
0.19	0.2	0.478128	0.090844	0.1	0.2	0.478128	0.047812
0.19	0.3	0.500143	0.095027	0.1	0.3	0.500143	0.050014
0.19	0.4	0.483584	0.091881	0.1	0.4	0.483584	0.048358
0.19	0.5	0.441168	0.083822	0.1	0.5	0.441168	0.044116
0.19	0.6	0.380280	0.072253	0.1	0.6	0.380280	0.038028
0.19	0.7	0.305325	0.058011	0.1	0.7	0.305325	0.030532
0.19	0.8	0.218593	0.041532	0.1	0.8	0.218593	0.021859
0.19	0.9	0.120643	0.022922	0.1	0.9	0.120643	0.012064
0.19	0.95	0.067213	0.012770	0.1	0.95	0.067213	0.006721
0.19	1	0.0105	0.001995	0.1	1	0.0105	0.00105
	c. NACA 0006:			d. WHITE WHALE(RHS): BOSE et al (1990): Table 3. Fluke Section Offsets			
0.06	0	0	0	0.19	0	0	0
0.06	0.0125	0.157825	0.009469	0.19	0.0125	3.4	0.034
0.06	0.025	0.217893	0.013073	0.19	0.025	4.2	0.042
0.06	0.05	0.296223	0.017773	0.19	0.05	5.7	0.057
0.06	0.075	0.349991	0.020999	0.19	0.075	6.8	0.068
0.06	0.1	0.390230	0.023413	0.19	0.1	7.7	0.077
0.06	0.15	0.445430	0.026725	0.19	0.15	8.7	0.087
0.06	0.2	0.478128	0.028687	0.19	0.2	9.1	0.091
0.06	0.3	0.500143	0.030008	0.19	0.3	9.2	0.092
0.06	0.4	0.483584	0.029015	0.19	0.4	8.5	0.085
0.06	0.5	0.441168	0.026470	0.19	0.5	7.4	0.074
0.06	0.6	0.380280	0.022816	0.19	0.6	6.3	0.063
0.06	0.7	0.305325	0.018319	0.19	0.7	5	0.05
0.06	0.8	0.218593	0.013115	0.19	0.8	3.8	0.038
0.06	0.9	0.120643	0.007238	0.19	0.9	2.7	0.027
0.06	0.95	0.067213	0.004032	0.19	0.95	1.9	0.019
0.06	1	0.0105	6.30000E	0.19	1	U	#VALUE!

OFFSET COMPARISON(NACA # VS White Whale's)

Legend:
- NACA 0019
- NACA 0010
- NACA 0006
- WHITE WHALE

Y-axis: Delta / c
X-axis: Chord (x 100%)
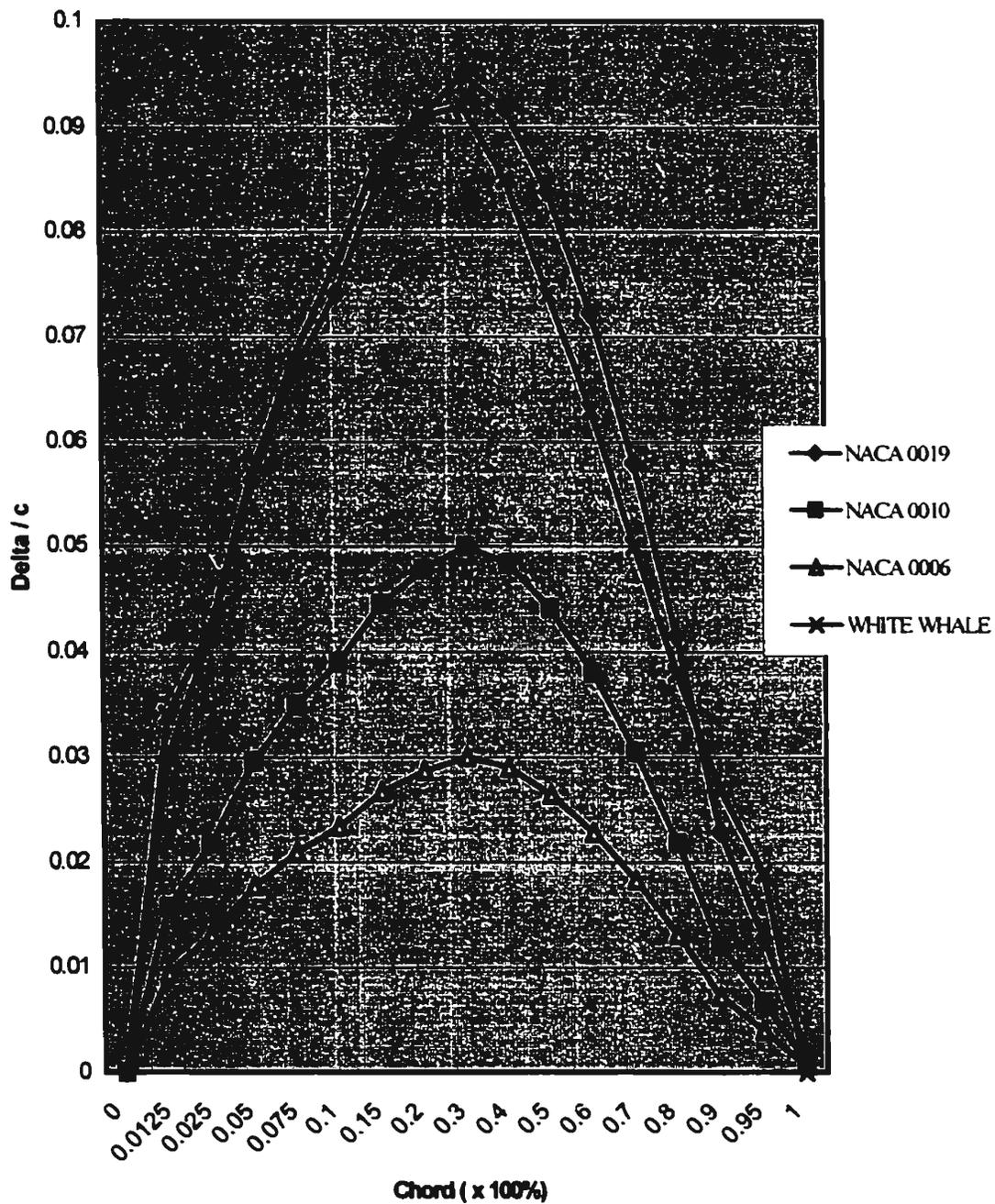
Comparison of Load and Thrust Cells' Record in Lbs
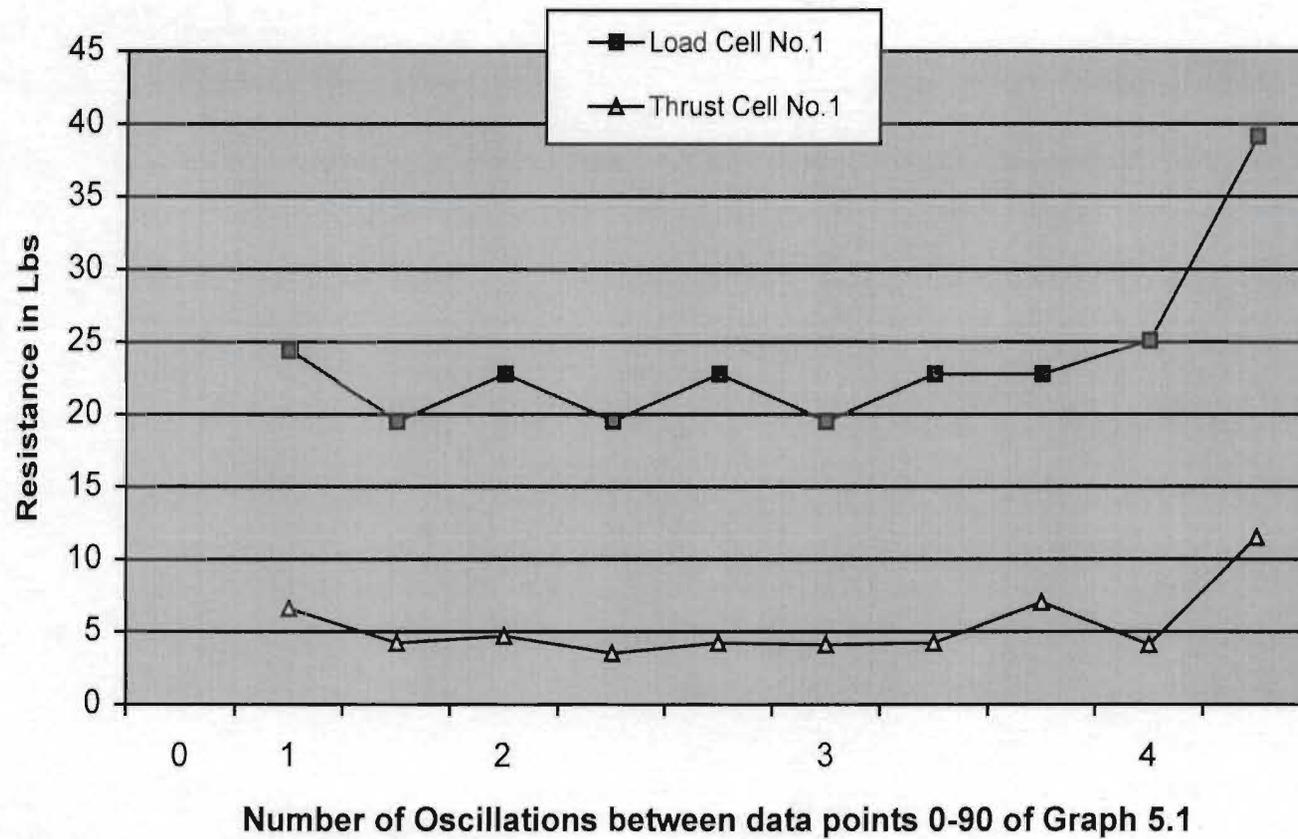
"LABTECH NOTEBOOK"
"Data file"
"Time is 11:57:19.01."
"Date is 8-10-   Conversion
1999."   from"ue" to "lbs"

"load a"	"load b"	"strain a"	"strain b"	"load c"	"load d"
"lbs"	"lbs"	"ue"	"ue"	"lbs"	"lbs"
137.1288	-97.5943	-46.8254	-123.631	67.38643	-177.917
117.5976	-175.719	-49.2668	-113.865	70.89985	-163.863
117.5976	-156.188	-39.5012	-104.099	56.84618	-149.809
156.6601	-253.844	-24.8528	-87.0094	35.76566	-125.215
156.6601	-214.782	-22.4113	-82.1266	32.2521	-118.188
156.6601	-234.313	-22.4113	-82.1266	32.2521	-118.188
137.1288	-214.782	-19.9699	-82.1266	28.73868	-118.188
156.6601	-234.313	-22.4113	-82.1266	32.2521	-118.188
156.6601	-214.782	-19.9699	-82.1266	28.73868	-118.188
156.6601	-234.313	-17.5285	-82.1266	25.22526	-118.188
156.6601	-234.313	-19.9699	-77.2437	28.73868	-111.161
176.1913	-214.782	-19.9699	-82.1266	28.73868	-118.188
156.6601	-195.251	-17.5285	-82.1266	25.22526	-118.188
156.6601	-214.782	-17.5285	-79.6852	25.22526	-114.675
156.6601	-214.782	-17.5285	-77.2437	25.22526	-111.161
176.1913	-195.251	-15.0871	-77.2437	21.71185	-111.161
156.6601	-214.782	-19.9699	-74.8023	28.73868	-107.648
176.1913	-214.782	-17.5285	-79.6852	25.22526	-114.675
176.1913	-195.251	-15.0871	-77.2437	21.71185	-111.161
156.6601	-214.782	-17.5285	-74.8023	25.22526	-107.648
137.1288	-195.251	-17.5285	-77.2437	25.22526	-111.161
176.1913	-195.251	-12.6457	-72.3609	18.19843	-104.135
156.6601	-234.313	-17.5285	-72.3609	25.22526	-104.135
137.1288	-195.251	-15.0871	-74.8023	21.71185	-107.648
137.1288	-195.251	-15.0871	-74.8023	21.71185	-107.648
156.6601	-214.782	-12.6457	-77.2437	18.19843	-111.161
137.1288	-214.782	-15.0871	-74.8023	21.71185	-107.648
137.1288	-214.782	-17.5285	-74.8023	25.22526	-107.648
156.6601	-214.782	-19.9699	-74.8023	28.73868	-107.648
156.6601	-195.251	-17.5285	-74.8023	25.22526	-107.648
137.1288	-253.844	-19.9699	-74.8023	28.73868	-107.648
156.6601	-195.251	-17.5285	-77.2437	25.22526	-111.161
137.1288	-214.782	-19.9699	-77.2437	28.73868	-111.161
137.1288	-253.844	-19.9699	-77.2437	28.73868	-111.161
117.5976	-253.844	-19.9699	-77.2437	28.73868	-111.161
137.1288	-195.251	-17.5285	-77.2437	25.22526	-111.161

111

Record in Lbs {Input VS Thrust}
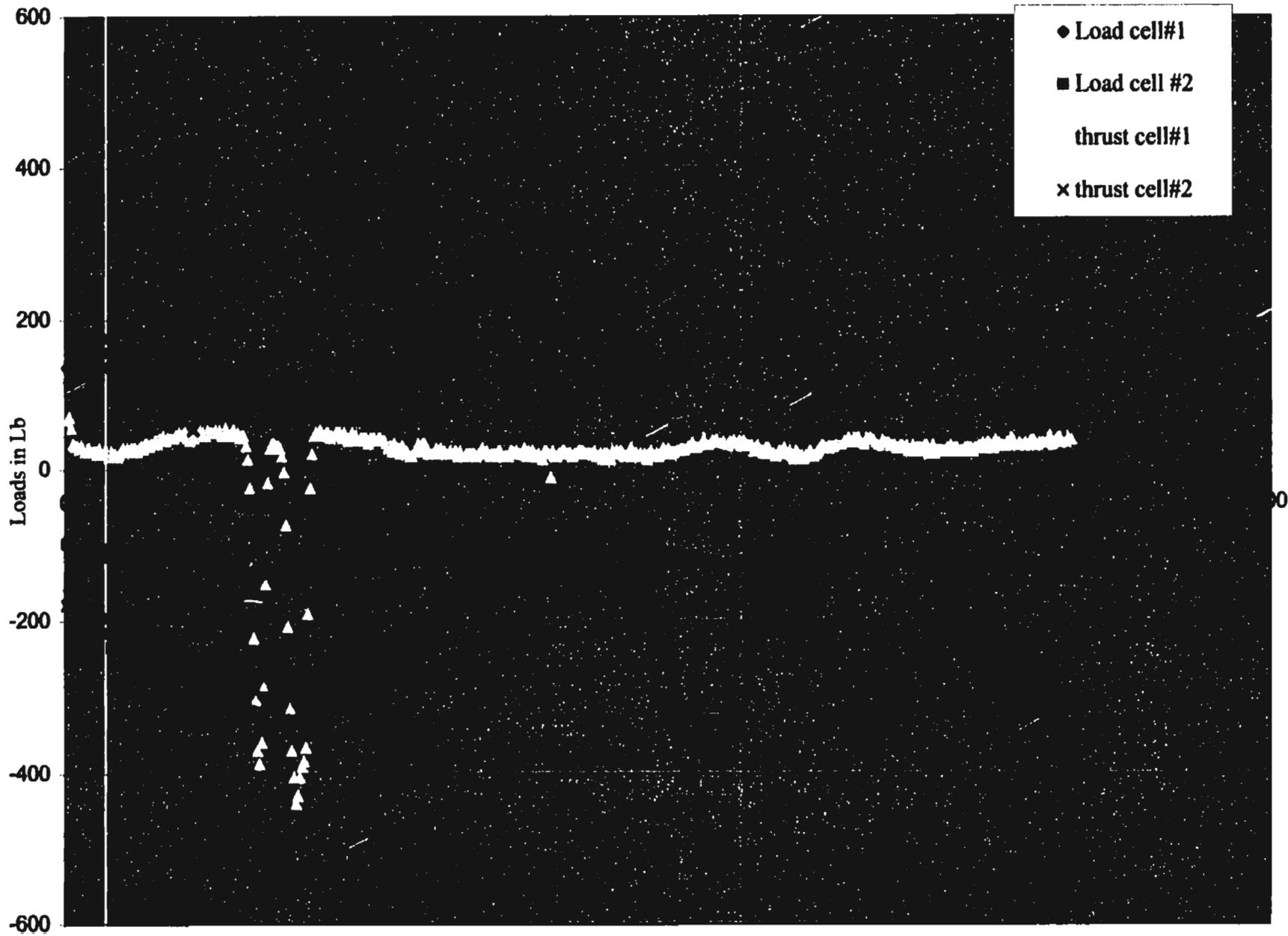
LABTECH NOTEBOOK
Data file
Time is 11:41:34.01.   Conversion from strain to lbs
Date is 8-14-1999.

load a	load b	strain a	strain b		strain c	strain d
lbs	lbs	ue	ue		lbs	Lbs
-13398	-37929.6	-3979.93	-338.474		-5727.52	-487.098
-16034.7	-40781.2	-4355.91	-721.775		-6268.59	-1038.71
-17128.5	-41914	-4499.95	-856.052		-6475.88	-1231.95
-17499.6	-42363.2	-4578.08	-919.529		-6588.31	-1323.29
-17460.5	-42265.6	-4541.45	-897.556		-6535.61	-1291.67
-17441	-42304.6	-4539.01	-885.349		-6532.09	-1274.11
-17362.9	-42148.4	-4521.92	-939.06		-6507.5	-1351.4
-17226.2	-42031.2	-4507.27	-853.611		-6486.42	-1228.43
-17226.2	-41953.1	-4495.07	-863.377		-6468.85	-1242.49
-17128.5	-41894.5	-4492.63	-860.935		-6465.34	-1238.97
-17128.5	-41816.3	-4477.98	-851.17		-6444.26	-1224.92
-17069.9	-41757.8	-4468.21	-843.845		-6430.2	-1214.38
-17011.3	-41699.2	-4460.89	-834.08		-6419.66	-1200.32
-16952.7	-41660.1	-4463.33	-831.638		-6423.18	-1196.81
-16913.7	-41621	-4451.12	-824.314		-6405.61	-1186.27
-16816	-41542.9	-4446.24	-814.549		-6398.58	-1172.22
-16874.6	-41542.9	-4438.92	-816.99		-6388.04	-1175.73
-16913.7	-41640.6	-4456	-814.549		-6412.64	-1172.22
-16698.8	-41445.3	-4431.59	-795.017		-6377.5	-1144.11
-16698.8	-41425.7	-4429.15	-799.9		-6373.99	-1151.14
-16659.7	-41367.1	-4419.38	-790.134		-6359.94	-1137.08
-16679.3	-41308.5	-4412.06	-790.134		-6349.39	-1137.08
-16562.1	-41328.1	-4419.38	-777.927		-6359.94	-1119.52
-16542.6	-41328.1	-4419.38	-777.927		-6359.94	-1119.52
-16562.1	-41328.1	-4421.83	-780.369		-6363.45	-1123.03
-16737.9	-41347.6	-4426.71	-797.459		-6370.48	-1147.62
-16523	-41249.9	-4407.18	-765.72		-6342.37	-1101.95
-16816	-41542.9	-4438.92	-812.107		-6388.04	-1168.7
-16737.9	-41464.8	-4436.47	-812.107		-6384.53	-1168.7
-16796.5	-41484.3	-4456	-824.314		-6412.64	-1186.27
-16698.8	-41386.7	-4421.83	-792.576		-6363.45	-1140.6
-16640.2	-41464.8	-4448.68	-792.576		-6402.1	-1140.6
-16737.9	-41425.7	-4426.71	-799.9		-6370.48	-1151.14
-16405.8	-41289	-4446.24	-782.81		-6398.58	-1126.54
-16757.4	-41386.7	-4419.38	-797.459		-6359.94	-1147.62
-16640.2	-41406.2	-4434.03	-797.459		-6381.02	-1147.62

113

Comparison of Load and Thrust Cells' Record in Lbs

Number of Oscillation between data points 228-275 of Graph 5.5
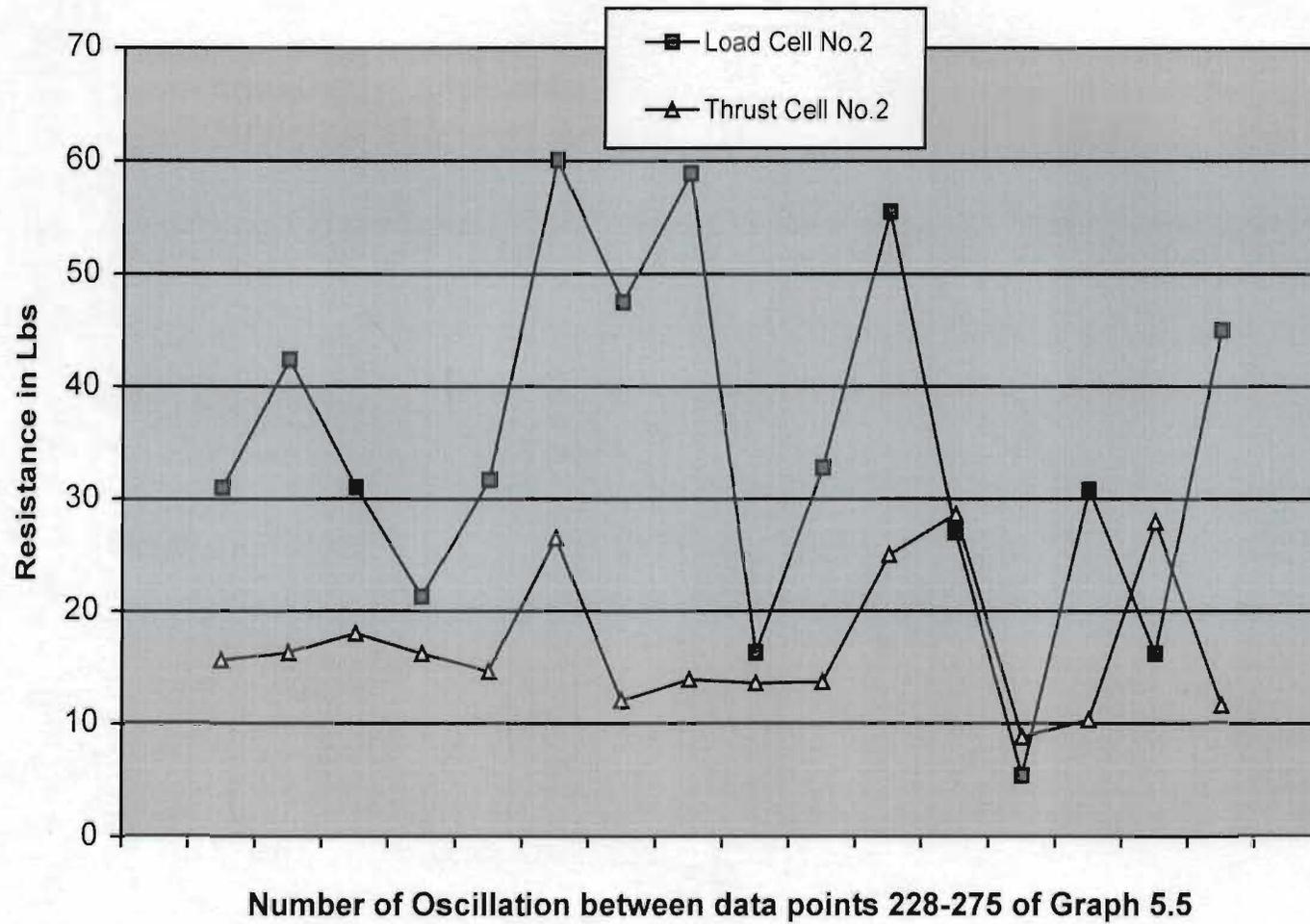
LABTEC H NOTEBOOK				
Data file				
Time is 11:31:11.10.				
Date is 10-20- 1999.				
sg 1	sg 2	Sg3		sg 5
ue	ue	ue		ue
-778.1899	-564.6019	-1423.8352		1306.7034
-889.4692	-662.014	-1516.1204		1231.0198
-912.7603	-700.4662	-1553.0344		1196.8401
-964.5181	-736.3549	-1592.5852		1162.6604
-990.397	-764.5531	-1621.5891		1135.8049
-995.5728	-795.3148	-1653.2297		1104.0667
-1047.3306	-820.9496	-1679.5969		1079.6526
-1070.6216	-846.5844	-1705.9641		1057.6799
-1073.2095	-869.6556	-1729.6946		1033.2659
-1127.5552	-897.8539	-1758.6985		1008.8518
-1143.0825	-920.9252	-1782.429		986.8792
-1145.6704	-943.9965	-1806.1594		964.9065
-1197.4282	-967.0677	-1829.8899		940.4924
-1200.0161	-985.0121	-1848.3469		925.844
-1210.3677	-1002.9564	-1866.804		906.3127
-1256.9497	-1026.0277	-1890.5344		884.3401
-1251.7739	-1043.972	-1908.9915		867.2502
-1282.8286	-1059.3529	-1924.8118		855.0432
-1311.2954	-1079.8607	-1945.9055		833.0706
-1308.7075	-1102.932	-1964.3625		815.9807
-1347.5259	-1118.3129	-1982.8196		798.8909
-1363.0532	-1133.6937	-2001.2766		781.801
-1370.8169	-1149.0746	-2017.0969		767.1526
-1394.1079	-1164.4554	-2030.2805		752.5042
-1404.4595	-1177.2728	-2043.4641		742.7385
-1425.1626	-1195.2172	-2064.5579		723.2073
-1445.8657	-1213.1615	-2083.0149		706.1174
-1461.3931	-1228.5424	-2098.8352		691.469
-1476.9204	-1243.9232	-2117.2922		674.3792
-1492.4478	-1261.8676	-2130.4758		662.1721
-1492.4478	-1274.6849	-2143.6594		649.9651
-1520.9146	-1287.5023	-2159.4797		635.3167
-1528.6782	-1300.3197	-2170.0266		623.1096
-1528.6782	-1315.7006	-2185.8469		610.9026

Record of Loads in micro strain

Legend:
- Load cell #1
- Load cell #2
- Strain gauge #3
- Strain gauge #4

Y-axis: Load in micro-strain (2000 to -3500)

X-axis: Time Lapse (2 Hz), values: 1, 8, 15, 22, 29, 36, 43, 50, 57, 64, 71, 78, 85, 92, 99, 106, 113, 120, 127, 134, 141, 148, 155, 162, 169, 176, 183
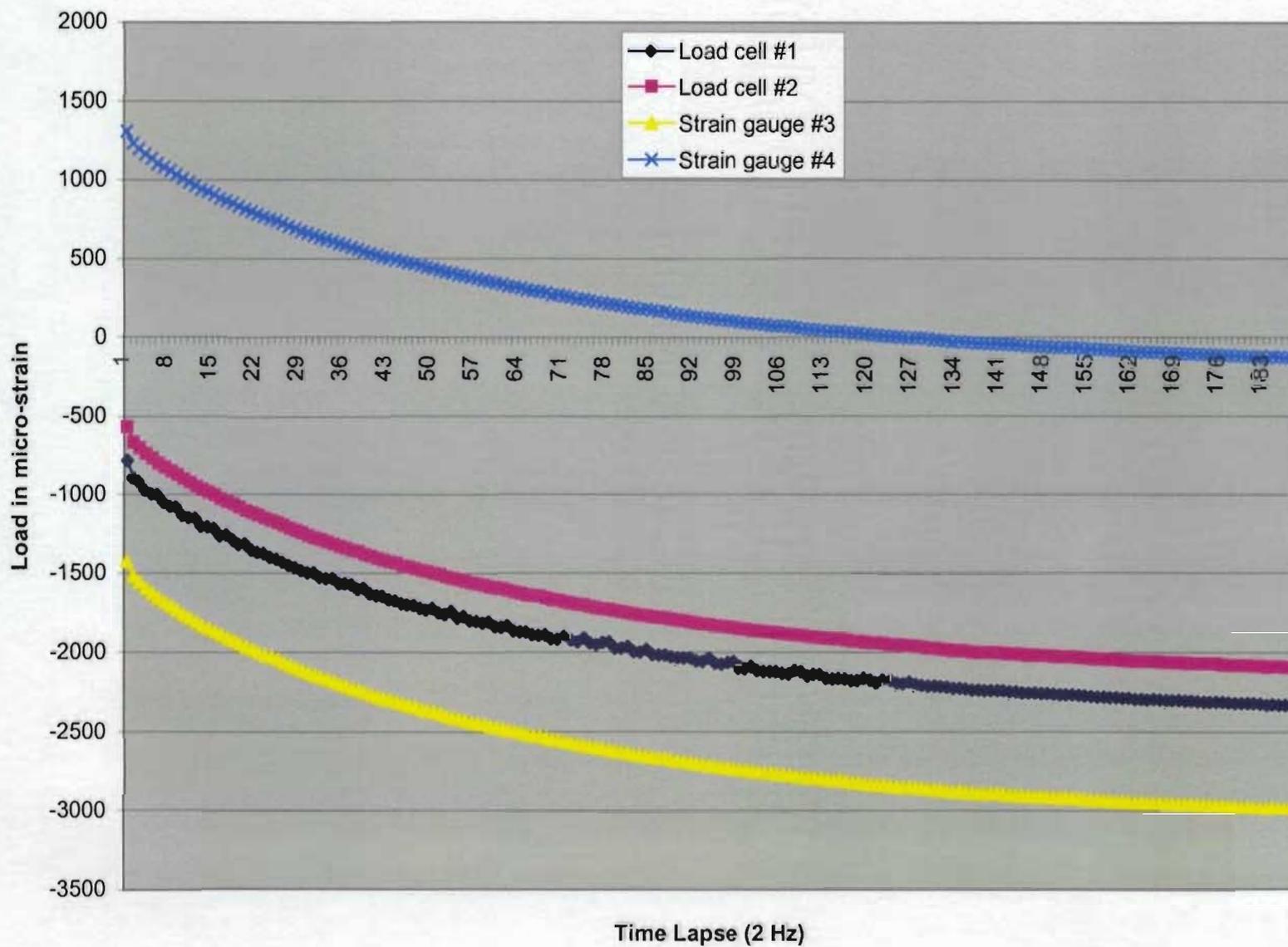
LABTECH NOTEBOOK				
Data file				
Time is 10:44:47.70.				
Date is 10-21-1999.				
sg 1	sg 2	Sg3		sg 5
ue	ue	Ue		Ue
1540.560	3042.209	5.2664		4211.977
1444.808	3057.590	5.2664		3491.762
1330.940	3203.708	-73.8352		2800.844
1473.274	3103.732	-0.0071		3386.781
1475.862	3075.534	-18.4641		2849.672
1442.220	3062.717	5.2664		4053.285
1439.632	3090.915	44.8171		3513.734
1465.511	3108.859	28.9968		2903.383
1470.687	3096.042	79.0945		3276.918
1457.747	3049.899	71.1843		2620.179
1447.396	3088.352	63.2742		3145.082
1501.741	3142.185	89.6414		2798.402
1470.687	3126.804	129.1921		3423.402
1478.450	3072.971	110.7351		2717.836
1465.511	3111.423	110.7351		3047.426
1413.753	3096.042	118.6453		3191.469
1470.687	3101.169	110.7351		2922.914
1470.687	3085.788	150.2859		3323.304
1447.396	3062.717	108.0984		2776.429
1452.571	3072.971	145.0125		3088.929
1431.868	3072.971	150.2859		3294.008
1356.819	3147.312	145.0125		2791.078
1447.396	3088.352	123.9187		3228.090
1455.159	3060.153	116.0085		2981.508
1426.692	3052.463	118.6453		3196.351
1426.692	3080.661	137.1023		3015.687
1408.577	3106.296	134.4656		3052.308
1442.220	3098.606	145.0125		2871.644
1437.044	3075.534	155.5593		3269.594
1429.280	3039.646	81.7312		2847.230
1385.286	2998.630	121.282		3923.890

117

Record of Loads in micro-strain{Thrust/Input}
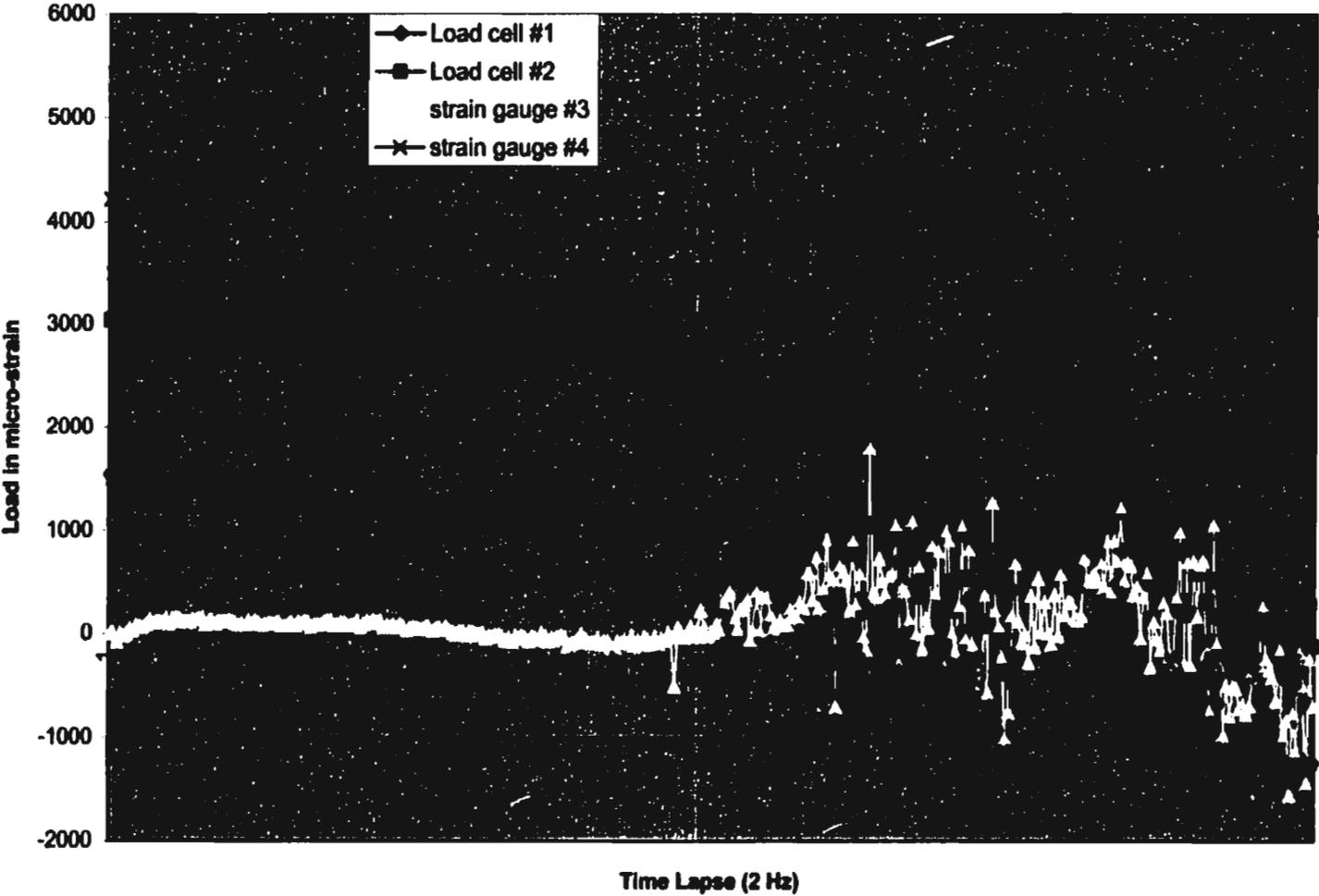
APPENDIX E

Sizing Of Beam, Shaft, key, Keyway,etc…

Lever Arm Beam Size:

The overall force attributed to the foil when oscillating at 5.23 rad/s was around 270 N. Use a factor of two to cover unexpected the loads at higher frequency. Then consider the lever as a balance beam below.

```
0.22 m          1749 N                    0.52 m
┌─────────────────────────────────────────────────────┐
│                      ▲                                │
▼                      │                                ▼
1229 N                 │                          520 N
```
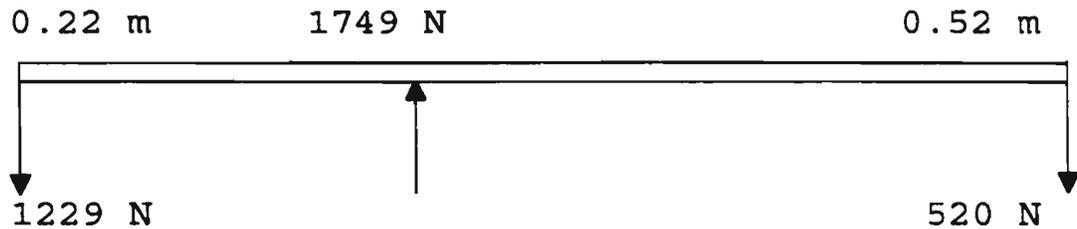
Maximum Bending Moment = 270.4 N m

Profile of beam, rectangular: (b x h), & b=14 mm (chosen because it was available)

Choose structural steel, cold drawn, 1020, s_y=441Mpa. Use σ_d= s_y/8 or 55Mpa. From s_y=M/I/c=55Mpa=270.4 N m/I/c, then I/c=4.9 x 10^{-6} m^3.

However, I/c=1/6 bh^2=2.33x10^{-3} h^2. Substituting, h^2=2.1x10^{-3} or h=0.046 m or **46 mm**.

Size of beam to be as close as possible to 14 mm x 46 mm I beam.

Power Take-off:

Given Conditions:

10 inch sheave via a cogged V belt (Gas engine rated at 12 hp, transmitted power to an efficiency range of 70-96%). Sheave had a common shaft with a 25 teeth sprocket chain drive. A chain roller was connected to a 10 teeth chain driver. This sprocket gear is splined to a small shaft, which was to be the power take-off for the oscillator mechanism.

Allowing slippage: 12 hp x 70% = 8.4 hp or 5280 ft-lb/s. $P=T\omega$ and if ω(working frequency)=22.6 rad/s, T= 234 ft-lb.

Section modulus of round shaft: J/c(J,Polar moment of inertia & c, radius) = $\pi/2$ $c^3=T/\tau_d$, but $\tau_d = S_y/2x6$ (Impact loading).

Using low carbon steel 1141 OQT 900, the designated yield strength is $S_y = 129$ ksi with 15% elongation. Let $\tau_d = 129ksi/12=10.75$ ksi. By substitution, $c^3=2T/\pi\tau_d$ =2(234 x 12)/3.14(10.75 ksi) = 0.1664 in^3 . The value of c was 0.55 in.

The diameter of shaft was **1 inch.**

Key (Shear Stress):

Power transmitting element, T=F(D/2) where T=torque, F=shearing force, & D=dia. of shaft.

Using values above, T=234 ft lb, D=1 in. then F=2(234 x 12)/1=5616 in lb.

Choose 1040 cold drawn, S_y=82 ksi at 10% elongation. Let $\tau_d = S_y/2x4$(repeated loading) = 82 ksi/8=10250 psi, which was the design allowable stress.

Since the shaft was only an inch in diameter, the maximum width of cut was 0.25

in. and 0.125 in. deep. This matches well with the manufacturer's keyway opening of the

flexible rubber, steel coupling.

Finding the length was A=0.25L=5616/10250=0.54.

Solving for L, led to 2 1/8 in. This was split into two since the other half was for the

reducer input shaft.

Bolts and Pins:

Use size appropriate for the load.

Coupling:

Used for mis-aligned shaft in angular or lateral fit.

It also absorbs impact loading due to fluctuation.

This project used a compression type light load coupling for 1 in. size shaft as described

in the power take off shaft.

APPENDIX F

ANNOTATED DATA for:

A. Record Test no. 1, data points 1 to 84 and its graph presentation

B. Record Test no. 4, data points 228 to 275 and its graph presentation

A. **Annotated data points 1 to 84**

	"load a"				"load c"			
	"lbs"		Difference	Average	"lbs"		Difference	Average
1	137.1288				67.38643			
2	117.5976	19.5312	19.5312		70.89985	-3.51342	3.513419	
3	117.5976	0	0		56.84618	14.05367	14.05367	
4	156.6601	-39.0625	39.0625		35.76566	21.08051	21.08051	
5	156.6601	0	0		32.2521	3.513563	3.513563	
6	156.6601	0	0		32.2521	0	0	
7	137.1288	19.5313	19.5313		28.73868	3.513419	3.513419	
8	156.6601	-19.5313	19.5313		32.2521	-3.51342	3.513419	
9	156.6601	0	0	24.41408	28.73868	3.513419	3.513419	6.587678
10	156.6601	0	0		25.22526	3.513419	3.513419	
11	156.6601	0	0		28.73868	-3.51342	3.513419	
12	176.1913	-19.5312	19.5312		28.73868	0	0	
13	156.6601	19.5312	19.5312		25.22526	3.513419	3.513419	
14	156.6601	0	0		25.22526	0	0	
15	156.6601	0	0		25.22526	0	0	
16	176.1913	-19.5312	19.5312		21.71185	3.513419	3.513419	
17	156.6601	19.5312	19.5312	19.5312	28.73868	-7.02684	7.026837	4.216102
18	176.1913	-19.5312	19.5312		25.22526	3.513419	3.513419	
19	176.1913	0	0		21.71185	3.513419	3.513419	
20	156.6601	19.5312	19.5312		25.22526	-3.51342	3.513419	
21	137.1288	19.5313	19.5313		25.22526	0	0	
22	176.1913	-39.0625	39.0625		18.19843	7.026837	7.026837	
23	156.6601	19.5312	19.5312		25.22526	-7.02684	7.026837	
24	137.1288	19.5313	19.5313		21.71185	3.513419	3.513419	
25	137.1288	0	0	22.78645	21.71185	0	0	4.684558
26	156.6601	-19.5313	19.5313		18.19843	3.513419	3.513419	
27	137.1288	19.5313	19.5313		21.71185	-3.51342	3.513419	
28	137.1288	0	0		25.22526	-3.51342	3.513419	
29	156.6601	-19.5313	19.5313		28.73868	-3.51342	3.513419	
30	156.6601	0	0		25.22526	3.513419	3.513419	
31	137.1288	19.5313	19.5313		28.73868	-3.51342	3.513419	
32	156.6601	-19.5313	19.5313		25.22526	3.513419	3.513419	
33	137.1288	19.5313	19.5313	19.5313	28.73868	-3.51342	3.513419	3.513419
34	137.1288	0	0		28.73868	0	0	
35	117.5976	19.5312	19.5312		28.73868	0	0	
36	137.1288	-19.5312	19.5312		25.22526	3.513419	3.513419	
37	117.5976	19.5312	19.5312		28.73868	-3.51342	3.513419	
38	98.0663	19.5313	19.5313		32.2521	-3.51342	3.513419	
39	137.1288	-39.0625	39.0625		28.73868	3.513419	3.513419	
40	137.1288	0	0		35.76566	-7.02698	7.026981	
41	117.5976	19.5312	19.5312	22.78643	35.76566	0	0	4.216131
42	137.1288	-19.5312	19.5312		32.2521	3.513563	3.513563	

Data Points for Load and Thrust Cell No.1

43	117.5976	19.5312	19.5312		35.76566	-3.51356	3.513563	
44	117.5976	0	0		35.76566	0	0	
45	98.0663	19.5313	19.5313		39.27908	-3.51342	3.513419	
46	117.5976	-19.5313	19.5313		35.76566	3.513419	3.513419	
47	117.5976	0	0		42.7925	-7.02684	7.026837	
48	98.0663	19.5313	19.5313		42.7925	0	0	
49	98.0663	0	0	19.53126	46.30592	-3.51342	3.513419	4.099037
50	98.0663	0	0		39.27908	7.026837	7.026837	
51	117.5976	-19.5313	19.5313		42.7925	-3.51342	3.513419	
52	117.5976	0	0		42.7925	0	0	
53	98.0663	19.5313	19.5313		42.7925	0	0	
54	117.5976	-19.5313	19.5313		42.7925	0	0	
55	98.0663	19.5313	19.5313		46.30592	-3.51342	3.513419	
56	98.0663	0	0		46.30592	0	0	
57	117.5976	-19.5313	19.5313		49.81934	-3.51342	3.513419	
58	78.5351	39.0625	39.0625	22.7865	46.30592	3.513419	3.513419	4.216102
59	98.0663	-19.5312	19.5312		49.81934	-3.51342	3.513419	
60	78.5351	19.5312	19.5312		49.81934	0	0	
61	98.0663	-19.5312	19.5312		42.7925	7.026837	7.026837	
62	78.5351	19.5312	19.5312		39.27908	3.513419	3.513419	
63	98.0663	-19.5312	19.5312		46.30592	-7.02684	7.026837	
64	78.5351	19.5312	19.5312		42.7925	3.513419	3.513419	
65	78.5351	0	0		53.33276	-10.5403	10.54026	
66	98.0663	-19.5312	19.5312		46.30592	7.026837	7.026837	
67	98.0663	0	0	22.7864	53.33276	-7.02684	7.026837	7.026837
68	78.5351	19.5312	19.5312		49.81934	3.513419	3.513419	
69	98.0663	-19.5312	19.5312		49.81934	0	0	
70	117.5976	-19.5313	19.5313		46.30592	3.513419	3.513419	
71	78.5351	39.0625	39.0625		53.33276	-7.02684	7.026837	
72	98.0663	-19.5312	19.5312		49.81934	3.513419	3.513419	
73	117.5976	-19.5313	19.5313		49.81934	0	0	
74	98.0663	19.5313	19.5313		49.81934	0	0	
75	78.5351	19.5312	19.5312		53.33276	-3.51342	3.513419	
76	78.5351	0	0	25.1116	49.81934	3.513419	3.513419	4.098989
77	78.5351	0	0		53.33276	-3.51342	3.513419	
78	98.0663	-19.5312	19.5312		46.30592	7.026837	7.026837	
79	98.0663	0	0		49.81934	-3.51342	3.513419	
80	78.5351	19.5312	19.5312		56.84618	-7.02684	7.026837	
81	98.0663	-19.5312	19.5312		49.81934	7.026837	7.026837	
82	98.0663	0	0		46.30592	3.513419	3.513419	
83	98.0663	0	0		49.81934	-3.51342	3.513419	
84	98.0663	0	0		53.33276	-3.51342	3.513419	
		98.0663	98.0663	39.16498		53.33276	53.33276	11.49755
		Oscillation	Load C.#1	Thrust C.#1				

		0							
		1	24.41408	6.587678					
			19.5312	4.216102					
		2	22.78645	4.684558					
			19.5313	3.513419					
			22.78643	4.216131					
		3	19.53126	4.099037					
			22.7865	4.216102					
			22.7864	7.026837					
		4	25.1116	4.098989					
			39.16498	11.49755					
			23.84302	5.41564	Approx. Efficiency:		22.71373		

Comparison of Load and Thrust Cells' Record in Lbs

Legend:
- Load Cell No.1
- Thrust Cell No.1

Y-axis: Resistance in Lbs (0, 5, 10, 15, 20, 25, 30, 35, 40, 45)

X-axis: Number of Oscillations between data points 0-90 of Graph 5.1 (0, 1, 2, 3, 4)
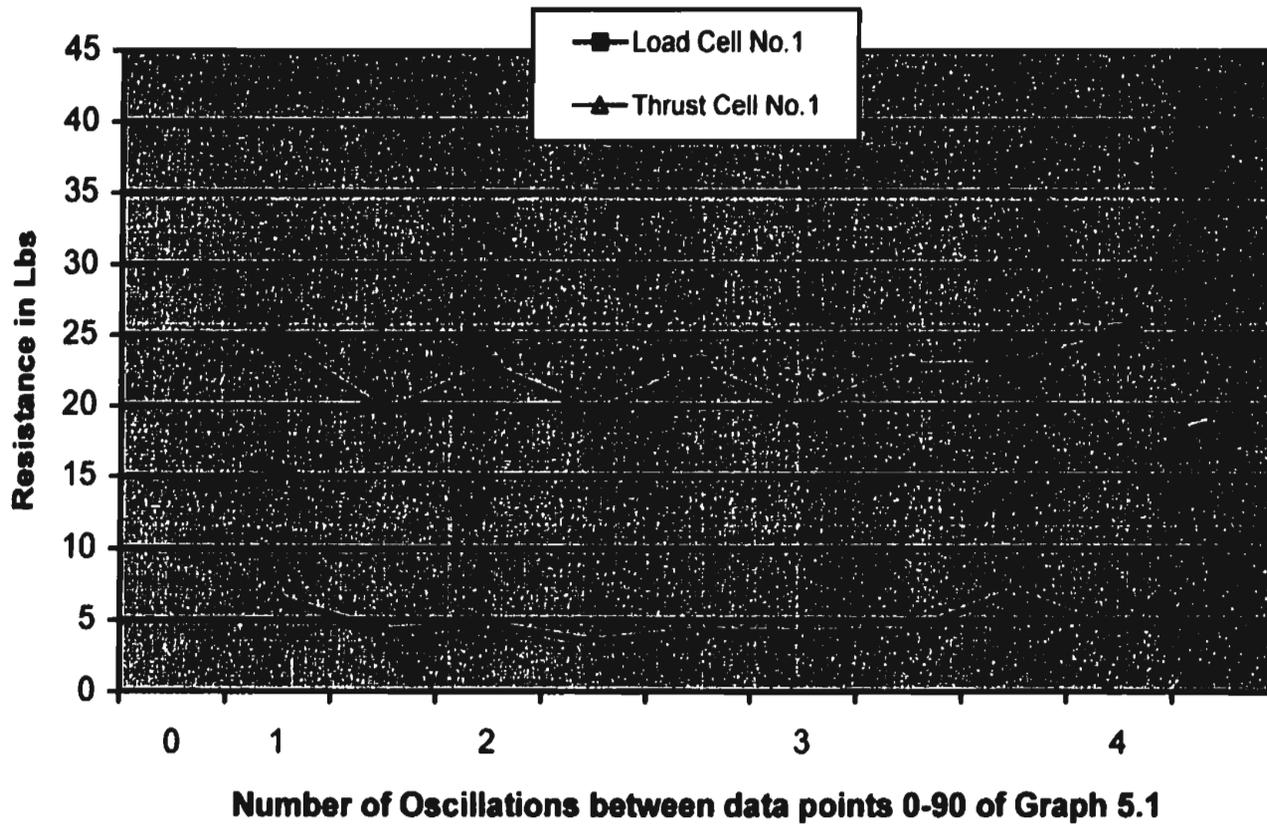
B.   **Annotated data points 228 to 275**

	Annotated data for Load cell #2			3points	Average	20#~ 600 ue	Annotated data for Thrust cell #2				Average	20#~60 0ue
	micro-strain											
228	2491.06					"lb."	4607.48					"lb."
229	1329.81	1161.25	1161.25				4873.6	-266.11	266.113			
230	1865.57	-535.77	535.767				4126.53	747.07	747.07			
231	778.66	1086.91	1086.91	2783.94	927.978	30.9326	4517.15	-390.63	390.625	1403.81	467.936	15.5979
232	2839.69	-2061	2061.04				4695.38	-178.22	178.223			
233	2980.69	-140.99	140.991				4121.65	573.731	573.731			
234	1365.7	1614.99	1614.99	3817.02	1272.34	42.4113	4834.54	-712.89	712.891	1464.84	488.281	16.276
235	319.798	1045.9	1045.9				4656.31	178.223	178.223			
236	222.385	97.4122	97.4122				4426.82	229.492	229.492			
237	1875.83	-1653.4	1653.44	2796.75	932.251	31.075	3218.32	1208.5	1208.5	1616.21	538.737	17.9579
238	1065.77	810.059	810.059				4553.77	-1335.4	1335.45			
239	1047.82	17.9444	17.9444				4512.27	41.5039	41.5039			
240	2134.74	-1086.9	1086.91	1914.92	638.306	21.2769	4431.7	80.5664	80.5664	1457.52	485.84	16.1947
241	1122.17	1012.57	1012.57				4683.17	-251.46	251.465			
242	1096.53	25.6347	25.6347				4526.92	156.25	156.25			
243	2914.04	-1817.5	1817.5	2855.71	951.904	31.7301	3618.72	908.203	908.203	1315.92	438.639	14.6213
244	1393.89	1520.14	1520.14				4724.67	-1106	1105.96			
245	2621.8	-1227.9	1227.91				5083.56	-358.89	358.886			
246	-39.089	2660.89	2660.89	5408.94	1802.98	60.0993	4158.27	925.293	925.293	2390.14	796.712	26.5571
247	2488.5	-2527.6	2527.59				4568.42	-410.16	410.156			
248	1183.69	1304.81	1304.81				4229.07	339.356	339.356			
249	740.208	443.482	443.482	4275.88	1425.29	47.5098	4553.77	-324.71	324.707	1074.22	358.073	11.9358
250	2665.38	-1925.2	1925.17				5125.06	-571.29	571.289			
251	383.884	2281.49	2281.49				4529.36	595.703	595.703			
252	1478.49	-1094.6	1094.6	5301.27	1767.09	58.903	4614.81	-85.449	85.4492	1252.44	417.48	13.916
253	363.377	1115.11	1115.11				4082.58	532.227	532.227			
254	547.947	-184.57	184.57				4434.15	-351.56	351.563			
255	714.573	-166.63	166.626	1466.31	488.77	16.2923	4092.35	341.797	341.797	1225.59	408.529	13.6176
256	1588.72	-874.15	874.146				4627.02	-534.67	534.668			
257	963.23	625.488	625.488				4436.59	190.43	190.43			
258	2419.28	-1456.1	1456.05	2955.69	985.229	32.841	3960.51	476.074	476.074	1201.17	400.391	13.3464
259	232.639	2186.65	2186.65				3657.78	302.734	302.734			
260	2483.37	-2250.7	2250.73				4761.29	-1103.5	1103.52			
261	1924.53	558.838	558.838	4996.22	1665.41	55.5135	3911.68	849.61	849.61	2255.86	751.953	25.0651
262	501.804	1422.73	1422.73				4519.59	-607.91	607.91			
263	235.203	266.602	266.602				3591.86	927.735	927.735			
264	973.484	-738.28	738.281	2427.61	809.204	26.9735	4634.34	-1042.5	1042.48	2578.13	859.375	28.6458
265	2024.51	-1051	1051.03				4517.15	117.188	117.188			
266	540.257	1484.25	1484.25				4226.63	290.527	290.527			
267	2867.89	-2327.6	2327.64	4862.91	1620.97	54.0324	3843.32	383.301	383.301	791.016	263.672	8.78906
268	327.488	2540.41	2540.41				3982.48	-139.16	139.16			
269	140.354	187.134	187.134				3606.51	375.977	375.977			

270	94.2115	46.1426	46.1426	2773.68	924.561	30.8187	4014.22	-407.71	407.715	922.851	307.617	10.2539
271	112.156	-17.944	17.9444				3320.86	693.359	693.359			
272	817.112	-704.96	704.956				4434.15	-1113.3	1113.28			
273	83.9576	733.154	733.154	1456.05	485.352	16.1784	3728.58	705.567	705.567	2512.21	837.403	27.9134
274	2401.34	-2317.4	2317.38				4536.68	-808.11	808.106			
275	670.994	1730.35	1730.35				4302.31	234.375	234.375			
276			1000	5047.73	1682.58	56.0859				1042.48	347.494	11.5831

	Values of Load and Thrust cells No. 2											
	Load cell	Thrust cell										
0												
1	31	15.6										
2	42.4	16.3										
3	31	18										
4	21.3	16.2										
5	31.7	14.6										
6	60.1	26.5										
7	47.5	12										
8	58.9	13.9										
9	16.3	13.6										
10	32.8	13.7										
11	55.5	25										
12	27	28.6										
13	5.4	8.8										
14	30.8	10.3										
15	16.2	27.9										
16	56	11.6										
	563.9	272.6										
	35.2438	17.0375	Approx. Efficiency:		48.3419							

Comparison of Load and Thrust Cells' Record in Lbs

Legend: Load Cell No.2, Thrust Cell No.2

Y-axis: Resistance in Lbs (0, 10, 20, 30, 40, 50, 60, 70)

X-axis: Number of Oscillation between data points 228-275 of Graph 5.5
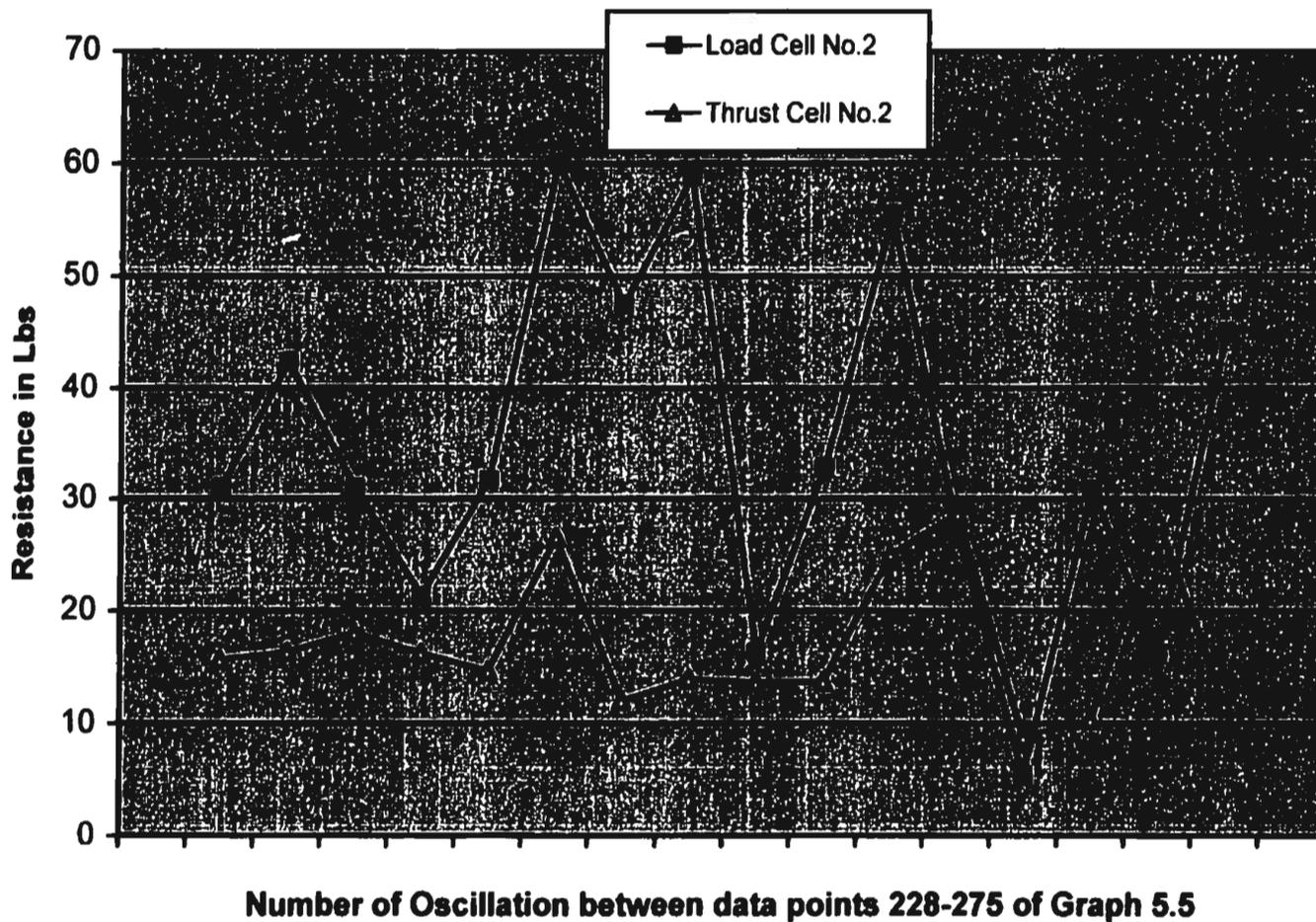
APPENDIX G

Schematic Drawing for the Load and Thrust Cell

(Load & Thrust
Cells use Quarter
Bridge Circuit)

CYEXP-GP
8 Channel
Expansion
Multiplexing
Terminal
Panel

Typical Screw Terminals

37 Pin Connector

Cable Connector
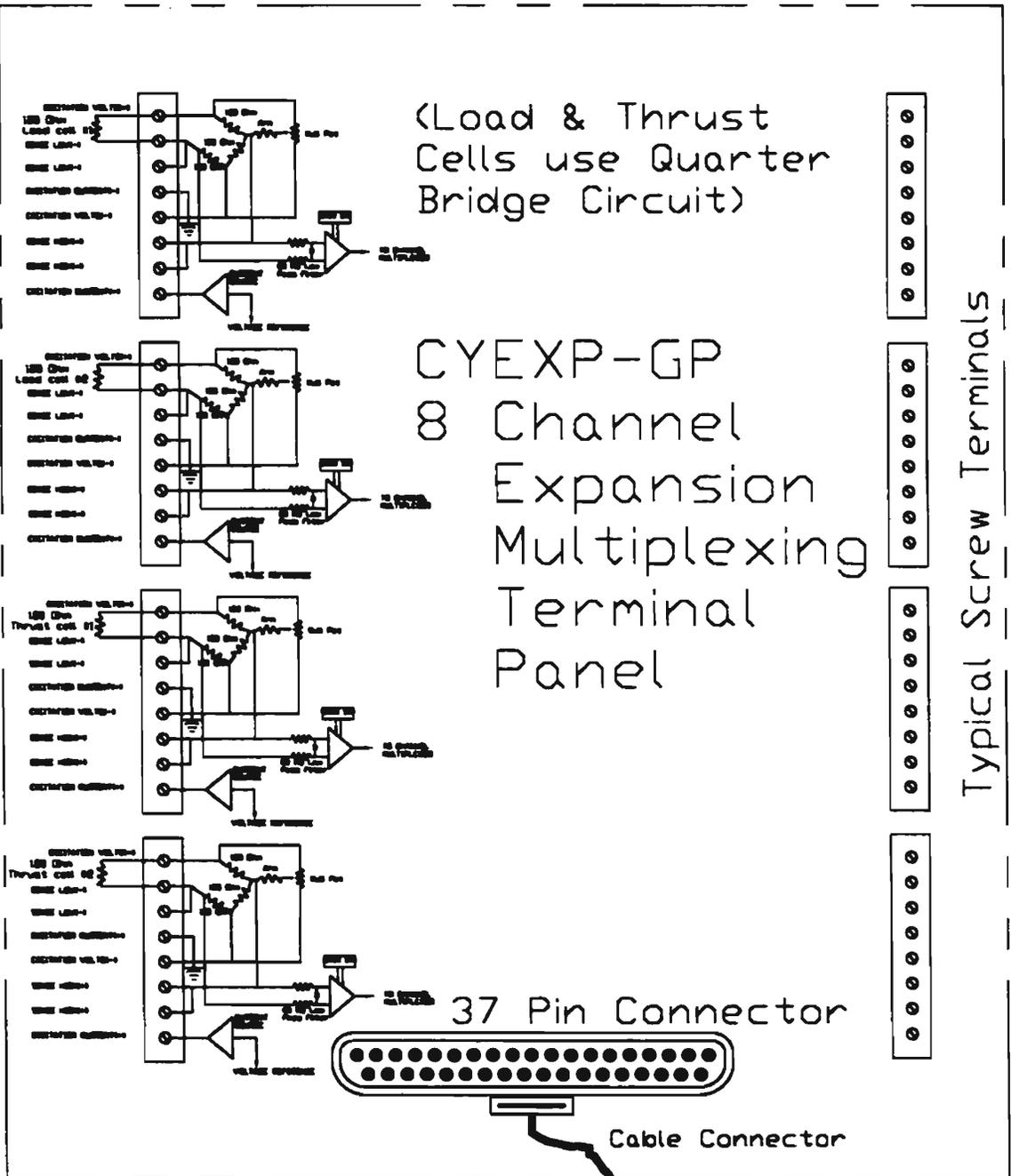
To 37 Pin Connector
of the CYDAS-1400
Series Board Slotted to a 486 PC's mother-board

DWG. NO.09	TITLE: LOAD AND THRUST CELLS SCHEMATIC	DESIGNED BY: T. CALDERON

APPENDIX H

A PROPOSED FOIL RE-DESIGN TO IMPROVE PERORMANCE

-

NOTE:
Material: Aluminum
1/4" × 1" Typical
Area of foil, A=0.2
Aspect ratio;AR=+6

Hinge or Pitch
Enclosure

Profile of
Structure

Ø1.00
Typ.

23.00

17.75

58°

11.50

9.50

3.05

4.00 4.00 4.00 4.00

1.78

1.72

Ø0.75
Typ.

1.09

1.00

1.00

22.5

FRONT VIEW

SIDE VIEW